CONTENTS

Publication Details

2020-21

Sl No	Name of Faculty	Title	Journal	Index
1	Kiran M D	Sliding Wear Behaviour of Nickel-Coated Short Fibre-Reinforced Al7075 Composites	Journal of Failure Analysis and Prevention, Springer, DOI https://doi.org/10.1007/s11668-020-00955-1, 11 August 2020.	Scopus Web of Science
2	Praveen Kumar T N, H K Govindraju	Axial Crushing Behaviour of Foam, Pyramidal and Tetrahedral Structure Filled Aluminium Square Tubes	Journal of Critical Reviews ISSN- 2394-5125 VOL 7, ISSUE 14, 2020	Scopus
3	Keerthi kumar N	Design and Implementation of Solar Based Smart Mobile Charging System	International Journal of Mechanical and Production Engineering Research and Development (IJMPERD) ISSN (P): 2249–6890; ISSN (E): 2249–8001, Vol. 10, Issue 4, Aug 2020, 229–238	Scopus
4	Keerthi kumar N	i-Trasher- Smart Waste Management System	International Journal of Mechanical and Production Engineering Research and Development (IJMPERD), ISSN(P): 2249–6890; ISSN(E): 2249–8001, Vol. 10, Issue 3, Jun 2020, 7577–7586	Scopus
5	Keerthi kumar N	Advanced Decision Support System for Precision Agriculture Using WSN	International Journal of Mechanical and Production Engineering Research and Development (IJMPERD), ISSN(P): 2249–6890; ISSN(E): 2249–8001, Vol. 10, Issue 3, Jun 2020, 7561–7568	Scopus
6	Keerthi kumar N	Impact of injection timing on simarouba seed oil-fueled CI engine	Materials Today: Proceedings, 2214-7853, https://doi.org/10.1016/j.matpr.2020.10.329 2214-7853, 2020	Scopus

7	Sangmesh	Numerical investigation on heat sink with fluid pockets for high power LEDs	Indian Journal of Engineering & Materials Sciences Vol. 27, pp. 1018-1026, October 2020.	Scopus
8	Kiran M D	Fracture Toughness of CNT Filled Carbon Fabric Reinforced Epoxy Composites	Materials Research Innovations, Volume 25, Issue 2 (2021).	Scopus
9	Kiran M D	Fracture toughness study of epoxy composites reinforced with carbon fibers with various thickness	Materials Today: Proceedings, Volume 46, Part 7, Pages 2630-2634, 2021.	Scopus
10	H K Govindraju Kiran M D	Three-point bending and impact behaviour of carbon/epoxy composites modified with titanium dioxide nanoparticles	Materials Today: Proceedings, Volume 43, Part 2, Pages 1755-1761, 2021.	Scopus
11	Keerthi kumar N	Performance and Emission Characteristics of C.I Engine Fuelled with Hybrid Biodiesel	International Journal of Vehicle Structures & Systems, 13(1), 6-9, ISSN: 0975-3060 (Print), 0975-3540 (Online), doi: 10.4273/ijvss.13.1.02	Scopus
12	Madhu M C	Hybrid DC-AC homes with roof top solar power	E3S Web of Conferences 239, 00025 (2021)	Scopus
13	Keerthi Kumar N	Performance and Emission Characteristics of 4-Stroke Diesel Engine Using Simarouba and Graphene Nanoparticles	5th International Conference on Advanced Research in Mechanical, Material and Manufacturing (ICAMMME-2021) organized by REVA University on 9th and 10th July 2021	International Conference

TECHNICAL ARTICLE—PEER-REVIEWED

Sliding Wear Behaviour of Nickel-Coated Short Fibre-Reinforced Al7075 Composites

Nithin Kumar · M. D. Kiran · S. S. Sharma · B. Ravikiran Kamath · R. K. Veeresha

Abstract In the present study, Aluminium-7075 alloy is reinforced with nickel-coated short carbon fibres in the form of short fibre. These composites were prepared by stir casting method with 2, 4, 6 and 8 wt.% of nickel-coated carbon fibres. Wear resistance of aluminium alloy and its composites were analysed according to the ASTM standards. The experiments were conducted using pin-on-disc wear test and rig wear test method with different loads. From the wear test, it was found that aluminium composites with 8% nickel-coated carbon fibre rate of wear are minimum. Worn and fractured surfaces of cast aluminium alloy and the developed composites are analysed by SEM. The test results reveal that the wear resistance of the prepared MMCs improves with the addition of carbon fibre.

Keywords Al7075 alloy · Pin on disc · Wear resistance · SEM

Introduction

Aluminium and its alloys are known for excellent corrosion resistance as well as good mechanical properties. In terms of wear properties, they are poor. Tribological applications like pistons, components of brake-system, engine blocks, wear resistance components and other various aircraft, and defence equipment's [1]. Metal matrix composites are prepared using aluminium and its alloys to develop newer material to achieve the better tribological properties [2–5]. Hence, requirements for enhancements in wear resistance and service loads of materials in all these applications have forced researchers to develop and synthesise aluminium-based composites.

Silicon carbide, alumina, titanium carbide and fly ash improve the strength, hardness and wear resistance of the composites. Problems are encountered during machining of metal matrix composites due to the addition of hard dispersoids to these composites. Matrix alloy has higher surface finish when compared with the hard-reinforced metal matrix composites. Also, the thermal and electrical conductivity of aluminium is changed by the addition of ceramic reinforcements. Reinforcement also influences machinability index [6].

In the case of Al6061 reinforced with TiO_2, it was observed that composites exhibit lower wear coefficient and better hardness as compared with the matrix alloy [7]. The volumetric wear loss is high because of increased loads and sliding distances, but the coefficient of wear is low in both matrix alloy and its composites. The high strength aluminium alloys Al7010, Al7009 and Al2024 reinforced with SiC particles exhibit significantly better sliding wear characteristics than that of alloys due to the addition of SiC particles [8]. Aluminium matrix composites

N. Kumar (✉) · B. Ravikiran Kamath · R. K. Veeresha
Department of Mechanical Engineering, NMAMIT, Nitte 574110, India
e-mail: na.hebbar@yahoo.co.in

M. D. Kiran
Department of Mechanical Engineering, BMS Institute of Technology and Management, Bengaluru, India

S. S. Sharma
Department of Mechanical and Manufacturing Engineering, MIT, Manipal 576104, India

reinforced with short steel fibres show decrease in wear rate by increasing the reinforcement fibres decreased the rate of wear and coefficient of friction at different loading conditions [9]. Metal matrix composite of Aluminium-7075 with nickel-coated carbon fibres in the form of short fibres shows increase in fatigue strength with increase in reinforcement loading [10]. Surface coating on carbon fibres increases the wettability, and it increases the interfacial reaction between matrix and carbon. And it overcomes the arduous of obtaining better interface bonding between fibres matrix. Coating of nickel on surface of carbon fibre exhibits better interface bonding among matrix and fibres and also increases the oxidisation resistance, strength of the composites with both metal and polymer matrix [11, 12].

In present investigation, Al7075 alloy reinforced with nickel-coated short carbon fibres of 2, 4, 6 and 8 wt.%. was prepared using stir casting method. The wear behaviour of prepared composites was studied using pin-on-disc method. The surface, subsurface and the fragments are studied using scanning electron microscopy to analyse the wear mechanisms [13, 14].

Experimental Details

The composites were prepared by reinforcing Al7075 alloy with varying percentage of carbon fibres coated with nickel using stir casting process. This test was conducted to find out the wear property of the material. The specimens are prepared according to ASTM standard G99. The rate of wear is investigated by using a pin-on-disc method for different loading conditions. Before the experiments, wear specimens are held in a holder and abraded against the sheet of abrasive paper on rotating steel disc to get a flat wear surface. Initially, the specimen is weighed in the
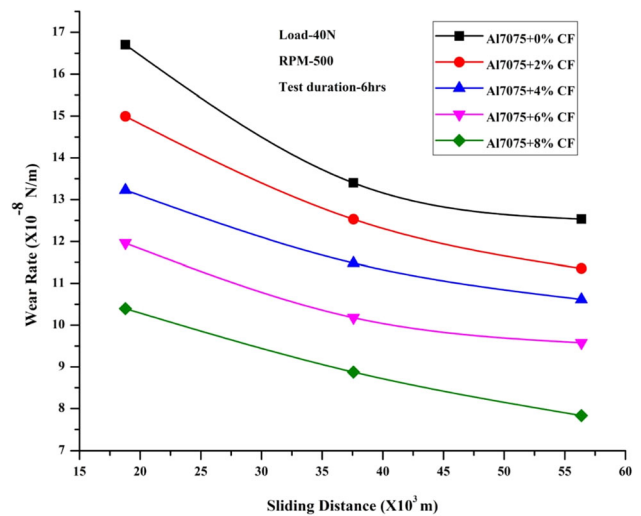

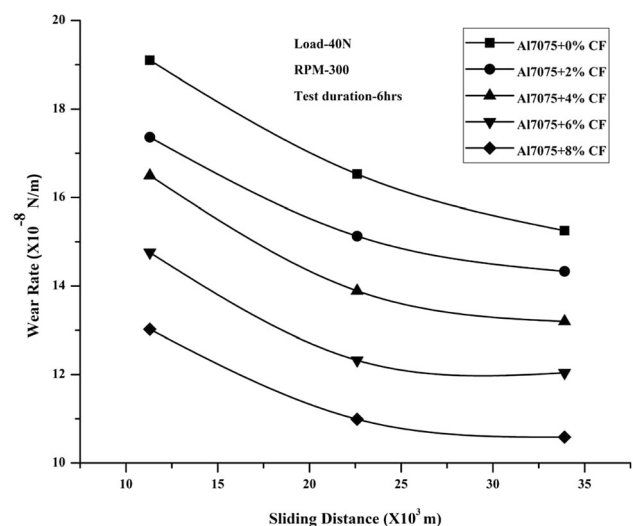Fig. 2 Specimen before and after test

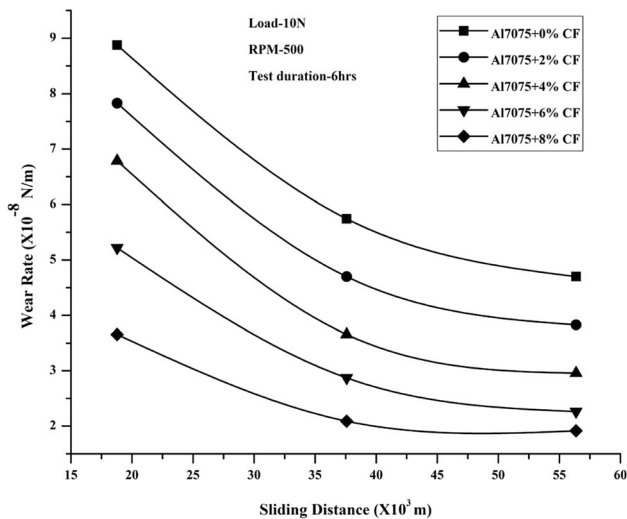Fig. 3 Wear rate at 10 N load

Fig. 4 Wear rate at 20 N load

Fig. 1 Pin-on-disc test rig

Fig. 5 Wear rate at 30 N load

Fig. 6 Wear rate at 40 N load

Fig. 7 Volumetric wear rate at normal load

Fig. 8 Specific wear rate at normal and 300 rpm load and 300 rpm
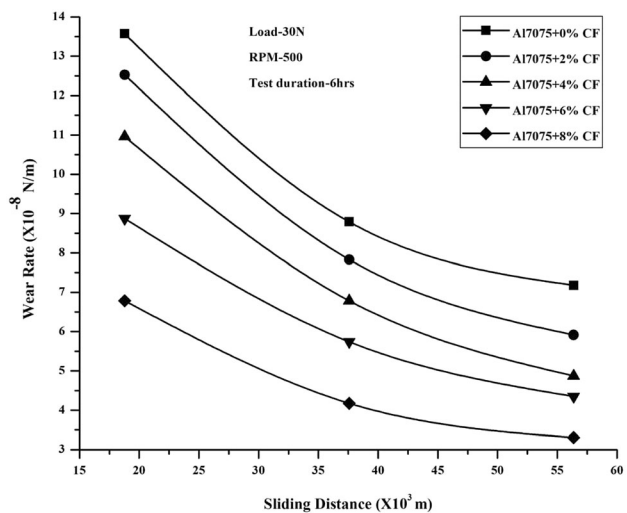
microbalance, and then, it is inserted to the collet of pin-on-disc machine. The specimen along with collet is calibrated at a particular track diameter. The track diameter is changed after each test. During the test, the specimen remains fixed and only the disc rotates. The disc is rotated with the help of a DC motor, having a speed range 0–2000 RPM with wear track diameter 50–180 mm, and it is capable of obtaining sliding speed of 0–10 m/s. A controller is used to vary the speed of the disc. A dead weight loading system is used to apply the required load and press the pin against the disc. Normal load and other parameters are set to a constant value throughout the test for a single specimen.

Each set of trials are conducted for a duration of 6 h. After every two hours run, the test specimens were removed from the collet, cleaned with acetone solution and weighed. The difference in weight of the specimen before and after the test is used to calculate wear rate. Figure 1
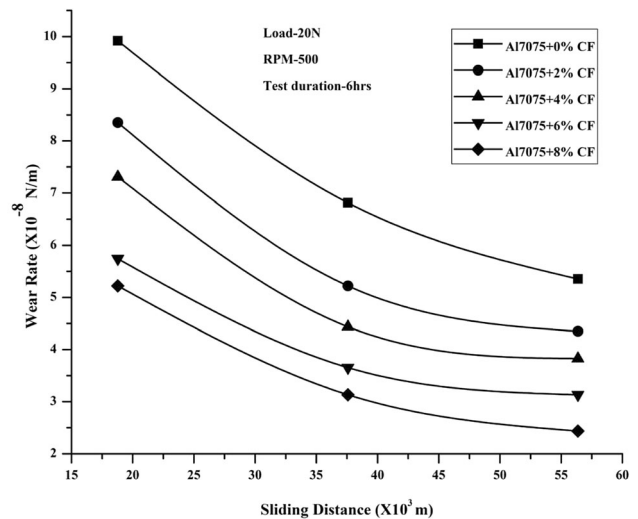
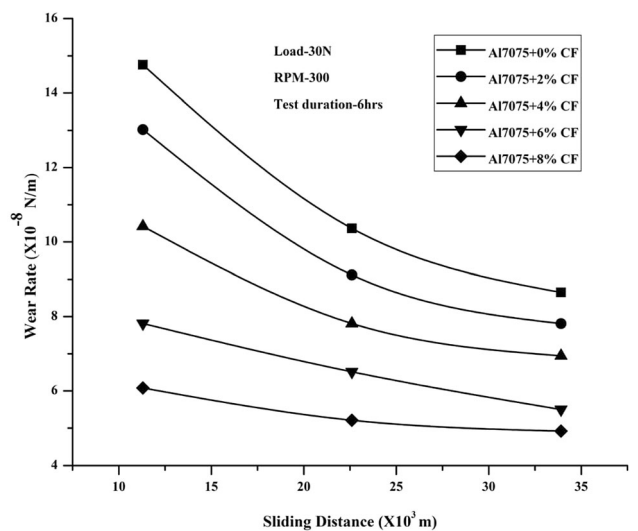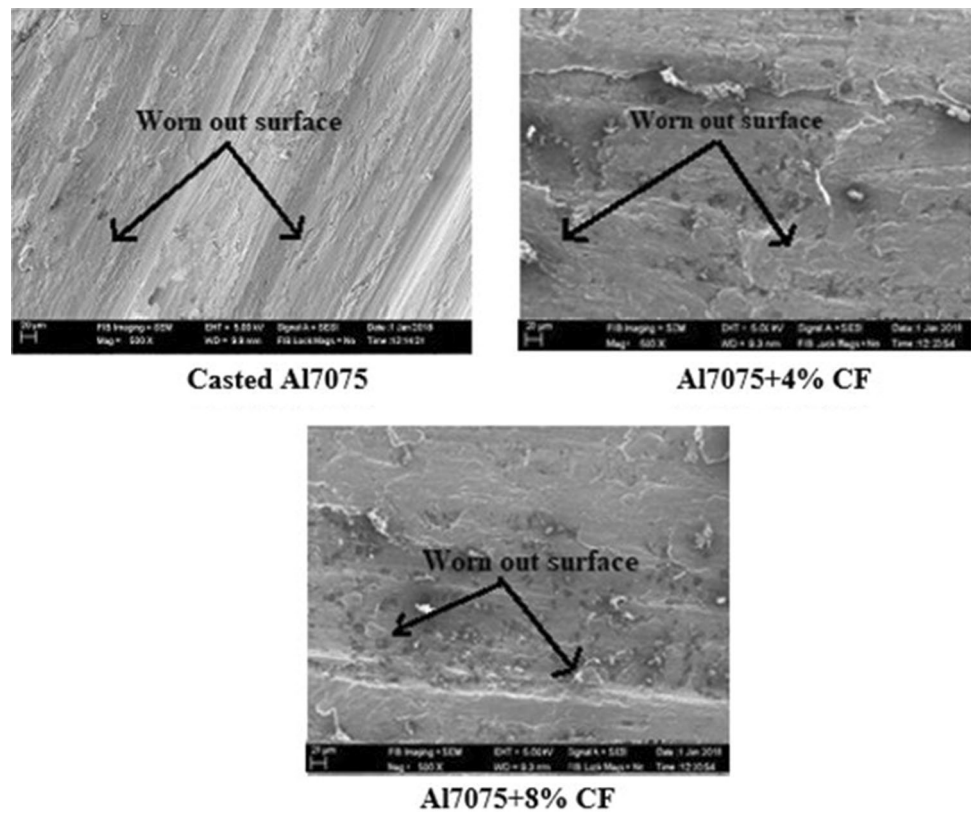shows the setup of pin-on-disc test rig. Figure 2 shows wear test specimen before and after the test.

Calculations

Wear rate is calculated by calculating the loss of mass of the specimen after each test. It is cautioned that after each test, wear debris is avoided from the specimen. The relation

Fig. 9 SEM morphology
300 rpm

Casted Al7075

Al7075+4% CF

Al7075+8% CF

between wear rate, loss of mass (Δm) and the sliding distance (L) is obtained using the formula:

$$W_r = \Delta m/L$$

The relation between volumetric wear rate W_v of the composite, the density of the composite (ρ) and the test duration (t) is obtained using the formula:

$$W_v = \Delta m/\rho t$$

Specific wear rate method is used to characterise the composite for wear behaviour. The specific wear rate is the volume loss of composite due to abrasive wear per unit sliding distance and unit applied normal load. The specific wear rate is obtained by the formula:

$$W_s = W_v/V_s F_n$$

where V_s is the sliding velocity, and F_n is the normal load applied.

Results and Discussion

The results obtained from the pin-on-disc wear testing setup for different volume fractions, loads and RPM revealed that the addition of short carbon fibres decreased the wear rate of the Al7075 composite. The composite formed by reinforcing 8 wt.% carbon fibre with Al7075

matrix showed the least wear rate with increasing sliding distance for normal loads ranging from 10 to 40 N at 300 RPM. The experiment was repeated for the same normal loads at 400 RPM and 500 RPM. It was observed that the trends were similar to that observed for 300 RPM and 8 wt.% reinforced composite showed minimum wear rate. However, for the initial sliding distance the wear rate increased; after some duration, it decreased and then remained almost constant for the entire duration of the test.

Figures 3, 4, 5, 6, 7 show the change of volumetric wear rate with normal load for 300 RPM. The results indicated an increase in the volumetric wear rate with the increase in normal load owing to the fact that, for significantly greater amounts of normal load, the frictional thrust was observed to have increased and resulted in increased de-bonding and fracture that caused more volumetric wear loss. The volumetric wear rate for Al7075 reinforced with 8 wt.% carbon fibre was found to be much lesser when compared to casted Al7075.

An additional increase in the load triggered the commencement of delamination which resulted in a higher volumetric wear rate for both the aluminium matrix alloy and its composites as observed by several researchers. Similar plots were observed at 400 and 500 RPM.

Figure 8 displays the change of specific wear rate with normal load for 300 RPM. The results revealed that increase in normal load decreases the specific wear rate.

Fig. 10 SEM morphology 500 rpm

Casted Al7075

Al7075+4% CF

Al7075+8% CF
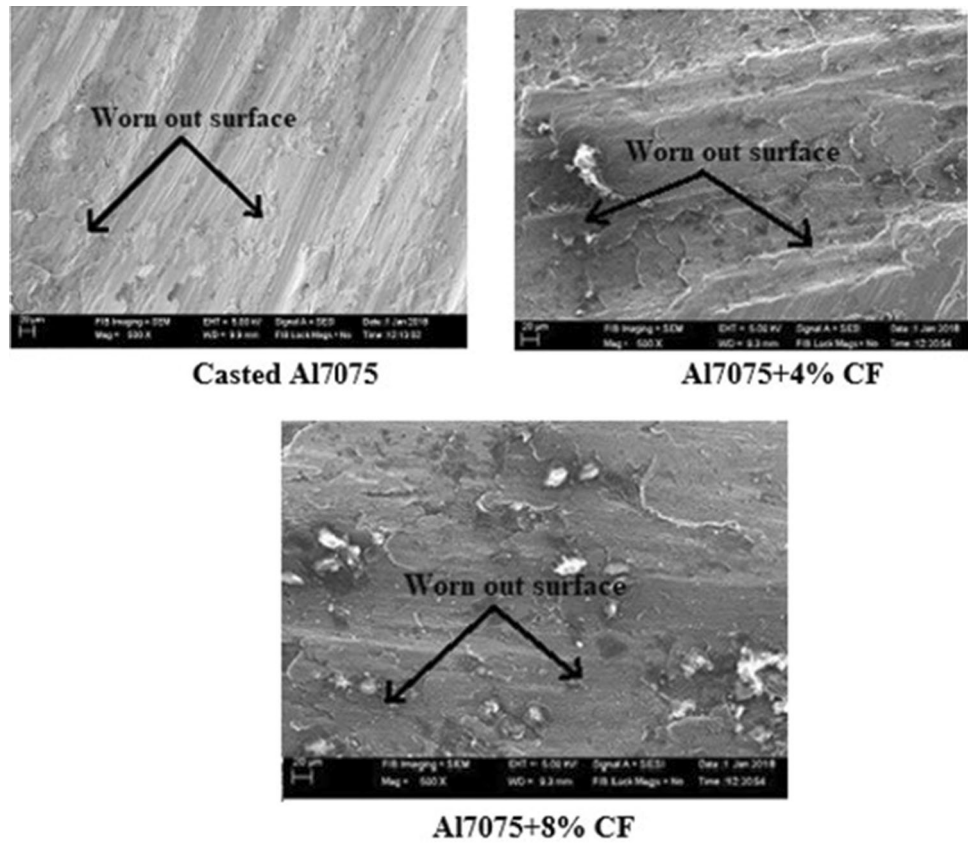
The specific wear rate for Al7075 reinforced with 8 wt.% carbon fibre showed a nearly horizontal trend and was found to be much lesser when compared to casted Al7075.

For lower speeds and loads, the difference between the specific wear rates for each specimen was large which decreased with the increase in speed and load. However, for higher speeds of 400 RPM and 500 RPM, the rate of specific wear decreases with the increase in normal load values including the 8 wt.% reinforced composite specimen.

To comprehend the wear mechanism of aluminium alloy and its composite, SEM observation of the wear surfaces was carried out. Figures 9 and 10 show the SEM images of worn out surfaces at 300 RPM and 40 N Load for 6 hours test duration and at 500 RPM and 40 N load for 6 hours test duration, respectively. The white layers atop of worn out surface of the composites indicate that the temperature at the surfaces is very high.

It is observed that as the load increases, the fine scratches on the surface change into distinct grooves and result in wear loss, which increases with the rise in the sliding speed. It is evident from the fact that the grooves on the worn surfaces for 500 RPM were more than that of 300 RPM. From the images, it can be seen that extent of grooves in 8 wt.% of carbon fibre-reinforced composite is much less than 4 wt.% carbon fibre-reinforced composite and as cast Al7075 alloy in both the cases. Hence, it is clear from the figures that adding carbon fibre increases the wear resistance of the composite.

Conclusions

The wear rate is found to be decreasing with increase in wt.% of short carbon fibre for the different conditions like change in the sliding distance, change in the sliding velocity and change in the applied normal load, and at 8 wt.% of the short carbon fibre as reinforcement, the wear rate was found to be minimum.

References

1. P.J. Blau, Friction and wear of aluminium-silicon alloys. ASM Handb. Friction Lubr. Wear Technol. **18**, 785–794 (2013)
2. M.G. Vassilaros, D.A. Davis, G.L. Stecker, J.P. Gudas, in *Proceedings of the Tri- Service Conference on Corrosion US Air Force Academy, Colorado*, Vol II, (1980)

3. A.I. Onen, B.T. Nwufo, E.E. Ebenso, R.M. Hlophe, Titanium (IV) oxide as corrosion inhibitor for aluminium and mild steel in acidic medium. Int. J. Electrochem. Sci. **5**, 1563 (2010)

4. S. Biswas, A. Shantharam, N.A.P. Rao, K. Narayana Swamy, P.K. Rohatgi, S.K. Biswas, Performance of graphic aluminium particulate composite materials. Tribo. Int. **13**(4), 171–176 (1980)

5. M. Saxena, B.K. Prasad, T.K. Dan, Corrosion characteristics of aluminium alloy graphite particulate composite in various environments. J. Mater. Sci. **27**, 4805–4812 (1992)

6. S.K. Biswas, B.N. Pramila Bai, Dry wear of aluminum graphite particle composites. Wear **68**, 347–358 (1981)

7. C.S. Ramesh, A.R. Anwar Khan, N. Ravikumar, P. Savanprabhu, Prediction of wear coefficient of Al6061–TiO2 composites. J. Wear **259**, 602–608 (2005)

8. R.N. Rao, S. Das, Effect of matrix alloy and influence of SiC particle on the sliding wear characteristics of aluminium alloy composites. Mater. Des. **31**, 1200–1207 (2010)

9. D. Mandal, B.K. Dutta, Wear and friction behavior of stir cast aluminium base short steel fiber reinforced composites. Wear **257**, 654–664 (2004)

10. N. Kumar, H.C. Chittappa, A.A.D. Mello, M.D. Kiran, Fatigue behaviour of carbon fiber reinforced aluminum metal matrix composites. Adv. Sci. Eng. Med. **10**(3), 1–4 (2018)

11. Z. Hua, Y. Liu, G. Yao, L. Wang, J. Ma, L. Liang, Preparation and characterization of nickel coated carbon fibers by electroplating. J. Mater. Eng. Perform. **21**, 324–330 (2012)

12. M.D. Kiran, H.K. Govindaraju, T. Jayaraju, Evaluation of fracture toughness of epoxy-nickel coated carbon fiber composites with Al2O3 nano filler, in *Advances in Polymer Composites: Mechanics, Characterization and Application,* AIP Conf. Proc. 2057, 020002-1–020002-5; https://doi.org/10.1063/1.5085573

13. S. Arivukkarasan, V. Dhanalakshmi, A. Suresh Babu, M. Aruna, Performance study on fatigue behavior in aluminium alloy and alumina silicate particulate composites. J. Appl. Sci. Eng. **16**, 127–134 (2013)

14. C.S. Ramesh, M. Safiulla, Wear behavior of hot extruded Al6061 based composites. J. Wear **263**, 629–635 (2007)

AXIAL CRUSHING BEHAVIOUR OF FOAM, PYRAMIDAL AND TETRAHEDRAL STRUCTURE FILLED ALUMINIUM SQUARE TUBES

PRAVEEN KUMAR T N[1], H K GOVINDRAJU[2], UJVAL CHAKRAVARTHY B N[3]
S VENKATESWARAN[4], S SEETHARAMU[5]

[1,2,3] BMS Institute of Technology and Management
[4] Atria Institute of Technology
[5] R.V. College of Engineering
[1] tnpmech@bmsit.in

ABSTRACT: The present investigation involves the study of the crushing behaviour of Al- 6063 thin walled empty tubes and tubes filled with periodical structures and polyurethane foam under axial loading. From the axial crushing test, it was observed that, when the crushing load increased the tube was folded axially and tube undergoes large plastic deformation with symmetric mode folding. The large plastic strain was concentrated on the corner areas of the tube and on the horizontal folds, the other areas the tube will undergo small plastic deformation. It was observed that the tube filled with pyramid structure and polyurethane foam showed 57% more crushing strength when compared with the empty tube.

I.   INTRODUCTION

Thin walled structures are used to convert the energy absorbed by the material in to plastic energy during the impact loads to protect the people and structures during accident. Thin walled structures perform well in energy absorbing in terms of its low weight, larger displacements and total energy absorption [1]. The geometry places an important in failure mode and the corresponding energy absorption properties. Circular tubes will be crushed in a ring mode or a diamond mode or a mixed mode. Mainly it depends upon diameter to wall thickness ratio. Similarly, in square tubes it depends upon width to wall thickness ratio [2-9]. In spite of having the desirable properties, crushing force is not uniform during the deformation process particularly in high initial peak force and subsequent fluctuation conditions. The surface of a tubes generates the lower initial peak force and a more uniform crushing process with side effect of reduced total energy absorption [10]. Under quasi-static loading, different types of deformation modes were observed for different kind of specimens, these are diamond deformation mode, concertina deformation mode, mixed deformation mode, axisymmetric deformation mode and global bending mode [11]. The energy absorbing capacity of materials and structures of different types of structures such as rectangular, circular, hexagonal, triangular, pyramidal, foam filled, cellular etc[12] are used. The crushing mechanism on the thin-walled part using the concept of super-folding element the pattern of the folding shell elements were used [13]. The folding mechanism is shown in Fig. 1.
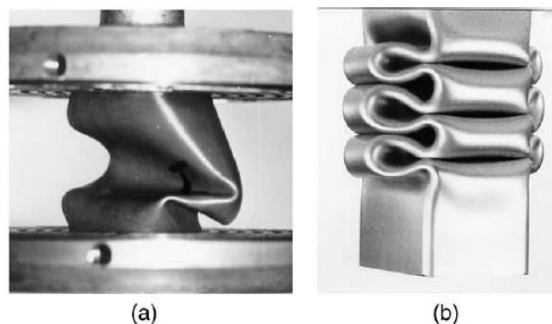

(a)   (b)

Fig. 1. Folding patterns of crushed shell structures

The mechanism considered in the plastic element folding are, bending occurs along stationery hinged line, conical surface opening, deformation of floating, toroidal surface, rolling deformations, bending along hinge line, inclined, stationery. Some of the authors reported that the progressive folding mode observed initially and later stages of loading, splitting occurs at the corners in case of tube filled with honeycomb and filled with polyurethane [14] shown in Fig. 2.
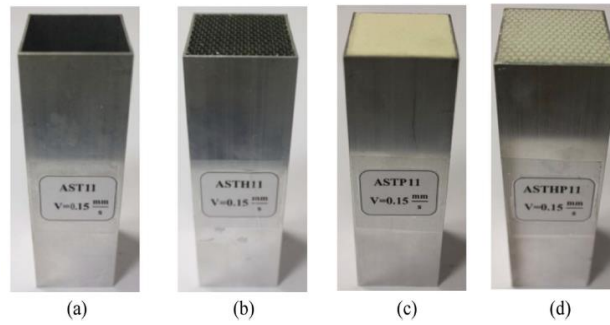
Fig.2 (a) Hollow aluminium tube (AST); (b) Honeycomb-filled tube (ASTH); (c) Foam-filled tube (ASTP); (d) Foam and honeycomb-filled tube (ASTHP).

From this study it is understood that, the configurations of hollow tube filled with polyurethane and honey-comb is the better solution in terms of axial crashworthiness. There is 88.5 % increase in mean crushing force for the sum of all configurations compared and tested separately. To determine and improved the energy absorbing capacity of these materials, the extensive numerical, experimental and research has been conducted. Lattice Truss Topologies are absorbing more energies when compared with empty tube structures. (Fig.3)
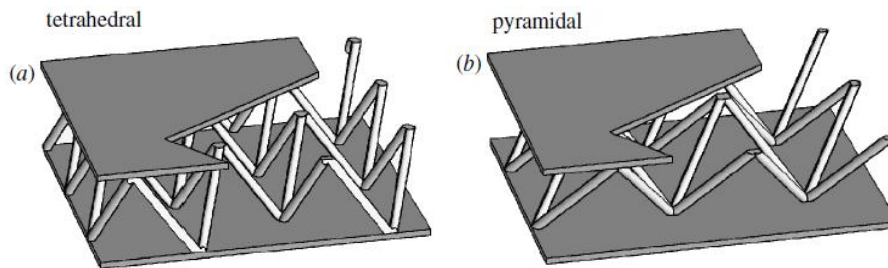

Fig.3: Lattice truss sandwich panel structures. (a) Tetrahedral lattice, (b) Pyramidal lattice

From the broad literature survey it was found that energy absorption is improved when filler material is used as fillers in the tubes rather than using empty tubes. The present investigations conducted on tubes filled with micro studs, filler materials with periodic structures. These materials are used in crash box of automobiles, aerospace and railway systems.

II.   MATERIALS AND METHODOLOGY

In order to understand the crash worthiness of structures, the crushing behaviour tests were conducted using the Universal Testing Machine (UTM). Since the thin walled structures are having stable collapsible behaviour under crushing load, these materials are commonly and widely used as energy absorbing structures.

Table: 1 Chemical Composition of Aluminium 6063

	Mg	Si	Fe	Cr	Cu	Ti	Mn	Zn	traces	Al
Element %	0.80	0.54	0.25	0.08	0.08	0.05	0.05	0.05	0.05	98.05

The specimens were prepared for a size of 50 mm x 50 mm x 100 mm with wall thickness of 3 mm. all the specimens were prepared and tests were conducted as per the ASTM – D - 1621 – 16 test standards. The compressive load was applied in a load controlled mode till the specimen takes maximum load. Load displacement were recorded.

III.   TESTING OF TUBES

The empty tubes and filled tubes were tested along the axial direction under the compression load and the load displacement values were tabulated. The tubes were tested along the axial direction; different stages of crushing for different tubes are shown in Fig. 4 to Fig. 9. In this test it was observed that, when the crushing load increases the tubes are folded axially and tube undergoes large plastic deformation, at this stage the energy dissipation will occur. The large plastic strain is concentrated on the corner areas of the tube and on the horizontal folds and other areas the tube will undergo small plastic deformation. The folding behaviour observed for the aluminium empty square tube is in symmetric mode.

Fig. 4. Axial Crushing of Empty Tube at different stages of loading

Fig. 5 Axial Crushing of Tube filled with polyurethane foam at different stages of loading
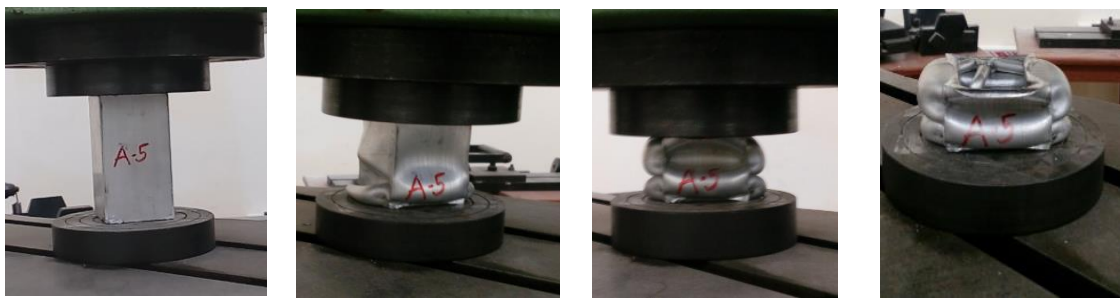

Fig. 6:   Crushing of Tube filled with Tetrahedral Structure

Fig. 7 Crushing of Tube filled with Pyramid Structure

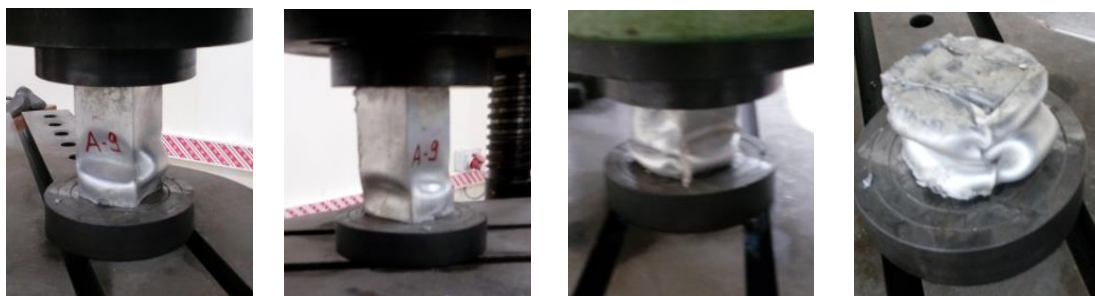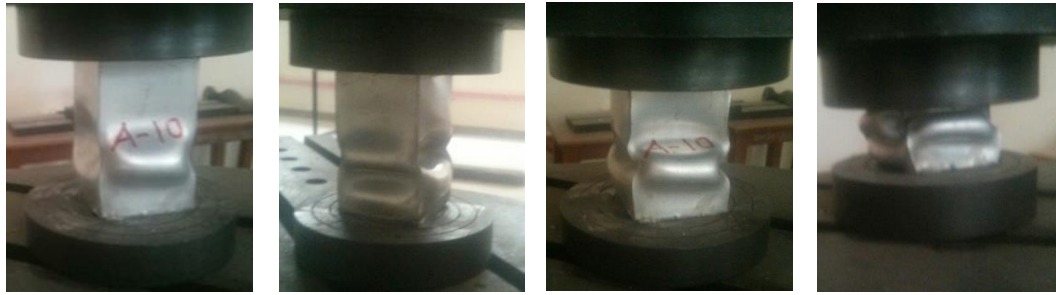**Fig. 8 Tube filled with Tetrahedral Structure and Polyurethane Foam**

Fig. 9 Crushing of Tube filled with Pyramid Structure and Polyurethane foam

IV. RESULTS AND DISCUSSION

The folding behaviour observed for the empty aluminium square tube is in symmetric mode. From Fig. 10 it is observed that an empty has taken a maximum load of 117KN for the first fold, the load bearing capacity increased till the formation of second fold up to a maximum load of 82KN. The third fold has taken a load of 54KN. The load displacement diagram of all the tubes are shown in Fig. 10.

The tube filled with pyramid structure and with polyurethane foam at different stages of loading taken under axial crushing load is 142kN. After reaching maximum crushing load, the first folding starts from the top side and the crushing load starts decreasing.
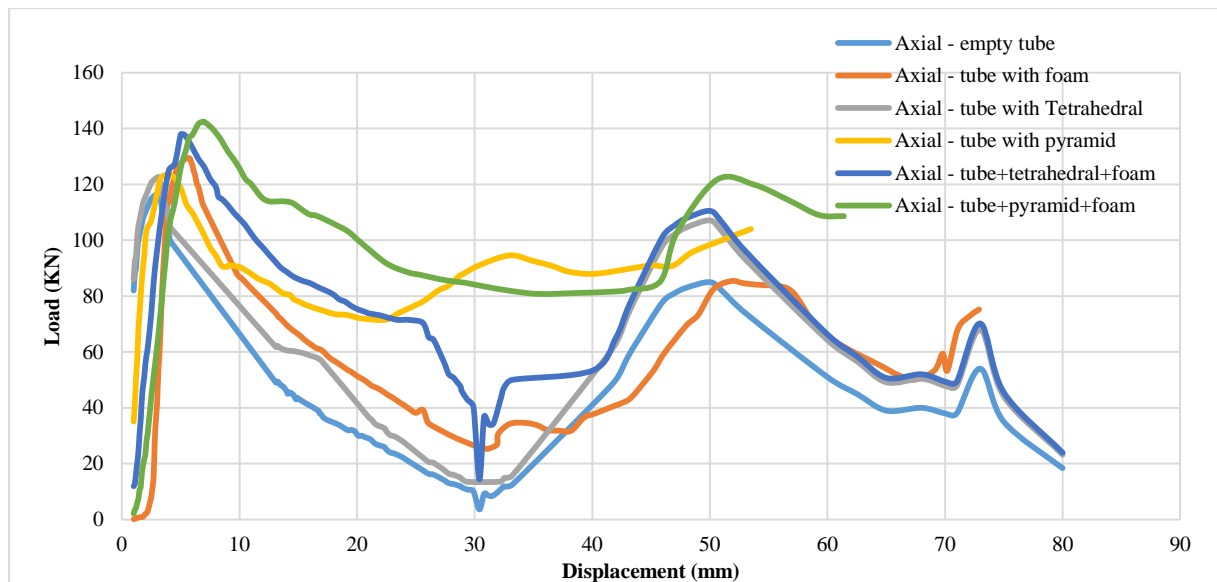

Fig.: 10 Load versus displacement plot for crushing of the empty and filled tubes

From the Fig. 10 the total energy absorption, specific energy absorption and mean crushing force for axial crushing are tabulated in the below Table 2.

Table 2. Results of axial crushing of empty and filled tubes

Specimen	Crushing load (kN)	Deflection (mm)	Energy absorption (J)	Specific energy absorption (J)	Mean crushing force (kN)
Aluminum empty tube	117	3.1	3812	226	1229
With foam	130	5.6	4253	225	759
Tube With tetrahedral	121	3.1	4687	224	1511
Tube With pyramid	123	4.0	4682	218	1170
Tube With tetrahedral & Foam	138	5.2	5727	249	1101
Tube With pyramid & Foam	142	6.9	5993	255	868

From the investigations it was found that aluminium tubes filled with foam has taken a maximum crushing load of 130 KN with a maximum deflection of 5.6mm when compared with pyramid structures and empty tubes. The load bearing capacity has been further increased to 138 KN when tubes filled with foam and tetrahedral structures in tubes. Also with pyramid structures it is further increased to 142 KN. Shown in table 2. Correspondingly energy absorption capacity and deflection of the tubes increased in all the tubes.

V. CONCLUSION

From the investigation it was found that the energy absorption under the axial loading is improved by 3% in foam filled tubes, 33% with tetrahedral structure, 35% with pyramid structure, 85% with foam & tetrahedral structure and 150% with foam & pyramid structure when compared with empty tubes.

From the above investigation it is concluded that the tube having pyramid structure filled with foam showed higher energy absorbing capacity.

VI. ACKNOWLEDGMENT

REFERENCES

1. G. Lu, T.X. Yu, Energy Absorption of Structures and Materials, Woodhead Publishing,Cambridge, UK, 2003.
2. A.A. Singace, H. Elsobky, T.Y. Reddy, On the eccentricity factor in the progressive crushing of tubes, Int. J. Solids Struct. 32 (1995) 3589–3602.
3. A.G. Pugsley, On the crumpling of thin tubular struts, Q. J. Mech. Appl. Math. 32 (1979) 1–7.
4. A. Pugsley, The large-scale crumpling of thin cylindrical columns, Q. J. Mech. Appl. Math. 13 (1960) 1–9.
5. A.A. Singace, Axial crushing analysis of tubes deforming in the multi-lobe mode, Int. J. Mech. Sci.41 (1999) 865–890.
6. K.R.F. Andrews, G.L. England, E. Ghani, Classification of the axial collapse of cylindrical tubesunder quasi-static loading, Int. J. Mech. Sci. 25 (1983) 687–696.
7. S.R. Guillow, G. Lu, R.H. Grzebieta, Quasi-static axial compression of thin-walled circular aluminium tubes, Int. J. Mech. Sci. 43 (2001) 2103–2123.
8. W. Abramowicz, N. Jones, Dynamic axial crushing of square tubes, Int. J. Impact Eng. 2 (1984) 179–208.
9. W. Abramowicz, N. Jones, Dynamic progressive buckling of circular and square tubes, Int. J. Impact Eng. 4 (1986) 243–270
10. A.A. Singace, H. El-Sobky, Behaviour of axially crushed corrugated tubes, Int. J. Mech. Sci. 39 (1997) 249–268.
11. Chih-Cheng Yang, "Dynamic Progressive Buckling of Square Tube" The 27th Conference on Theoretical and Applied Mechanics, Tian, Taiwan, R.O.C., 12-13(2003)
12. Haydn N. G. Wadley "Multifunctional periodic cellular metals", Phil. Trans. R. Soc. A (2006) 364, 31–68 Doi:10.1098/Rsta.2005.1697
13. W. Abramowicz "Thin Walled Structures as Impact Energy Absorbers", Thin Walled Structure, Vol-41(2003) 91-107.
14. Rafea Dakhil Hussein, "Crushing Response of Square Aluminium Tube Filled with PolyurethaneFoam and Aluminium Honeycomb", Thin Walled Structures, Vol-110(2017) 140-154.

DESIGN AND IMPLEMENTATION OF SOLAR BASED SMART MOBILE CHARGING SYSTEM

PRATHIBA N[1], RAGHUNANDAN G. H[2], VINUTHA B[3] & KEERTHI KUMAR N[4]

[1,2]Department of Electronics and Telecommunication Engineering, Bengaluru, India

[3]Departmentof Electronics and Communication Engineering, Bengaluru, India

[4]Department of Mechanical Engineering, BMS Institute of Technology and Management, Bengaluru, India

ABSTRACT

In the current trends of society, cell phones have emerged as the smost demand communication source. The necessity to provide charging service to the public is very much required in day today life, the reason that most of the people moving out from the place they stay are likely to leave their charger maybe at their residing place or in lodges and so on. The paper here presents a system based on coin insertion for cell phone charging and is designed using solar tracking. This can be of use in rendering service to exurban regions that often lacks in grid power. The proposed system enables charging the battery by harnessing the energy from the sun which can be used anytime without the need of any electricity. The user has to insert a coin in the insertion slot of the coin sensor and just connect the cell phone to the input port which initiates the battery charging. This ensures the required charge to switch on the mobile from off state but not to the fullest charged state. This is quite helpful that at least minimum charging has been done of cell phone battery so that some important calls or any emergency calls can be made use of with the mobile. The greatest advantage is that it is one- time funding since the coin sensor will receive back the coin. The system design is based on Node MCU which performs the countdown timings for duration of 1 minute and LCD display is used to show the leftover time.

KEYWORDS: Mobile Charging, Solar Based, Solar Panel & Coin Sensors

Original Article

1. INTRODUCTION

Movements from one place to another with cell phones have emerged as a very essential mode of communication across the whole global area world. The cell phone plays a key role in connecting people no matter in which country they stay. It is a casual tendency among certain people who fail to remember where they left mobile charger maybe like at home or in their work place. This leads to the thinking of the other way to find charging. One way is the proposed coin based cell phone charging system which helps charging the cell phones that can be placed in public places where a coin is made use of similar to STD booth.

These days, frequent charging of phone is essential as maximum usage of it takes place. Different forms of battery chargers are available in the market like simple, solar chargers timer based, battery charger-analyzers which are universal, pulse, fast, inductive, intelligent, USB and motion powered chargers. The aforesaid chargers are application oriented that differ from application to application like battery charger for vehicles, cell phone charger, battery chargers used for electric vehicle and charge stations. The usage of energy sources of various kinds are utmost spread widely across the global area in the world. The sun is also a very good natural source of divergent energies of which the light energy is valued to be highly incredible.

The electrical energy is obtained from light energy conversion using Solar panel. By orienting the panel in line with the sun, efficiency can be maximized. This paper proposes designing a system for tracking the sunlight which provides a genuine and modest method of positioning the panel of solar towards the sun. In these modern times, there have been lots of emerging progresses rapidly in technologies that are being developed for charging the cell phones. In most of the cases, energy from the sun is used for charging the cell phones. Sun's energy converts light energy into direct current and hence this can be used for charging the mobile phones. The chosen solar panel is of fixed size 635x550x38mm, 37WP.The maximum amperes made use of are 2.0 amps to charge the mobile phones. The sensor for tracking sunlight is mounted. The result of this device is used to compare outputs of all for equalization. If they are all equal, then the structure of the collector is almost vertical to the sun. This indicates that the error in tracking is minimized. According to the renewable energy, sunlight is the main source of one of the renewable energy sources and called as solar energy. This energy generation is sufficiently very high because the solar panel will be positioned vertically to the rays of the sun. In addition, an IoT is also used so that the mobile phone can be charged successfully. In this framework, it keeps track of the light energy as well as power of the battery when the coin is inserted into the slot of coin box. The moment the coin gets detected, it sends signals to the Raspberry pi by which the relay gets triggered and the LCD displays the countdown time. The Thing Speak which acts as an open source of Internet of Things can collaborate with the outside world for tracking the location, data storing and retrieving and so on. The voltage obtained from a relay is fed as input to the cell phones.

2. EXISTING SYSTEMS

The challenges of the implementation of mobile charging systems are of great importance. There are many similar proposed systems which are not implemented anywhere in the India. Mobile charging systems based on inserting a coin was reviewed. G.Priyanka et al[1] have proposed the work on Coin Based Mobile Charger this system. On coin insertion, the slot that accepts it detects for the validation of the coin. For every per capita, the availability of the power is solely for a restricted period. The time is calculated using arduino in response to the insertion of number of coins count. As the panel size of the solar is being fixed 635x550x38mm, 37WP is made use of for charging the mobile phones with the greatest value being 2.0 amps. The system is centered on the Atmega 328.

The authors R.J.Sapkal et al[2], have proposed the work which use Coin Detection and Solar Panel for Automatic Gadget Charger. The mobile battery charger begins to charge in response to a mobile being connected to it the moment it detects coin insertion in the slot of the coin insertion being the initial stage. The size and coin type is sensed and displayed on the LCD .This indicates the user if the coin inserted is of the desired type and size. If the right choice of the coin is not satisfied then the coin will be sent back to the refund box. The coin of the right choice is accepted into the battery charging unit. This readily starts charging the mobile battery for an allotted time which in turn is under the control of the microcontroller software used. The microcontroller board is Arduino328 that is based on the ATmega328. Aditya Kamat et al [3], have proposed the work on the system involves a digital locker based system consisting of charging slots the users have to select the duration of charging their phone. They need to use the coin insertion system for paying the charges as well. Then the user needs to create a password for the locker which will provide security to the slot. The user can keep his mobile in charging slot to charge and the slot will get locked so that no one other than the user can open it. An Arduino UNO a microcontroller board based on the ATmega328P. Is programmed for all the controlling applications including the password protection and locking system.

Authors Aparna D. Pawar et al[4] have proposed the work on coin based solar mobile charger. Once any coin is inserted in to the slot, it is compared with a reference image coin already stored as data for comparison. Image processing plays a key role for comparing the inserted coin with the image of the coin saved. MATLAB software is made use of for comparing task to be performed. On detection of the correct inserted coin, a message is displayed as "plug the mobile phone". The charging takes place depending on the coin rate. The charging done is approximately 10% for a 1 Re coin inserted. Similarly, for 2Rs, 5Rs, 10 Rs coins and so on, the phone gets charged as per the software specified time. In this proposed system, ARM Microcontroller version 7 TDMI is used as it incorporates high storage capacity. The microcontroller receives power from the battery and makes use of solar energy. Stepper motor is made use of to control the mechanical movement of solar panel. Intensity of LDR present in its architecture system will be changed in accordance with the movement of the sun. The more the sunlight intensity, less is the LDR intensity. The motor rotates with the less LDR intensity indicating that the maximum energy of sunlight is achieved.

The authors S.B. Sridevi et al [5] have proposed the work on mobile charging using coin insertion as well as solar tracking system. This system uses coin for charging the mobile phone. This system also have solar tracking depending on the intensity of the LDR(Light dependent resistor) the solar will track the sunlight. The main design work proposed in this paper is automatic control of the solar panel by positioning it in such a way that it is oriented towards the sun. This is achieved by the mechanical movement control of the solar panel. It is a fact that sun rises in the east and sets in the west. The normal systems when positioned towards the east cannot be oriented towards the direction of the sun on set. This has a disadvantage for the panel of not receiving the required light energy. To overcome this lag, the work was designed using ATMEL 89c51 which is a 40-pin microcontroller to countdown the duration period of 3 minutes. LCD was used to display the actual time leftover. The output of the relay is latched and completing the timing in progress of the timing period. In this paper, Coin based mobile charging system is designed by tracking the solar energy. In fact, the normal solar panel is positioned only in one direction and there is shortage of light energy because of this reason for its proper operation. Hence this paper presents a controller for the solar panel with its power optimization is done to overcome the shortage of sunrays. LDR readings helps in rotating the panel. This leads to the fullest utilization of sunlight to work. By using the LDR, power optimization is also done.

In this paper, the work proposed is to upgrade a very good microcontroller based solar charger. The work carried out makes use of a coin insertion to charge mobile phone. This acting as mobile battery charger provides a distinctive service to the rural areas where there is a lack of grid power for either partially or for the whole day and an origin acting as a source of revenue to the site providers. In any business premises, the mobile battery coin based charging system may be rapidly and easily installed in the available out space.

Several times it may be noticed that the charging goes low where battery sets off while communicating in the halfway of one's conversation especially at awkward times while access to a standard charger is also highly impossible. To overcome this difficulty, a coin-based mobile battery chargers are designed as a solution which maybe satisfactory. The user has to insert a specific coin and then plug the mobile phone into the available adapters. It is observed that the phone will be provided with a micro-pulse for charging. This does not bring a mobile from 'dead' to fully charged state.

3. PROPOSED SYSTEM

The system network comprises of a number of units as shown in figure 1. NodeMCU is used which contains its own Wi-Fi model which can be used to upload and download data from the internet. Here its application is used to control and monitor

the system through cloud. Solar tracking system is implemented to solar panel to maximize the radiation of the Sun to fall the solar panel per unit area per unit time. The tracking system of light energy is developed based on node microcontroller. A minimum number of components is used in this system with the aurdino based circuit. Stepper motors are made use of that enables accurate tracking of the sun. Exploring the available intelligence in the available data table thereafter, it has been manifested that the light energy tracking systems are capable of accumulating maximum energy than a fixed panel system can gather. This leads to high efficiency throughput obtained through this tracker, and so it can be observed that the developed solar energy tracking system is a realistic process of increasing the energy of light that is obtained from the sun. Thus this method proves to be an efficient tracking system for gathering solar energy. The block diagram of the proposed system consists of three human machine interface devices which are LCD, fingerprint sensor and keypad. It also consists of stepper motor(s), DC motor, ARM microcontroller, voltage regulator, GSM module, Relay and a submersible mini-pump.
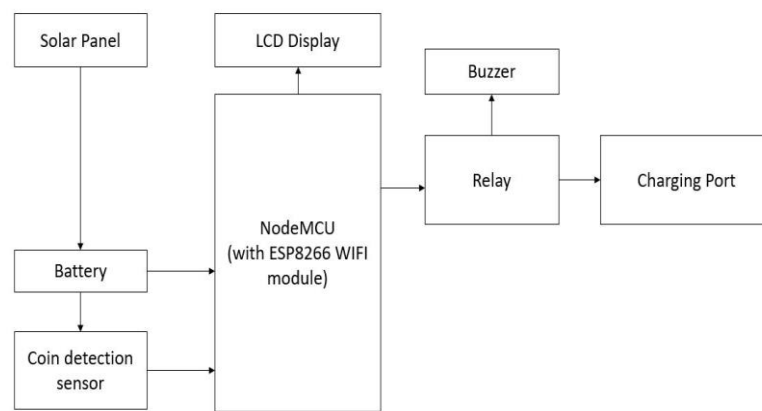

Figure 1: Block Diagram of the Coin Based Mobile Charging System.

The slot of coin insertion is the input stage wherein a coin is inserted. Followed by this, mobile is connected to the mobile battery charger and charging begins. The coin is accepted based on its size and the type. This data will then be exhibited on the LCD panel for the knowledge of user, and so could be helpful for verifying correct coin insertion. If the coin is of a different size and type, then it will be returned back to the refund box. A mechanical slot is fixed along with electrical triggering in coin insertion slot. If the inserted coin is of the desired requirements it transmits a pulse to the control unit permitting the start of charging the mobile battery connected to the device. Then the coin insertion slot accepts the coin into the battery charging unit and start charging the mobile battery for a particular period of time as directed by the software of the microcontroller.

The Controller section acts according to the input signal from the sensor circuit. The diameter of the coin accepted range is approximately 18mm to 29mm. And the thickness of coin accepted ranges from 1.2mm to 3.0mm. Coins outside this range will not be accepted. This further leads to provoking microcontroller accompanying with the LCD interface, displaying the chosen mobile option. And if a specific mobile is chosen for charging then the similar process is activated followed by charging the mobile for a particular period. On completion of the task, the message "Charge complete" is displayed on the LCD panel. Likewise at the same time, more than four different mobiles can be charged with the same procedure. The LCD displays all the information to the customer as and when required. On connecting battery of the mobile a message is displayed as "Insert Coin". When charging begins then the message "Charging" gets displayed on LCD . Finally on completion of charging another message "Charge completed" gets displayed. If it has to be charged

repeatedly, then the coin is supposed to be inserted when the completed message gets displayed. The output has 10 terminals for connecting different types of mobile batteries and for charging mobile batteries of different make 7 of them are connected internally.

The noteworthy aspect of the cell phone battery charger of universal nature is that it draws power from the solar energy during the day time for charging the internal battery of the controller. In case if any power is required additionally, then the power used is the grid power. For supplying 230v, 50Hz, a micro inverter based solar has been designed. This is helpful as both the powers namely grid and the solar are being connected parallelly along with a switch so that it can to switch over from one another as per the requirement. The system flow is as shown in figure 2 below. In the input stage of the insertion slot, on inserting a coin, the mobile phone battery charger begins charging with mobile connected to it.
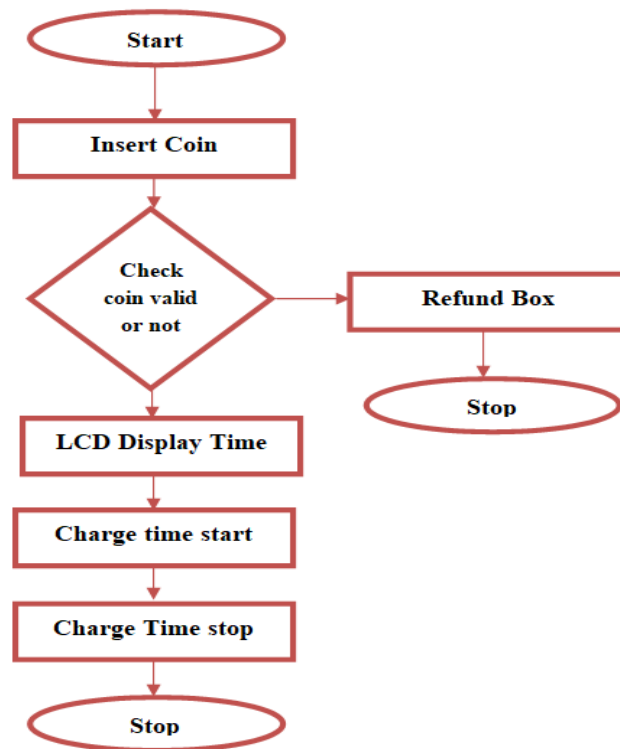
Figure 2: System Flow Chart.

The valid coin to be inserted will be displayed at the LCD panel for the user convenience. This helps the user to insert the correct type and size of the coin into the coin insertion module used which is authenticated for 5 different types of coins to be accepted. If the coin is inserted turns out to be valid, the contiguity sensor recognizes the coin then coin detection system gives out a signal in pulse form to the control unit permitting it to begin charging of the cell phone battery by turning on the relay which acts as switch. The required voltage and current for charging mobile is supplied by a regulator. The panel of the solar is used to harness the light energy. Meanwhile four Light Dependent Resistor's and stepper motor is used to trace the Sunlight to obtain the desired increased efficiency. Circuit Design and PCB layout: In this phase, simulation tools are used for designing the basic circuit which in turn helps to check the overall working of the circuit to be used in the development of smart coin mobile charging system. Many parts were collected with the aid of the simulator tool. Circuit testing was performed on the simulator to ensure proper working. PCB Layout was built granting to the circuit designed, leading to the integration of the hardware components to be set up accordingly. Assembling: In this

phase of system progress, the elements together are assembled as per the designed circuit and Printed Circuit Board layout comparatively shown in the early phases. Testing was performed following the component assembling. Figure 1 shows the block diagram of overall system indicating the functional parts that checks every single correlated components working with one another. Parallel testing was performed for the hardware set up. In Software phase incorporates two intermediate steps as follows: a) Microcontroller programming: The first step in this microcontroller programming involved generating an .asm file of the code assembly which was coded related to the operation and performance of controller. This is followed by burning microcontroller with the accumulated files of this code developed. The second step involved developing a C program that was designed to interact with .asm file code. The interaction of the whole operation is being performed by calling the functions of .asm file through the C program. b) Usage of MATLAB for performing image processing techniques: This involved value of coin detection by picture processing techniques that helped in tracing the size and type. The related techniques were masking, extracting the features, usage of Hough Transformation, matching the related patterns and so on. In correlation with the beginning hardware setup, the detection of value of coins is performed by a range of threshold value matching technique. Coin value calculation: Followed by the development of above mention codes, integration with the hardware setup was performed. Task debugging and compilation of the code developed using microcontroller is performed. On confirmation of error free code, the files compiled are passed on to the controller for its operation. On detection of some coin inside, it allows the coin - holder to move in-front of the camera and the image of the coin is captured. The value of the real time captured image is sent to the MATLAB for calculation. Finally, the power is turned ON by sending an instruction to the controller for a specific defined time duration.

4. IMPLEMENTATION RESULTS

The proposed system was tested and the results obtained are as shown in the following figure 3. The LCD displays the data and time set for the mobile charging system before coin is inserted.
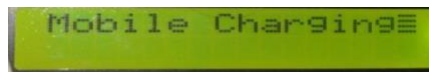

Figure 3: Initial Message on LCD Display.

If the time elapses then the LCD displays the alert message as shown in the figure 4.

Figure 4: LCD Displaying the 'TIME OUT' Message.

Monitoring the output from IoT is presented in the figure below. ThingSpeak used displays the data stating the name of the person, channel ID and status of the access.

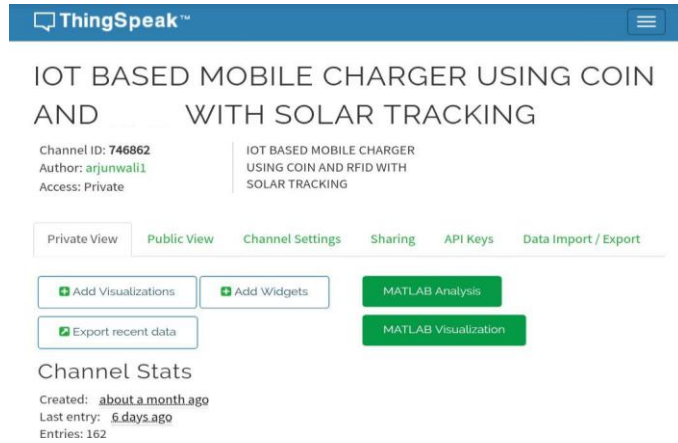**Figure 5: Data Displayed with Name, ID and Access Status.**
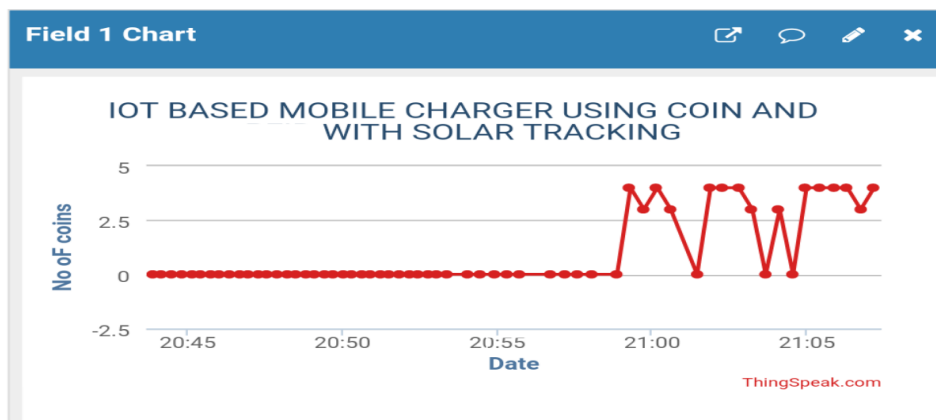

Figure 6: Field Chart of Coins Versus Date.

The graph represents the field chart displaying coins and the date.

The status of the signals is also being monitored and displayed. The two following field chart figures display the current and voltage signal status with respect to time.
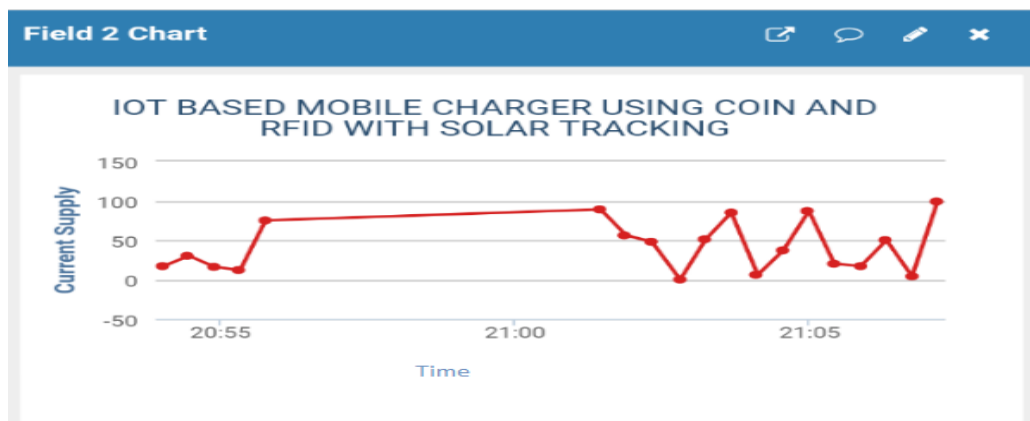

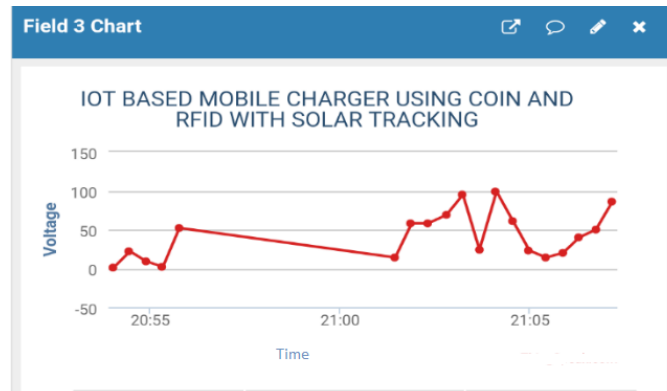**Figure 7: Field Chart of Current Versus Time.**

Figure 8: Field Chart of Voltage Versus Time.

5. FUTURE WORK

The modeled sensor is developed for a specific type of coin. In future, the scope can be extended by enhancing the system with such fabrication that can accept varied types of coins, so that it may be very useful and can be implemented in many public areas. By using digital image processing in coin module, different types of coin can be detected. Project has a scope too for extension as charging of electric vehicle.

6. CONCLUSIONS

In the proposed system, the developed sunlight energy tracking system is based on NodeMCU. The NodeMCU employed circuit is used in the working system with a lowest number of components. To target accurate tracking of the sun the use of enabling stepper motors is performed. After examining the data obtained, conclusion can be drawn stating that the presented solar tracking system is a feasible method of maximizing the energy of light received from the sun.

REFERENCES

1. *G.Priyanka,S. Anisha,P. PadmaShri "Coin based Mobile charger", 2018 International Journal of .Pure and Applied Mathematics, Volume 119 No.12 2018,13695-13701.*

2. *R.J.Sapkal, Snehal .N.Shinde, Madhuri. B.Sathe, Roshani .M.Waghmare "Automatic Gadget Charger using Coin Detection and Solar Panel "(IJESC) May 2017.*

3. *Nguyen, Khuong Vinh, and N. A. M. Nguyen-Quang. "Design and Simulation of a Photovoltaic-Based Energy System for Mobile Device Chargers At Public Place." International Journal of Electrical and Electronics Engineering Research (IJEEER) 5.1, Feb 2015, 111-118*

4. *Aditya Kamat Aniket Kulkarni, Raju Kasturi, Nazahat Balur "Digital locker based system consisting of charging slots," International journal of latest research and applications (IJLERA) ISSN: 2455-7137, May 2015.*

5. *Aparna D. Pawar,"Coin based solar mobile charger" International Journal of Engineering and Technical Research (IJETR) ISSN: 2321-0869, Volume-3, Issue-5, May 2015.*

6. *S.B. Sridevi, A.Sai Suneel "Coin based Mobile Charging using solar tracking" International Journal of Advanced Research in Electronics and Communication Engineering (IJARECE) Volume 2, Issue 9, September 2013.*

7. *Usikalu, M. R., Anuoluwapo H. Shittu, and Leke N. Obafemi. "Construction of an intelligent and efficient light control system." International Journal of Mechanical and Production Engineering Research and Development 8.4 (2018): 1025-1034.*

8. *Kajal S.Bondade, Kirti G. Parate, Prathmesh D. Patle, Shubham S.Verma "RFID Based Mobile Charger By using Solar Panel India,ISSN NO: 2454-1958 Volume 2 : Issue 2 - February 2017.*

9. *Navjeet Kumar, Dorathy R, Shruthi M, Dr. Anusuya S" IOT Based Smart Charger" International Journal of Pure and Applied Mathematics Volume 115 No. 8 2017, 565-570.*

10. *Gaurav V. Chamate, Vishwanath Kommulwar, Jayant V. Wankhade "Coin Based Mobile Charger using Solar tracking system" International Research Journal of Engineering and Technology (IRJET) e-ISSN: 2395-0056 Volume: 04 Issue: 01 Jan -2017.*

11. *Pawar, A. N. J. A. L. I., and S. A. N. D. I. P. Rahane. "Opportunities and challenges of wireless communication technologies for Smart Grid applications." International Journal of Computer Networking, Wireless and Mobile Communications (IJCNWMC) 3.1 (2013): 289-296.*

12. *Prashanth K Sangmesh, Praveen Kumar, Ruchitha.C, Rashmi k "Unsecured Coin Based Cell Phone Charger with RFID "(IJSEM) Vol2 Issue 11, November 2017.*

13. *Rishabh Srivastava, Satyam Gupt, Shyam Chaudhary "Coin based mobile charging system" Research (IJETR) ISSN: 2321-0869, Volume-3, Issue-5, May 2018.*

i-TRASHER- SMART WASTE MANAGEMENT SYSTEM

RAGHUNANDAN. G H[1], KEERTHI KUMAR. N[2], KARUNYA SANKAR[3] & RUSHANK PRABHUDESAI[4]

[1,3,4]Department of Electronics and Telecommunication Engineering, BMS Institute of Technology and Management,

Bengaluru, India

[2]Department of Mechanical Engineering, BMS Institute of Technology and Management, Bengaluru, India

ABSTRACT

All day to day activities required to manage waste from the time to time. It should be safely disposed is collectively called waste management. Waste management is a crisis growing in terms with environmental pollution which is a major public health issue. Waste management System will serve as a solution for this rising issue. This system plays a very vital role in the development of smart waste management system. Most of the waste collected is not treated and as a result harmful-gases are released. This proposed system in this paper serves the purpose to convert these waste materials into useful product. The waste is treated from the time of its inception making it friendlier to the environment. It reduces the spread of infections and bugs which may contaminate the environment when waste is left open. The proposed system i-Trasher is faster and eco-friendly in converting waste to compost. The compost generated can be used in gardens, agriculture and farming. The compost has many benefits for the soil making it a conditioner, a fertiliser and a natural pesticide for the soil. The main aim of i-Trasher is to produce pure and utilisable compost in an efficient manner and faster rate. Our proposed system not only deals with the organic waste, it also deals with the plastic waste which is non-biodegradable. The proposed system demonstrates its capability of effectiveness and rapid processing, and also its smartness.

KEYWORDS: Waste Management, Compost, Smart recycling, Organic, Plastic

Original Article

INTRODUCTION

The disposal of garbage, sewage, and other waste products, transportation and collection of it in simple terms is known as waste management. Treating of solid and liquid waste is also a part of this process. There are multiple solutions for recyclable items which cannot be categorised as trash. The whole idea of waste management is narrowed down to reusing the waste products as valuable resources. This could be useful for household as well as business purposes. There are many advantages that come with the treating and management of waste in correct manner. The biggest advantage is that a better, clean and disease free atmosphere is created to live in. This can only be experienced when the disposal and treatment of the waste is done in the right manner. Reduction is pollution is the second advantage. Impact from Harmful gases such as carbon di oxide, methane, carbon monoxide can be reduced by managing waste in the right way which does not eliminate the unwanted products. Speaking about its role in the conservation of energy, this can be seen the process of recycling paper. Recycling paper helps in the reduction of cutting down trees while it also helps in the reduction of carbon footprints. It helps in the development and generation of employment for people in a large scale. This in turn leads to more people adapting eco-friendly practices. The two major factors that contribute to waste generation are growth in population and industrialisation which has created a major concern of waste disposal for several decades. Though there is some advancement being made in waste disposal methods they aren't adequate enough. Looking as some of the methods we have:

Reduction & Preventive Measures of Waste Generation

The main cause of waste formation know so far is the extensive use of unnecessary products and constant buying of new products. The rapid growth in population has also added excessive generation of waste. To control the growth of waste judiciously a conscious decision has to be taken to use all the existing products efficiently at personal and professional level.

Recycling

Recycling means changing or transforming wastes into new products of similar kind by processing it industrially. Some of the recyclable products are glass, paper, aluminium and plastics. The reuse of wastes rather than disposal is environmentally friendly but also economical.

Incineration

The process of transforming waste products to their base components by combustion is known as incineration. Energy is derived by trapping the generated heat. Some of the by-products of incineration are assorted gases and inert ash. Varied degrees of pollution are caused depending on how the incinerator is designed and nature of the combusted waste. This method can be used for getting rid of hazardous and toxic wastes.

Composting

The process of decomposing of organic waste using microbes by keeping it accumulated in a lit for a very long time is known as composting. This compost is rich in nutrients and can be used as fertilisers for plants. This is a very slow process and a significant area of land is also consumed. The fertility of the soil can be improved by reprocessing it biologically.

Sanitary Landfill

The dumping of waste in a landfill is what is done in this method. To avoid contamination of the ground water by chemical substances a protective lining is lauded in between the waste and the ground water which acts as a barrier. This protective lining is also known as the base. To reduce odour from the waste the waste layers are coated with sand. The vulnerability of toxic chemical being leaked accidentally is avoided by the soil. Places with low ground water level and far from sources which can cause floods are suitable for a landfill.

Disponal in Ocean/Sea

Generally this method is used only for radioactive active elements. The waste is generally dumped in faraway oceans very far from human habitats. This could be a threat to aquatic habitats which is the reason why it is being challenged by environmentalists.

Plasma Gasification

The method of waste disposal to recycle municipal solid waste in landfills to sources of energy is known as plasma gasification. Syngas is prepared by converting the carbon-based materials, exposing them to high temperatures. Though there are several methods to dispose wastes as a mass quantity, the control in the pollution and littering can only be got by the small scale and early disposal stages. This is nothing but the disposal at every house in an individual level. The mass disposal methods mentioned above are done only after the wastes from houses are picked up. If processing of the disposed wastes is done at the early stage itself, there will be reduction in the chaos a pollution caused. Making use of the products

obtained by this processing can also cut the cost of buying new products and can also be used for profit. According to recent statistical reports, Organic, paper and plastic wastes are the most disposed and hence i-Trasher specifically on the major part of the disposed waste. According to the statistics, 43% of the wastes disposed comes under the category of organic wastes, 26% under paper and 13% under paper.
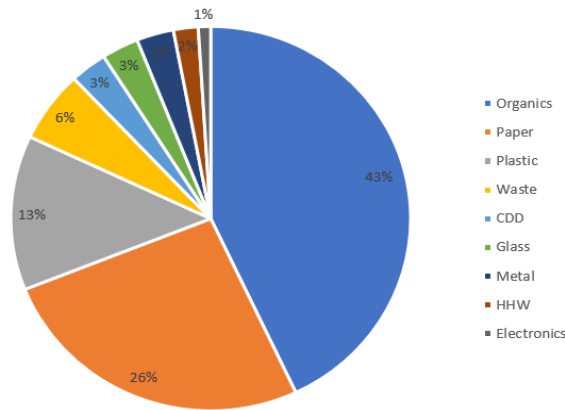

Figure 1: Types of Wastes Disposed.

Another statistical report (Fig.2) shows that 44% of wastes produced are food and green which are again under the category of organic wastes 17% paper and cardboard wastes and 12% plastic wastes. Through both the reports it can be concluded that i-Trashes focus on the major parts of the wastes produced.
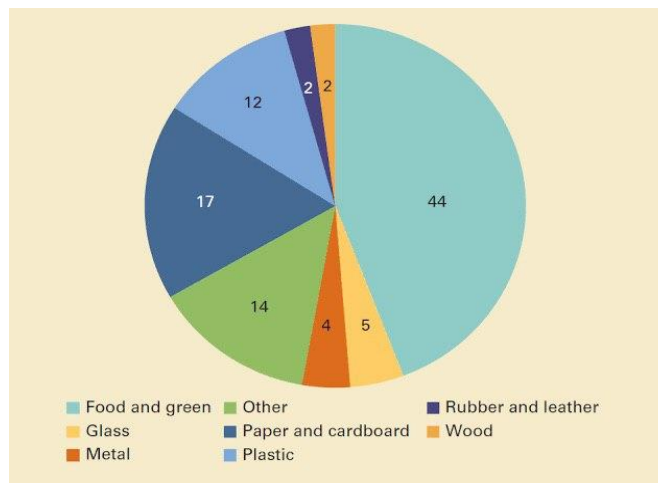

Figure 2: Category of Wastes Disposed.

Next set of report speaks about the origin of wastes (shown in Fig.3). Majority of the wastes, i.e. about 43% of the wastes is domestic household wastes, 15% is from the hotels and restaurants. The target audience of i-Trasher is the same set of categories along commercial establishments which is 8% of the production source.
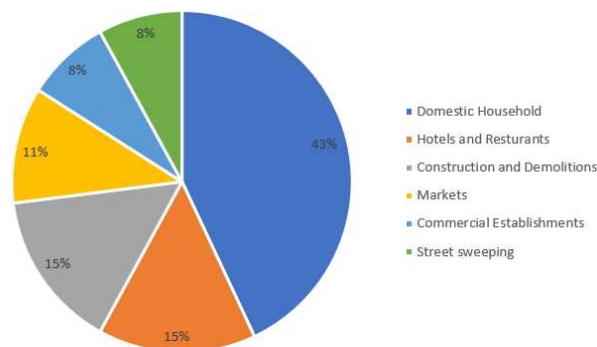
Figure 3: Source of Disposed Waste.

The next section will speak about the various existing waste management systems along with their specific roles in bring out development in the field of waste management. Every system has its own contribution to bring improvements in the existing systems.

EXISTING SYSTEMS

System [1] states that the main focus of this system is on the concept of connection of all bins to a common network to control and overview the trash bins present in the city making it helpful. The main aim of this system is to avoid overflow of waste and to help the workers in cleaning the bins. The idea of automation is being implemented for waste management all over the city using the i-bins. Technologies such as raspberry pi, IR/ultrasonic sensors and weight sensors have been used. The system only focuses on the overflow which is only one part of the growing crises. In [2] spilling out of waste from bins by over flooding brings about contamination to the public places. Infections are increased due to the breeding of huge amounts of bugs on them. The main aim of this system is to monitor the level of waste and disposal of waste automatically. This task of the system comes into action only after the disposal of wastes in the correct manner. In [3] it is stated that the main aim of this system is to detect the overflow of waste using wireless networks (WSN) and IoT. Sensors are deployed in the bins and WSN is used for networking them together. Data for every determined interval is collected using the sensors which are deployed. A request is raised to the garbage collector agent once the threshold is reached. All the filled vehicles are collected by the agent once requested using IoT framework. The functioning of this system is similar to the [2] but with a different technological approach. With [4] the research and development of a home composter specially designed for household is shown in this system. The organic kitchen and food waste can be utilised, disposed and managed at the source of waste generation. Easy usage and easy user interface have been ensured. The output compost is ready to use for the application of plants. Hence the kitchen waste bin is effectively replaced by the home composter. The system [5] introducing a practical solution to recycle the food waste instead of throwing them into the landfill. An eco-friendly machine is designed to convert food waste into fertilizer. The process is completely automated, it works under certain environmental conditions (i.e. temperature, humidity) to fasten the process. This can be a drawback as the environmental conditions vary a lot. In system [6], aims to convert waste to compost using the composting process. Temperature and humidity are maintained to certain levels in order to start the process. They aim to decrease the wastes dumped in landfills and to provide better quality of compost. Using the self-heating method for compost can be time consuming which can delay the composting process. In [7] have come up with a SMART Composting Machine. The machines can 10 to 15 kg of organic waste into usable compost. But it is not efficient system.
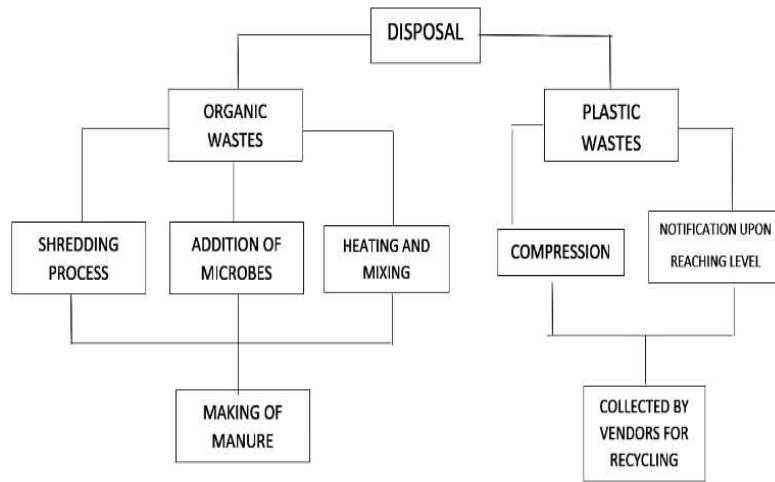
PROPOSED SYSTEM

Figure 4: Working of System.

The waste is first collected in two separate compartments, one for plastic and the other for organic waste. This organic waste is passed through a shredder and is shredded to fine pieces. This waste is simultaneously mixed with the microorganisms while being shredded. The mixture is then heated up to a certain temperature and constantly stirred. It takes 20-24 hours for the waste to get converted into compost. The compost is then drained out of its excess water and then collected in a tray which is removed out of the machine after this process ends. The plastic waste collected in the first compartment is compressed with the help of a piston which can be removed as the compressed plastic reaches a certain level which in turn would send a notification to the nearby plastic dealers to collect the plastic. These two processes in both the compartments take place simultaneously making this machine very efficient and smarter than the existing technologies.

IMPLEMENTATION

The design of i-Trasher consists of two compartments, the compartment at the top is for the plastic wastes and the compartment at the bottom is for organic wastes. There are two outputs on each side to collect the respective wastes after processing (shown in Fig.5).
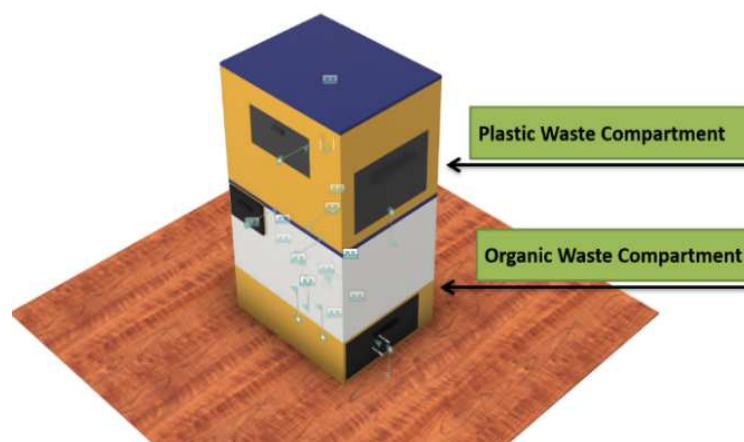
Figure 5: Outer Design with Compartments.

The plastic waste compartment is fixed with a piston for compression. The piston is attached with protruding needle-like structures which will help in removing the air from the plastic wastes.
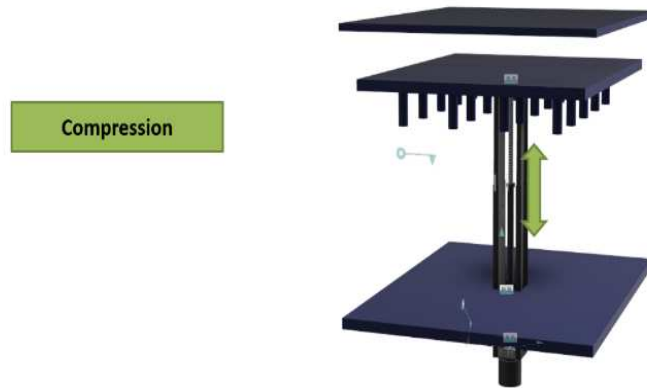
Figure 6: Plastic Waste Compression.

Once the waste are compressed and reaches a certain level, a notification will be sent for the plastic wastes to be collected.
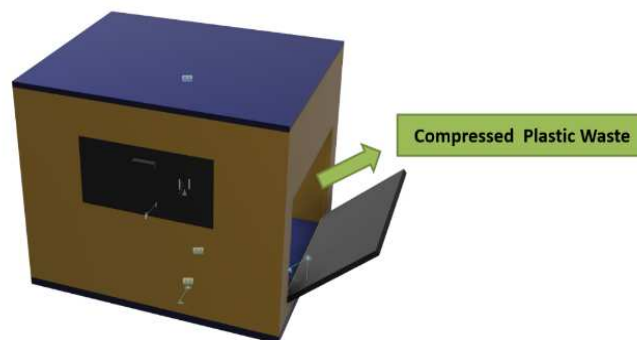
Figure 7: Plastic Waste Outlet.

The organic compartment is provided with an input and output port. A shredder has been installed to cut down the wastes into tiny particles which speeds up the process of conversion. We have a heater as well as microbes which help in the compost making process.
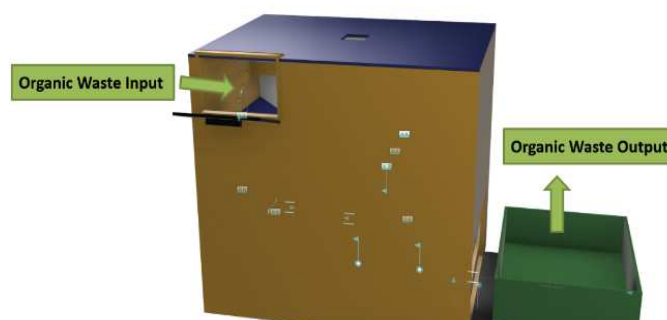
Figure 8: Organic Waste Compartment.

Once the compost is ready, they are transferred into the tray which can be opened as an outlet in order to access the converted compost.

Figure 9: Organic Waste Process and Outlet.

RESULTS AND EVALUATION

Waste management is very crucial in the present days. Recycling the materials is as important as disposing them in the correct manner. i-Trasher focuses on the majority part of the waste disposed and it efficiently converts them into useful products. Most importantly, the process starts at the beginning stage of disposal. It works on two categories of wastes simultaneously without any disturbances to their specific processes. It helps in segrega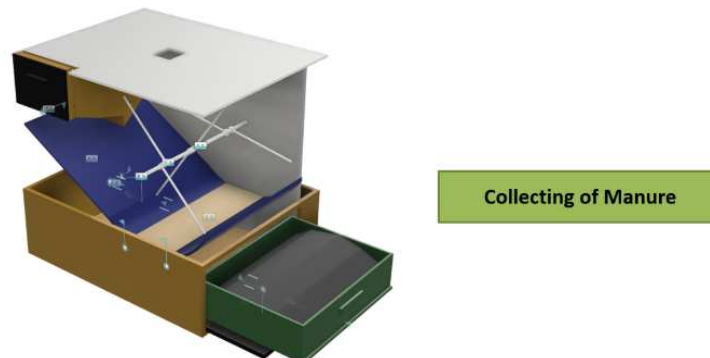tion as well as converting them into a useful set of products which can in turn be a source of profit for the user. i-Trasher is a product that made using smart technologies which makes it unique and easy to operate. It includes segregation, level detection, smart way to notify vendors as well as converting wastes to useful products. The targeted users are the main source of waste disposal. The system is made smart enough by equipping with IoT techniques. The network layer is responsible for transferring the measured information in the perception layer to the upper layers, where the processing systems are located, and uses ZigBee, Z-wire, GSM, UMTS, Wi-Fi, Infrared, 6LoWPAN. In addition to the basic assignments, the network layer also performs the cloud computing process and the data management process. The load sensor is coupled to a specific driver, such as HX711, which amplifies the signal emitted by the load cell in addition to providing interconnection with the microcontroller. The microcontroller based IoT system is used which automatically sends the message to the waste collector along with exact weight of the waste material and location. So this system will manages the waste systematically and waste descipation is also made easy. The farmers will be getting the compost and waste material collectors will be getting it in systematic way. The customer who is using this system will be paid by the farmers and waste material collectors based on the weight of compost and waste materials they receive.

Figure 10: Prototype of System.

CONCLUSIONS

i-Trasher converts the wastes into useful products. This is beneficial to the user because when the waste is recycled, they would not have to be reused to make the same products. The environmental benefits that come from recycling is that less waste which is thrown. This won't cause any harm to the people living in the area. i-Trasher can also help in making money or a source of profit. A waste collection business can also be started is a large amount of waste is being dumped. There will be people who will pay someone for getting their waste collected. The recycled products can be sold to manufacturers or vendors which could be another were of earning or making money. You can also use the converted compost as organic fertilizer. We can sell our compost to companies who make them in large numbers. It can also be used for feeding the soil with nutrients in the farm. i-Trasher starts the processing at early stages. This is an advantage because of the garbage is left for long it starts emitting harmful toxic gases by mixing up with other unwanted waste components. This means that pollution could be caused by the toxic material if the trash is not handled properly in the initial stages and will be harmful to humans and other living things. It will become a public hazard and can cause environmental destruction.

REFERENCES

1. *Krithika. S, Kaja Maideen J, Madan T K C,"An Automated Trash Monitoring System for Waste Management Using IoT– (I-Bin)", International Journal of Engineering and Advanced Technology (IJEAT), Volume-8, Issue-63, September 2019*

2. *S.Sreejith, R.Ramya, R.Roja, A.Sanjay Kumar, 2019 Smart Bin for Waste Management System, 2019 5th International Conference on Advanced Computing & Communication Systems (ICACCS),May 2019*

3. *Sivasankari, Bhanu Shri and Y.Bevish Jinila, "Smart Waste Management Using WSN and IoT", 2017 International Conference on Innovations in Information, Embedded and Communication Systems (ICIIECS 2017), March 2017.*

4. *Farooqi, Awais. "A Green Strategy towards the Miscibility Studies of Styrofoam in Organic and Inorganic Solvents by Using Materials Modelling and Simulation Method." Journal of General Engineering and Technology (JGET) 1 (2016): 11-18.*

5. *Nithika Sailesh, Vikas Shinde, Home composter: Domestic use composter,2015 World Congress on Sustainable Technologies (WCST) May 2015.*

6. *Gaurav Chiplunkar and Prof. (Dr.) Avinash More, Design of Kitchen Waste Composting Machine. International Journal of Trend in Research and Development, Volume 5(3),May – Jun 2018.*

7. *Asif, Muhammad Salman. "An Appraisal of Issues Faced by Manufacturing Companies, When Selecting an Enterprise Resource Planning (ERP) System." International Journal of Business and General Management (2018): 1-8.*

8. *Shada Bennbaia, Aseel Wazwaz, Alaa Abujarbou. Towards Sustainable Society: Design of Food Waste Recycling Machine Proceedings of the International Conference on Industrial Engineering and Operations Management Bandung, Indonesia, March 6-8, 2018*

9. *Swapnesh H. Bhaisare , Dr.Pramod Walke , Dr. D. S. S. Ganguly , V.M. Wankar. The Organic Compost Machine and Factors Effecting Performance of composting. International Journal of Engineering Science and Computing, December 2017.*

10. *Nurdin, Ismail. "Analysis and Utilization of Space as a City Area through Government Policy: Study in Solok District, Indonesia." International Journal of Humanities and Social Sciences (IJHSS) 8.5 (2019): 7-16.*

11. *Mohammed Adnan, Mohammed Elnour, Omer Mohammed Tawfeeq, Mohammed Awad. Waste Management System Using IoT. International Conference on Computer, Control, Electrical, and Electronics Engineering (ICCCEEE). IEEE. June 2018*

12. *Ravi Kishore Kodali, Venkata Sundeep Kumar Gorantla. Smart solid waste management. 3rd International Conference on Applied and Theoretical Computing and Communication Technology (iCATccT). IEEE. July 2017*

13. *Gopal Krishna Shyam, Sunilkumar S Manvi, Priyanka Bharti. Smart waste management using Internet-of-Things (IoT). 2nd International Conference on Computing and Communications Technologies (ICCCT). IEEE. March 2017*

14. *Amusan, L. M., et al. "Information on State of Challenges of Waste Management System in Nigeria Urban Housing System." International Journal of Mechanical and Production Engineering Research and Development 8.2 (2018): 75-86.*

15. *K N Fallavi, V Ravi Kumar, B M Chaithra. Smart waste management using Internet of Things: A survey. International Conference on I-SMAC (IoT in Social, Mobile, Analytics and Cloud) (I-SMAC). IEEE. June 2017.*

16. *Priyanka Shrivastava, Shivangi Mishra, S.K.Katiyar. A Review of Solid Waste Management Techniques Using GIS and Other Technologies. International Conference on Computational Intelligence and Communication Networks (CICN). IEEE. May 2015*

17. *Shubham Thakker, R Narayanamoorthi. Smart and wireless waste management. International Conference on Innovations in Information, Embedded and Communication Systems (ICIIECS). IEEE. October 2015*

18. *Fachmin Folianto, Yong Sheng Low, Wai Leong Yeow. Smartbin: Smart waste management system. IEEE Tenth International Conference on Intelligent Sensors, Sensor Networks and Information Processing (ISSNIP). IEEE. June 2015*

ADVANCED DECISION SUPPORT SYSTEM FOR PRECISION AGRICULTURE USING WSN

RAGHUNANDAN. G.H[1], VINUTHA. B[2], PRATHIBA. N[3] & KEERTHI KUMAR. N[4]

[1,3]Department of Electronics and Telecommunication Engineering, BMS Institute of Technology and Management, India

[2]Department of Electronics and Communication Engineering, BMS Institute of Technology and Management, India

[4]Department of Mechanical Engineering, BMS Institute of Technology and Management, India

ABSTRACT

Due to increased population food needs are increased which has leads to various agriculture techniques. Agriculture is a major economic sector for developing countries like India which plays a key role in economic development of the country. India ranks second worldwide in agriculture output. Digital agriculture or precision agriculture is an abstraction where the farmer will be able to access the parameters related to his farm and control them manually or automatically. The wireless sensor networks play a major role in achieving the need which involves computation, sensors for sensing and communication capabilities using wireless techniques. This proposed technology will improve the crop yield and maintain quality. In this paper, we have used various sensors in garden area. The collection of data from various sensors, decision making and relevant tasks are carried out based on the intelligence of the control system. This implementation of wireless sensor network technologies is also helpful for faraway surveillance in the various applications of the agriculture field.

KEYWORDS: GSM, Sensors.WSN, Agriculture, Precision

Original Article

INTRODUCTION

In the growth of Indian economy agriculture plays an important role in the predictable future. The 28 percent of GDP of our country is through agriculture and it plays an important role in giving employment. To have higher cropping patterns advanced technologies are needed in the place of traditional Indian agriculture techniques. Indian agriculture is having great diversity in needs, opportunities and futuristic approach. The growth of agriculture sector requires more sophisticated, rapid techniques which gives more yields less loss to farmers. These scope or challenges has lead to research in the field of precision techniques of agriculture. We prefer a sensor network which uses low cost components and required software.

The wireless sensor network is used in sensing various parameters related to agriculture productivity etc. The sensors works on the basic principle of Transducers. This information is communicated with the farmer by means of GSM technology, Zigbee, RF technologies etc. The data which is obtained from WSN will be stored in the database in central base station so that an individual can access the data from a web browser also. Due to the technological advancements, powerful sensor with low power utilization can be obtained. Sensor nodes are basic components necessary for the operation which comprise of computing, sensing and wireless communication unit. WSN interfaces with the network. In sensor networks, scattered control is used because in centralized control, if the central architecture fails the entire network will disintegrate. In this paper, Section II discusses about existing works, section III explains about new system proposed, section IV describes about implementation, section V is

about future works and conclusion is done section VI.

EXISTING WORKS

Research works related to precision agriculture is quite large in number. Some of the works of precision agriculture are discussed in this section. Precision farming solution [1] this research work provides the scope for analysing the applications of the soil sensor in precision agriculture. The motto of this research work is to estimate the fluidity or moist content of the soil. Since moisture of the soil required for variety of crops is different and it can be determined with the soil sensors. In paper [3] has documentation variety of sensors are used and working of each sensor is processed by wireless network. The data collected by each sensor is preserved by the sensor module which notes the working of the sensors the sensor module looks after the further exchange of preserved information intermediate to receiver and transmitter.

In system [4] the outcome of this work is to make out the operation of WSN to monitor the agriculture parameters. The System [5] the insight of this project is to appeal WSN for precision agriculture. IoT in precision agriculture applications using wireless moisture sensor network [6] in this paper we can go through the applications of WSN and WMSN in monitoring the moisture sensors. Many systems which are existing or developed are unique for a particular type of farm fields, crops and plantations. In growing countries where the farmers are having tiny piece of land may not be able to afford costly systems which are specific to a particular food grains. As they may be having multiple crop cultivation at same time. In this regard there is a high need to develop a system which is going to be cost effective and suitable for majority of applications related to farming.

PROPOSED SYSTEM

The system network comprises of a number of sensor nodes as shown in Fig.1. Each sensor node consists of a sensor unit, and a transmitter unit. Then, there is a receiver unit that receives information (the location of the node, status of the particular part of the field i.e. soil moisture content, temperature and humidity etc. from the sensor unit in the node) from the sensor node, processes it, makes decision to whether to irrigate or not to irrigate the field and notifies the farmer to take required action. In the sensing unit, there are four sensors (the soil moisture sensor, temperature and humidity sensor, sensor for rain detection and fire sensor) which sense the respective factors and the sensor values obtained are given to the transmitting unit. The transmitting unit takes the information from the sensing unit and through the RF module, sends it to the receiving unit. The receiving unit collects the information sent by the transmitting unit of the sensor node. The data received, is then processed and sent to the farmer (mobile phone) which happens through GSM. The farmer will thereby be notified about the respective node area and given options to turn ON/OFF the motor.
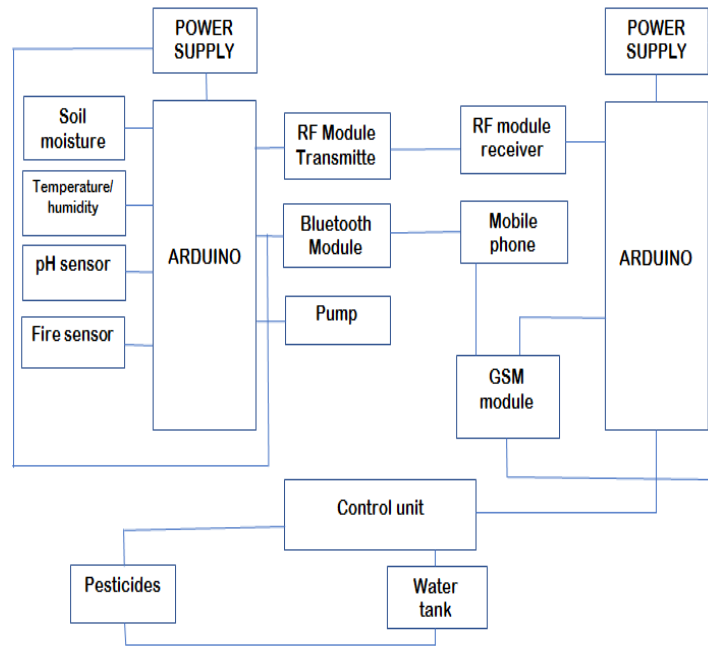
Figure 1: Concept of the New System.

The farmer now has to give the necessary command to the system. But if he fails to do so, the system gives a small amount of delay and does the task by itself. This makes the system more efficient as the farmer will be aware of each and everything happening in his farm even when there is nobody in the field. If the soil moisture level is low, the motor is turned ON and as soon as the soil moisture is retained, the motor is turned OFF. If the pre-set time period is say, 30 minutes, then every 30 minutes, the farmer will be notified about status of his field.

IMPLEMENTATION

The proposed system was implemented in the garden of BMSIT&M campus, Bengaluru. The soil was first examined before implementation of the system. The results obtained as shown in Table.1

Table 1: Test Results of Soil Considered

Organic Matter	2.8%
pH	7.6
Olsen Phosphorus	45 ppm
Bray 1 Phosphorus	40 ppm
Potassium	89 ppm
Sulfur	6 ppm

The ideal pH for grass and cereal soils vary, the optimum pH for grass is 6.3, while for cereals it is 6.5. If the pH value is lower or higher than these values, the supply of macro-nutrients (N, P, K and S) to the plant will be reduced, which will have a negative impact on the yield. As the pH of the soil was observed to be higher than the optimum value, it was neutralized by the usage of required amount of buffer index. Similarly, the concentration of Nitrogen, Phosphorous, and other essential nutrients were also optimized and the soil was made ready for implementation of the designed system. Two controlling units were used, one of which was placed near the field to which all the sensors were connected and the other controller, a little away from the field. The transmitter unit (Fig.2) is connected with an RF transmitter which helps in transmitting the data from one controlling unit to the other. The other controller at the receiver end (Fig.3) which is placed away from the field is connected to an RF receiver which receives the data transmitted from RF transmitter. Soil moisture

sensor, used to give the measure of the moisture content in the soil, is one of the most important sensors which is useful for the irrigation purposes. Based on the soil water content one can know how much to irrigate the field. A rain drop sensor is used to measure the amount of rainfall. A temperature and humidity sensor are used to measure the temperature of the soil and atmospheric humidity which helps the farmer to understand better about the necessities of the crop and decide the quantity of water required for it, type and amount of pesticides to be treated with, and other requirements, for the health of the crop. The temperature and the relative humidity of the surrounding environment majorly contribute to the health of the crop. Relative humidity is obtained by considering actual vapour pressure with respect to saturation vapour pressure expressed as a percentage.

$$RH = 100 \cdot \frac{e}{e_w}$$

(1)

A brief study was conducted with the help of the Professors of University of Agricultural Sciences (GKVK), Bengaluru, regarding the dependency of the occurrence of a disease on the temperature and relative humidity. Based on the inferences made, whenever the temperature and RH combination nears to the favourable condition for a disease, a small dosage of chemical or pesticide is mixed with the sprinkler system using valve control, as precautionary measure. If the favourable conditions sustain for long as shown in the Table.2, higher dose of pesticide is added. Different crops have different set points (temperature, RH factor) for different diseases.

Table 2: Set Points for Different Diseases

Disease	Temperature (^{o}C)	Rh (%)	Duration
Late blight	10-16°C	>90	>100hrs
Early blight	26-29°C	>80	4-5days
Leaf mold in green house tomato	24°C and 26°C	>85	10days
Powdery mildew	20°C to 30°C	>95	5-7days

All these determinations made are monitored in the controller at the transmitter end and are transmitted to the receiver through RF transmitter. The RF receiver connected to second controller, receives the data from the transmitter and sends it to the farmer (mobile) through GSM. Any message sent by the user is also received at the second controller any message from the farmer is also received by the receiver. The LM393 (soil moisture sensor) sensor used to advice the customer to water their plants, determines dielectric permittivity of the neighbouring medium. It works at 5V voltage. In soil, dielectric permittivity is considered to be a function of the water present in the soil. A dielectric permittivity related voltage is produced by the sensor .Based on the water content present in the soil. The average of the water content over the entire length of the sensor is considered for giving the measurements.

Figure 2: Transmitter Section of the Proposed System.

Figure 3 :Receiver Part of the Proposed System.

Figure 4 :Controlled Water Pumping Implementation.

The DHT11 is a temperature and humidity sensor which is used to sense the environment humidity. A humidity sensor and a thermally sensitive temperature sensor is used to find the temperature and humidity collection of the environment under consideration. It uses cost effective and efficient 8 bit microcontroller. It is easy to use but requires proper timing to get the required data. Rain observation is done using rain drop sensor. It determines rainfall intensity. The rain sensor is equipped with rain board and a controller board to sense the rain. Rain drops are collected on a printed circuit board. Lesser the resistance, the lesser the voltage output. Conversely, lesser water, the greater the output voltage on the analogue pin. The RF module, as the name suggests, operates at radio frequency. Radio frequency modules are used which includes transmitter and receiver part which has capability to transmit and receive the data for large distance.

An small sized RF module is used for transmitting radio wave by modulating it to carry the information. Transmitter is usually subject to modulating requirement which commands the maximum acceptable transmitter power output. At the receiver end the RF module has the super-regenerative receivers and super-heterodyne receivers. These Super-regenerative modules are a cost effective and less power consumption component which uses a series of amplifiers in order to separate modulated data from a carrier wave. A GSM modem is a device which can be either a mobile phone or a computer or any other processor communicated over a network using GSM modem. The SIM is inserted to the module to send the relevant SMS. The GSM modem accepts command 'STOP' to evolve an output at the MC when the program is executed. A wireless communication technology that is used to replace the cables connecting electronic devices is Bluetooth technology. RF technology known as 'star topology' is used to control these devices. Bluetooth networks can be built as piconets or scatter nets depending on the number of nodes in the network.

FUTURE WORK

In future the module can be equipped with numerous sensors which are advanced in technology. The system can be annexed with a camera by usage of which, the farmer can also get the visual status of the present situation of the field and its surroundings. Adding different sensors like pH sensor, leaf moisture sensor etc. can yield better results. Also, we can use technologies like Zigbee for wireless data transfer. Insufficient rainfall can be a major issue in agriculture. During rainfall there is no need of watering the farm land using water pumps .sensors helps in detecting rainfall and stop the water pump automatically. This will lead to automation in agriculture field .To overcome this issue, we can use sensors which detect the soil moisture, temperature, fire. This can help farmer in decision making about suitable amount of irrigation water. In future, it can also be foreseen that the farmers are given the basic knowledge of system being implemented, which also adds to efficiency of the yield and ease of practicing precision agriculture techniques for the farmer.

CONCLUSIONS

Precision has a major role in the field of agriculture. Primitive methods of irrigation and other agricultural practices that are still in existence in some parts of the world need to be improved. Proper implementation of advancement in science and modern technology with maximum efficiency both in terms of management and control and also economy, can prove to be of great help in achieving progress in agriculture..WSN has been used in majority of applications related to agriculture due to its flexibility and adaptability. Sensors are very useful in agriculture. We have successfully implemented the wireless sensor network in the field and the information was communicated to the user.

REFERENCES

1. George Eldho, *"A low cost WSN system for precision agriculture"*, Sixth International Symposium on Embedded Computing and System Design, 15-17 Dec. 2016.

2. Ibrahim, Rawidean, Kassim, Ahmad Harun, *"Precision agriculture applications using WSN"*, IEEE Malaysia International Conference on Communications, Nov. 2015.

3. Ibrahim Mohd R ,Mohd Kassim, Ahmad Harun, Ismail Mat Yusoff, *"IoT in Precision Agriculture Applications Using WMSN"*, IEEE Conference on Open Systems ,Oct. 2016

4. Attri, Arnav, Sahil Vashist Shubham, and Gagangeet Singh Aujla. *"An Advance Algorithm for Precision Agriculture Using Wireless Sensor Network."International Journal of Computer Networking, Wireless and Mobile Communications (IJCNWMC) 4.4, Aug 2014, 1-10*

5. Raghunandan. G .H, Akshata, *"Performance Analysis of Different WSN Based Systems in Precision Farming"*, Int. J. Advanced Networking and Applications Volume: 07 Issue: 05 Pages: 2893-2898 , May 05,2016.

6. Raghunandan.G.H. Archana R, Rachana, R Hegde *"Qualitative Analysis of Routing Protocols in WSN"*, IJANA, Volume: 08 Issue: 02 Pages: 3021-3025 (2016), Oct 20,2016.

7. Deshpande, Shripad V., and P. R. Devale. *"Recent trends in using wireless sensor networks in industrial environment."* International Journal of Computer Networking 3.3 (2013).

8. G. H. Raghunandan, S. Y. Namratha, S. Y. Nanditha, G. Swathi, *"Comparative Analysis of different Precision Agriculture Techniques using Wireless Sensor Networks"*, 2017 4th International Conference on Electronics and Communication Systems (ICECS), Feb. 2017.

9. Yousef. M. Hamouda, Basel ,Elhabil, *"Precision agriculture for greenhouses using a WSN"*, 2017 PICIT, May 2017.

10. John V , H Lu, Yeyini, *"Development and testing of a customised low cost UAS based on multispectral and thermal sensing for precision agriculture applications"*, 2017 International Conference UAS, June 2017.

11. Durgabai, R. P. L., and P. Bhargavi. *"Pest Management using Machine Learning Algorithms: A Review."* International Journal of Computer Science Engineering and Information Technology Research (IJCSEITR) 8.1 (2018): 13-22.

12. W Yitong, Yunbo, Xiaoyu, *"Design of Multi-parameter WSN Monitoring System in Precision Agriculture"*, Fourth International Conference on IMCC ,Sept. 2014.

13. Lei Xiao, *"The realization of precision agriculture monitoring system based on WSN"*, 2010 International Conference on Computer and Communication Technologies in Agriculture Engineering, Vol. 3, 12-13 June 2010.

14. Karyakarte, Mandar, Anil Tavildar, and Rajesh Khanna. *"Effect Of Mobility Models On Performance Of Mobile Wireless Sensor Networks."* International Journal of Computer Networking, Wireless and Mobile Communications (IJCNWMC) ISSN: 2250-1568.

15. Tagarakis A., Liakos V, Perlepes L, Fountas S, Gemtos T, *"WSN for precision agriculture"*, 15th Panhellenic Conference on Informatics, Oct. 2011.

16. Raghunandan.G.H, A. Shobha Rani; S. Y. Nanditha; G. Swathi, *"Hierarchical agglomerative clustering-based routing algorithm for overall efficiency of wireless sensor network"*, 2017 International Conference on Intelligent Computing, Instrumentation and Control Technologies (ICICICT), 6-7 July 2017.

17. *Divya U, A Dubey, P. Santhi T, "Application of Non-Linear Gaussian Regression-Based Clock Synchronization Technique for WSN in Agriculture", IEEE Sensors Journal Year: 2018, Volume: 18, Issue: 10, March 2018.*

18. *Camilo L, Alberto, C Mendoza, "Service Oriented Design Approach for a Precision Agriculture Data logger", IEEE Latin America Transactions, Volume: 14, Issue: 4, April 2016.*

19. *Prashant, Jagyasi, N Warke, Vaidya, "Design and development of WST for precision agriculture",7th International Conference on Communication and Networks ,January 2015.*

20. *S Marios, "Precision agriculture: Challenges in sensors and electronics for soil and plant monitoring", 2017 IEEE Biomedical Circuits and Systems Conference, Oct. 2017.*

Impact of injection timing on simarouba seed oil-fueled CI engine

N. Keerthi Kumar [a], T.K. Chandrashekar [b], N.R. Banapurmath [c]

[a] BMS Institute of Technology and Management, Doddaballapur Main Road Yelahanka, Bangalore 560064, India
[b] Mangalore Institute of Technology & Engineering, Moodabidri 574227, India
[c] Department of Mechanical Engineering, KLE Technological University, Hubballi 580031, Karnataka, India

ARTICLE INFO

ABSTRACT

In the present-day of world's economy, the supply of fossil fuels has reduced considerably due to increased growth rate of industrialization and transportation sector. Market economy has a highest impact due to the huge variation in demand and supply of petroleum-based fossil fuels. In this context, biofuels produced from non-edible vegetable seed oil are gaining more attention to use in generators and transportation sectors with less modification in engines. In the present work, Simarouba Oil Methyl Ester (SuOME) is being considered as fuel to run CI engine by advancing and retarding the injection timing (IT). Raw simarouba seed oil is processed and converted to their methyl ester via two stage transesterification process. Use of SuOME at an IT of 190bTDC, 230bTDC, 270bTDC and 310bTDC resulted in Brake thermal efficiency of 24.96%, 25.25%, 26.32% and 25.75% respectively. Reduction in tail pipe HC and CO emissions by 10% and 15% respectively were recorded for engine operating at IT of 270bTDC than standard IT. Marginal increase of NOx by 1.51% was observed due to the increased combustion temperature. Thus, the advancement of IT is a feasible choice to use SuOME in CI engine with higher performance and reduced toxic emission.

© 2020 Elsevier Ltd. All rights reserved.
Selection and peer-review under responsibility of the scientific committee of the International Conference on Advances in Materials and Manufacturing Applications.

1. Introduction

Major portion of worlds total energy consumed is derived from the burning of petroleum-based fossil fuels. Petroleum fuels used for transportation, power and agricultural application are depleting in an increasing rate. Toxic emissions produced owing to the burning of petroleum-based fossil fuels are major concern. This made many researchers to find the best alternative for the petroleum-based fuels. Biodiesel produced form nonedible vegetable seed oil is non-toxic, alternative renewable fuel to use directly to run the engine [1,2]. Simarouba oil methyl ester is one of the promising nonedible feedstocks which can be used to run the engine. Due to the higher viscidness of and fatty acid content of SuOME, raw oil is not feasible to use directly in the engine. In order to decrease viscosity, triglycerides are transformed into esters by transesterification process [3]. Biodiesels provides more advantages than diesel regarding engine wear, fuel cost and toxic emissions. Use of biodiesel improves the engine life by providing higher lubrication than diesel. Use of biodiesel tends to oxidize which causes the corrosion and degradation of engine components [4,5]. Due to higher viscosity, lower heating value and density of

vegetable oil than diesel, performance of engine is reduced. To improve the engine performance, varying the IT provides viable solutions [6]. The properties of compressed air vary as the IT is altered, and hence delay period varies. Early injection tends to increase the delay period due to the lower temperature and pressure of the compressed air. Delayed injection tends to reduce the delay period due to higher temperature and pressure of air within the combustion chamber. Hence variation of injection timings has influence on specific fuel consumption, brake thermal efficiency, peak pressure and NO_x emissions [7]. Effect of IT, injection pressure and nano particles were studied, improved performances with lower emissions were recorded for and IT of 19°bTDC injected at 240 bar. Reduced SFC of 12% and 52.94%, 62.22% and 28.22% reduction in CO, HC and Smoke opacity were noticed compared to diesel [8]. Retarding the injection than static IT provides reduced CO emissions for ceiba pentandra oil methyl ester operated CI engine, injection timing of 27°bTDC yielded higher performance with reduced smoke and other emissions. HC and CO emissions were reduced by 4 ppm and 0.02% respectively compared with standard IT [9]. Higher delay and slow burning were addressed by advancing the injection by 3.5°bTDC for rapeseed oil operated diesel engine,

advancing the injection timing showed reduced specific fuel consumption by 0.05 Kg/Kwh with increased in BTE of 4% than diesel [10]. Advancing the IT from 23°bTDC to 27°bTDC for lemon peel oil biofuel resulted in increased efficiency of 5.081% compared to diesel, use of EGR by 10 and 20% reduces the fuel consumption by 4.96% and 8.5% than diesel respectively [11]. Use of mango seed oil with B25 at injection of 23°bTDC and injection pressure of 200 bar gives the higher BTE of 1.83% 230 bar of injection [12]. Use of simarouba oil methyl ester to run the engine operating at standard operating condition reduces the performance, hence toroidal re-entrant combustion chamber with simarouba mode of operation showed reduced ignition delay by 0.3°CA and 1.3% higher brake thermal efficiency than hemispherical combustion chamber, while use of lateral dual swirl combustion chamber showed HC emissions of 56 ppm and CO emission as 0.18% [13,14]. Use of neat mahua and neem oil in conventional engine showed reduced performance, however, use of toroidal combustion chamber in engine showed increased brake thermal efficiency of 4.8% and 5.3% with mahua and neem oil respectively [15].

In the present investigation, four stroke water cooled single cylinder CI engine was used to evaluate experimentally the effect of IT and SuOME on performance, combustion and emission characteristics of engine. Finally the results were compared with results obtained from diesel mode operation.

1.1. Characterization of simarouba methyl ester

Simarouba seeds have been collected from GKVK, Bangalore, Karnataka. Pulp on the seeds were removed and the seeds were dried naturally to remove the moisture content. Raw simarouba seed oil has obtained by crushing the seeds using oil expeller. Transisterification process has been adopted to convert raw seed oil to its ester. The properties of the SuOME were determined as per Indian standards and observed to be in the property range of diesel fuel. Fuel properties and composition of fatty acids were shown in Table 1 and Table 2 respectively. Three trails have been carried to avoid the random error to record the properties of SuOME.

2. Test methods and sampling procedures

Test fuel SuOME is prepared using two stage transesterification process and the properties was evaluated as per Indian standards for biodiesel. Experiments are carried using single cylinder water cooled Kirloskar TV1 type CI engine. All the experiments were carried at constant engine speed of 1500 rpm. Fig. 1 is the schematic representation of engine setup used in present study. Technical specification of test rig is given in Table 3. Before collecting the data, the engine was preheated for 20 min using diesel as fuel

and at least 2 min between different sets of reading. SuOME was supplied to the engine from separate fuel tank. Reading was taken for all the engine loads of 0% to100% of full load (increment range of 20%) operating at an IT of 205 bar with compression ratio of 17.5:1only after attaining the steady state. Load on the engine was applied using eddy current type dynamometer. Exhaust gas emissions were recorded using 5-gas analyser and smoke was measured using HARTRIDGE smoke meter. Amount of fuel supplied was measured on volumetric basis. IT was varied by using shims. Four values of injection timings of 19°, 23°, 27° and 30°bTDC are used in this study.

3. Error analysis

After the experimentation and before recording the results, an error and uncertainty analysis must be carried out to avoid an erratic result. Hence, in the present work errors from various sources namely; instrument errors, errors due to testing methods and operating conditions have been considered. Total uncertainty has been calculated using square root method and all experimental results were recorded by considering average result of three set of experiments to avoid random errors. Total errors have been calculated and is it 4.71.

4. Results and discussion

The characteristics of DI CI engine are studied using neat SuOME at different IT. The results obtained are compared with base engine operation. The study of performance and combustion parameters obtained through experimentation provides a brief report on the appropriateness of neat SuOME for CI engine applications.

4.1. Brake thermal efficiency

Brake thermal Efficiency. Brake power of engine is directly proportional to Brake Thermal Efficiency (BTE). BTE is output of input heat shaped from the combustion of supplied fuel. It states the ratio of heat input to mechanical output. Fig. 2 represents the effect of IT on BTE. BTE of 100% SuOME at 80% load operating at different IT is lesser than diesel. Higher thickness and higher flash point of SuOME than diesel may be the reason for this trend. However, by advancing the IT from 19°bTDC to 27°bTDC, engine operated using SuOME gives increased BTE by 4.23%. This may be attributed as advancing the IT offers longer delay, which provides enhancement in air–fuel mixing and combustion process.

4.2. Peak pressure

Values of in cylinder pressure tell about the combustion behavior of the engine. Mass of the fuel burnt during the pre-mixed phase holds the maximum contribution towards the peak pressure. Fig. 3 represents the variations of peak pressure at different loads for diesel and SuOME at different injection timing. Higher peak pressure is observed for diesel than neat SuOME. This may be attributed as lower flash point and superior volatility of diesel gives the improved combustion and hence peak pressure. However, advancing the IT provides higher peak pressure up to 27°-bTDC due to earlier injection tends to accumulate more fuel and

Table 1
Properties of simarouba oil methyl ester.

Properties	Diesel	SuOME
Description of sample	–	Yellow Coloured Liquid
Calorific Value (Cal/g)	10,150	9,262
Flash point (°C)	56	162
Kinematic viscosity at 40 °C (cSt)	2.96	4.7
Density at 15 °C (g/ml)	0.833	0.815
Cloud Point (°C)	−16	21

Table 2
Properties of simarouba oil methyl ester.

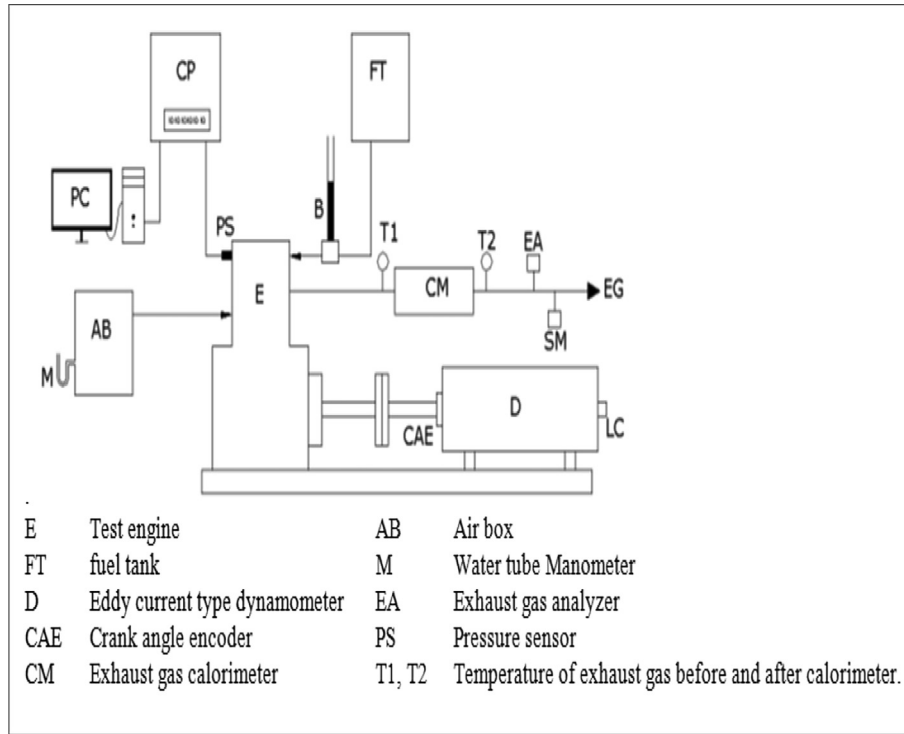| Parameters	Palmitic Acid	Stearic Acid	Oleic Acid	LinoleicAcid	Linolenic Acid	Arachidonic Acid
SOME	23.9%	13.2%	50.8%	5.6%	3.9%	1.2%

N. Keerthi Kumar, T.K. Chandrashekar and N.R. Banapurmath

Fig. 1. Schematic diagram of the experimental setup.

Table 3
Technical specification of engine.

Sl. No	Parameters	Specifications
1	Engine make	Kirloskar make
2	Engine type	Single cylinder, water cooled 4-stroke DI diesel engine
3	Injector pressure	200 to 260 bar
4	Rated power	5.2 kW @ 1500 rpm
5	Bore diameter	87.5 mm
6	Stroke length	110 mm
7	Compression ratio	17.5:1
8	Emissions	5-gas analyser
9	Smoke meter	HARTRIDGE smoke meter

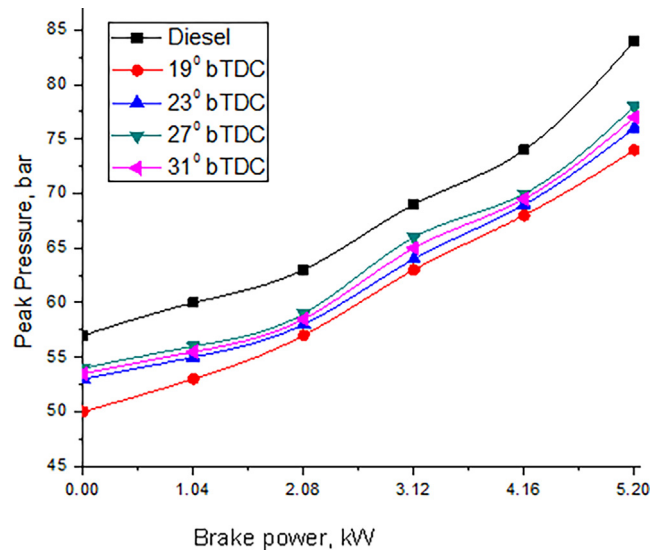**Fig. 2.** Effect of simarouba seed oil at various injection timing on BTE.

Fig. 3. Effect of simarouba seed oil at various injection timing on peak pressure.

burns rapidly giving higher peak pressure. On further advancing the IT leads to supply more fuel than intended and the power produced is wasted during compression process hence results in reduced peak pressure.

4.3. Combustion duration

Deviation in combustion duration (CD) with IT plotted in Fig. 4. CD is the time duration from the start of combustion to 90% of cumulative heat release. An increased CD was recorded for SuOME than diesel mode of operation; higher viscosity of SuOME may be the probable reason for this. Higher viscosity may cause improper
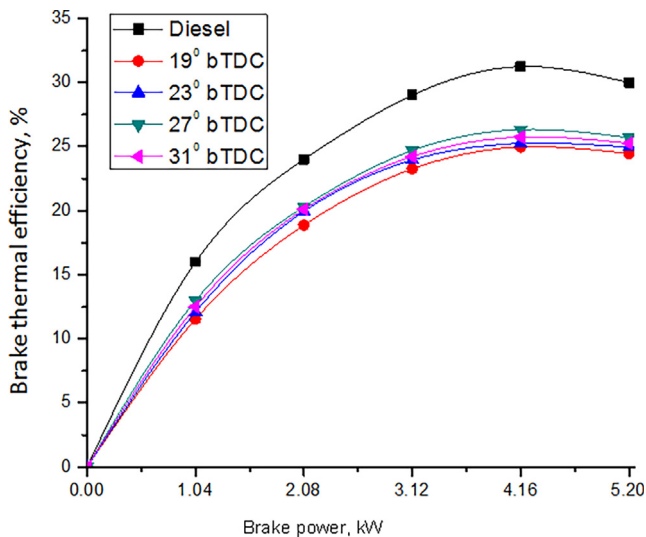
N. Keerthi Kumar, T.K. Chandrashekar and N.R. Banapurmath

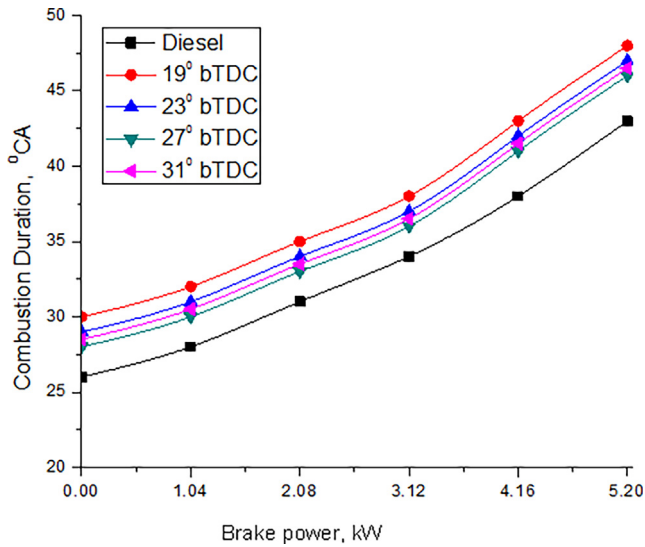Fig. 4. Effect of simarouba seed oil at various injection timing on combustion duration.

Fig. 5. Effect of simarouba seed oil at various injection timing on ignition delay.

fuel air mixing, reduced engine efficiency, combustion pressure and temperature. However reduced CD of 3.28% was observed for SuOME operating at 27°bTDC. This may be due to accumulation of more fuel which provides better combustion. Further advancing the IT gives the negative impact on combustion duration.

4.4. Ignition delay

The time period between the start of injection to the start of combustion is considered as Ignition delay (ID). Effect of SuOME at different IT on ID is shown Fig. 5. As the load increases, ID decreases due to the temperature within the combustion chamber of previous cycle and higher cetane number. ID is lower for diesel compared to SuOME operating at all the IT. This is due to the lesser flash point and higher colorific value of diesel provides earlier ignition than 100% SuOME. ID for SuOME operating at advanced IT of 27°bTDC the base line IT is lesser due complete combustion and higher BTE.

4.5. Hydrocarbon and carbon monoxide emission

Incomplete combustion of fuel produces HC and CO emissions. Factors effecting the both the emissions are oxygen content, ratio of air to fuel and cetane number. Fig. 6 and Fig. 7 shows the changes of HC and CO emissions respectively with different IT and brake power. Both emissions for SuOME are higher compared to diesel at all the brake power and this may be due to poor atomization capability of SuOME. However, HC emissions for SuOME at advanced IT of 27°bTDC is lesser by 10% compared to standard injection timing. CO emissions at IT of 27°bTDC is 15% lesser than IT of 19°bTDC. This may be due to, as the delay period increases in-cylinder temperature promotes the combustion process and hence provides better combustion than static IT. Advancing the IT above 27°bTDC provides higher HC and CO emissions.

4.6. Oxides of nitrogen

Higher combustion temperature is major reason for the formation of NOx emission. Variation of NOx emission with brake power and different IT is shown in Fig. 8. NOx emissions get reduced by retarding the IT. This may be due to reduced combustion process in retarding the IT. NOx emissions are lowest for IT of 19°bTDC
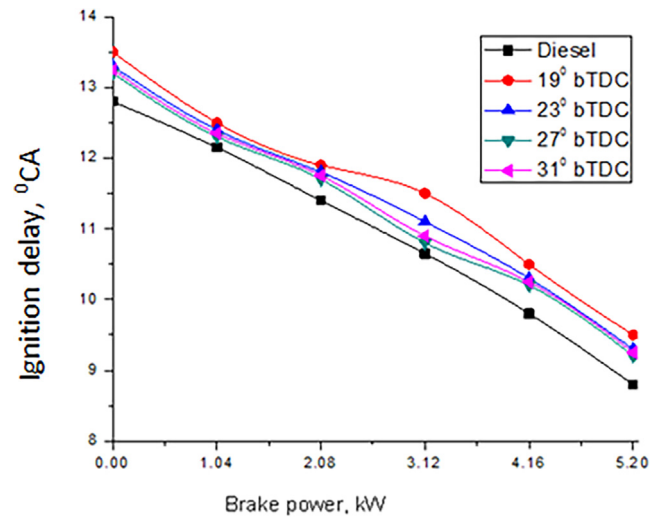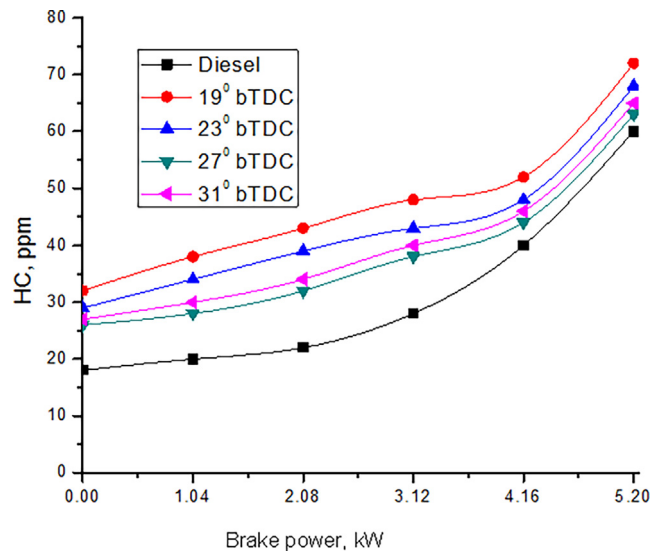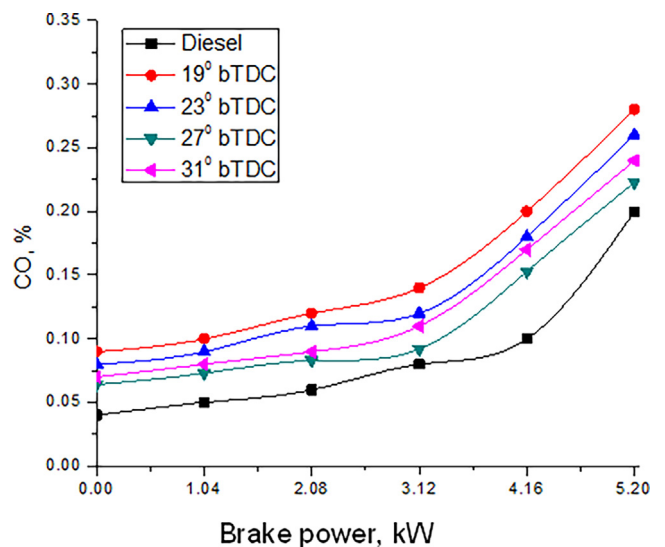

Fig. 6. Effect of simarouba seed oil at various injection timing on HC emission.

Fig. 7. Effect of simarouba seed oil at various injection timing on CO emission.
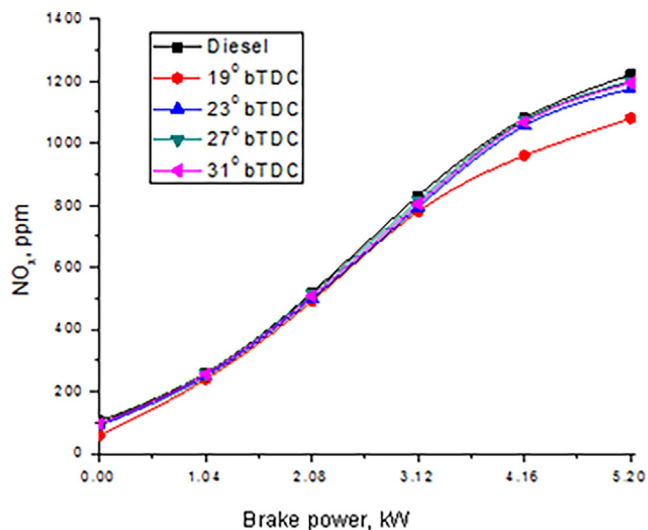
N. Keerthi Kumar, T.K. Chandrashekar and N.R. Banapurmath

Fig. 8. Effect of simarouba seed oil at various injection timing on NO$_x$ emission.
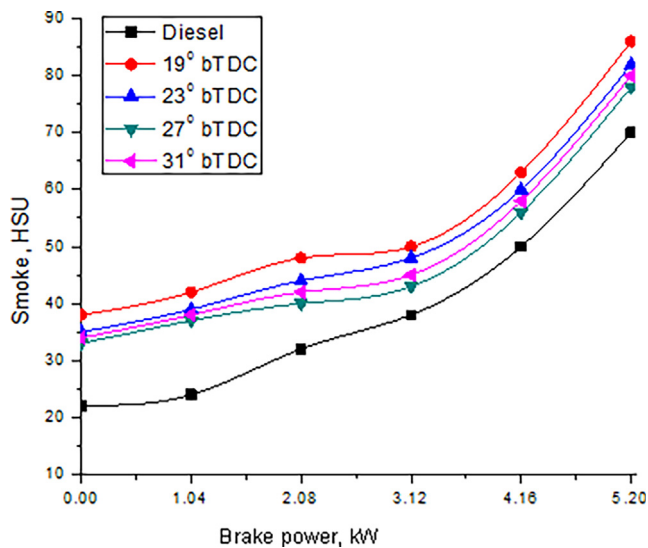

Fig. 9. Effect of simarouba seed oil at various injection timing on smoke.

for SuOME. NOx emissions for IT of 27°bTDC is 1.51% higher than standard IT for SuOME operation.

4.7. Smoke emissions

The variation of smoke emission with engine load for both diesel and SuOME fuel at various IT is plotted Fig. 9. Smoke emissions are clear indication of incomplete or partial combustion. Smoke emissions were lower for diesel compared to SuOME due to higher calorific value and lower viscosity tends complete combustion of diesel fuel. However, SuOME operating at 27°bTDC produces reduced smoke emissions by 6.66% compared to standard injection time operation. Further advancing resulted in increased smoke emissions due to the presence rich mixture inside the combustion chamber.

5. Conclusions

Through the detailed experimental work, it has been noticed that the performance of the diesel engine operating with SuOME

by early injection than standard IT indicated improvement in BTE. The following conclusions were drawn from the present study.

The following conclusions were drawn from the present study.

- Energy from Simarouba seed oil may be utilized as suitable supplement to the diesel.
- BTE for SuOME was less with standard operating condition due to its higher viscosity and lower heating value. An improved efficiency of 28.5% was observed for the advance IT of 27° bTDC than 25.25%, 26% and 27% for IT of 19°, 23° and 31°bTDC respectively.
- ID for SuOME was higher than the diesel due to more viscous nature of SuOME and hence, poor atomization. However, for SuOME operation at 27°bTDC, reduced ID of 10.1°CA was noticed compared to remaining IT.
- CD for SuOME was 43°CA and it is 5°CA higher than diesel mode of operation, due to higher self-ignition temperature of SuOME compared to diesel.
- HC and CO were high for the SuOME than diesel and observed to be 45 ppm and 0.17% respectively for IT of 27°bTDC. However, compared to other IT both the emissions were reduced noticeably.
- The smoke emission of SuOME was 12% greater than diesel, and 6.66% reduction in smoke was observed for engine operating at an IT of 27°bTDC compared operating at standard IT.
- Reduced NOx emissions were observed compared to diesel, however 1.51% increase in NOx emissions was recorded for 27°-bTDC than 23°bTDC.

It may be concluded that, by small adjustment in engine fuel IT, SuOME can be used effectively operate CI engine and act as suitable promising substitute for diesel. To reduce the NOx emissions a study of exhaust gas treatment can be done further.

Declaration of Competing Interest

The authors declare that they have no known competing financial interests or personal relationships that could have appeared to influence the work reported in this paper.

References

[1] S. Arbogast, D. Bellman, J.D. Paynter, J. Wykowski, Advanced biofuels from pyrolysis oil-opportunities for cost reduction, Fuel Process. Technol. 106 (2013) 518–525, https://doi.org/10.1016/j.fuproc.2012.09.022.
[2] K. Anand, R.P. Sharma, P.S. Mehta, Experimental investigations on combustion, performance and emissions characteristics of neat karanji biodiesel and its methanol blend in a diesel engine, Biomass Bioenergy 35 (1) (2011) 533–541, https://doi.org/10.1016/j.biombioe.2010.10.005.
[3] M.A. Fazal, A.S.M.A. Haseeb, H.H. Masjuki, Biodiesel feasibility study: an evaluation of material compatibility; performance; emission and engine durability, Renewable Sustain. Energy Rev. 15 (2) (2011) 1314–1324, https://doi.org/10.1016/j.rser.2010.10.004.
[4] S.A. Khan, R.M.Z. Hussain, S. Prasad, U.C. Banerjee, Prospects of biodiesel production from microalgae in India, Renewable Sustain. Energy Rev. 13 (9) (2009) 2361–2372, https://doi.org/10.1016/j.rser.2009.04.005.
[5] S. Jain, M.P. Sharma, Stability of biodiesel and its blends: a review, Renewable Sustain. Energy Rev. 14 (2) (2010) 667–678, https://doi.org/10.1016/j.rser.2009.10.011.
[6] Y. Zhao, K. Cui, J. Zhu, S. Chen, L.-C. Wang, N.K. Cheruiyot, J.K. Mutuku, Effects of retarding fuel injection timing on toxic organic pollutant emissions from diesel engines, Aerosol Air Qual. Res. 19 (6) (2019) 1346–1354, https://doi.org/10.4209/aaqr.2019.03.0112.
[7] M. Shahabuddin, A.M. Liaquat, H.H. Masjuki, M.A. Kalam, M. Mofijur, Ignition delay, combustion and emission characteristics of diesel engine fueled with biodiesel, Renewable Sustain. Energy Rev. 21 (2013) 623–632, https://doi.org/10.1016/j.rser.2013.01.019.
[8] R. Narsinga, K.S. Ranjith, Effect of fuel injection pressure and injection timing on performance and emissions of diesel engine using nanoadditive blends, RRJASI 1 (4) (2017).
[9] S.B. Nagesh, T.K. Chandrashekar, N.R. Banapurmath, Effect of injection timing and injector opening pressures on the performance of diesel engine fuelled

with ceiba pentandra oil methyl ester, Recent Adv. Petrochem. Sci. 1 (3) (2017) 555–564.

[10] O.M.I. Nwafor, G. Rice, A.I. Ogbonna, Effect of advanced injection timing on the performance of rapeseed oil in diesel engines, Renewable Energy 21 (3-4) (2000) 433–444, https://doi.org/10.1016/S0960-1481(00)00037-9.

[11] Ashok Bragadeshwaran, Nanthagopal Kasianantham, Muhammad Usman Kaisan, Dandu Madhu Sudan Reddy, Kunnappilly Murukesh, Influence of injection timing and exhaust gas recirculation (EGR) rate on lemson peel oil–fuelled CI engine, Environ. Sci. Pollut. Res. (2019), https://doi.org/10.1007/s11356-019-05369-7.

[12] K. Vijayaraj, C.G. Saravanan, Experimental investigation for various injection pressure and injection timing of a diesel engine using B25 methyl ester of mango seed oil 9(1) (2017) 31-44

[13] N. Keerthi Kumar, T.K. Chandrashekar, N.R. Banapurmath, Effects of combustion chamber profile on direct injection diesel engine operated with SuOME, AIP Conf. Proc. (2019), 2128, 050001-1 to 050001-13.

[14] N. Keerthi Kumar, T.K. Chandrashekar, N.R. Banapurmath, V.S. Yaliwal, Effect of combustion geometry on combustion, performance and emission characteristics of CI engine using simarouba oil methyl ester, Materials Science and Engineering Conference Series 376 (1) (2018) 012001.

[15] N.R. Banapurmath, A.S. Chavan, S.B. Bansode, S. Patil, G. Naveen, Tonannavar, M.S. Tandale, Effect of combustion chamber shapes on the performance of Mahua and Neem biodiesel operated diesel engines, J. Petrol. Environ. Biotechnol. 6 (4) (2015) 1.

Numerical investigation on heat sink with fluid pockets for high power LEDs

Sangmesh[a]*, Gopalakrishna Keshava Narayana[b], Sudhakar Kumarasamy[c], Mahendran Samykano[d],
Gowrishankar Thyagatur Panchaksharaiah[e] & Nagraj Patil[f]

[a]Department of Mechanical Engineering, BMS Institute of Technology and Management, Bangalore 560 064, India
[b]Jyothy Institute of Technology, Bangalore 560 082, India
[c]Faculty of Mechanical and Automotive Engineering Technology, University Malaysia Pahang, Pekan, Pahang 26600, Malaysia
[d]Department of Mechanical Engineering, College of Engineering, University Malaysia Pahang, Gambang, Pahang 26300, Malaysia
[e]Department of Mechanical Engineering, R L Jalappa Institute of Technology, Kodigehalli 561 203, India
[f]School of Engineering and Technology, Jain Deemed to be University, Bangalore 560 069, India

The present numerical study explores the use of fluid pockets in the heat sink to enhance heat transfer in high power LEDs. A robust heat sink model has been presented and evaluated the heat transfer characterization in terms of reduced LED junction temperature *via* natural convection and studied the effect of fluid flow in the pockets of heat sink. The junction temperature of the LED has been measured, for enhanced heat transfer and the results have been compared with conventional heat sink. The cooling fluid inside the fluid pockets absorbs heat generated by LEDs resulting in exchange of heat from heat sink surface to the liquid medium in the fluid pockets. The heat gain causes the fluid to flow against gravity due to density variation, raises the mixture of liquid inside the fluid pockets and flow back by gravity effect when it is condensed by the extended fin surface. The performance of the heat sink with fluid pockets has been found to be better than normal heat sink of same geometry due to its ability to conduct heat by the presence of liquid. Fluid pockets filled with de-ionized water in the heat sink have a noticeable effect on heat removal rate. A series of case studies have been done for accurate and efficient heat transfer output; these results then have been used as the benchmark to validate the experimental results. The numerical results have been found to be in good agreement with experimental results.

Keywords: ANSYS, De-ionized water, HSFP, LED, Heat sink

1 Introduction

Temperature of a LED has an adverse effect on lifetime of the LED. The luminous output of LED is entirely dependent on junction temperature by Daechan Jeon *et al.*[1]. The sophisticated packaging of LED, limited space, high temperature expected to raise the junction temperature which causes the LED to premature failure as given by Royston Marion *et al.*[2]. Further, Sung Jin Kim *et al.*[3] used different designs of heat sinks to minimize the junction temperature. S C Wong *et al.*[4] have conducted numerical analysis using finite element approach for multi fin heat sink design simulating the effects of the proposed design. The results indicated a positive effect with forced convection and was limited heat dissipation was obtained for natural convection in the investigation performed by Hui Huang Cheng *et al.*[5]. Whereas, Rasool Kalbasi *et al.*[6] studied the effect of varying fin

size and application of heat pipes for further reduction of temperature also proved to be promising. Another aspect that could be meddled with for enhancing the cooling effect is the fin geometry was performed by Qie Shen *et al.*[7]. A study performed by Shangsheng Feng *et al.*[8] on analytical solution of fin geometries on different boundary layers was found that at lower values of thermo-geometric parameter the error was high and for the higher values of the same the errors seems to be negligible and the same results have been seen by Santosh Chaudhary *et al.*[9]. The use of fluid pockets in the heat sink performed better compared to conventional heat sink studied by Sangmesh B *et al.*[10].

From the literature, it is found that numerous studies have been undertaken on fin geometries, forced convection. However a study on heat sink with fluid pockets has not been reported in the literature. Thus, the present investigation involves numerical study of the heat transfer characteristics of a heat sink with fluid pockets filled with De-ionized water as the cooling medium subjected to natural convection. The

———————
*Corresponding author
(E-mail: sangmesh.sangu293@gmail.com, sangmeshb@bmsit.in)

results obtained by numerical study are compared with the conventional heat sink without the fluid pockets.

2 Numerical analysis

In the present work, a three-dimensional computational fluid dynamics of different configurations is modeled with the help of ANSYS workbench. The computational modeling of a Novel heat sink was completed using the commercially available ANSYS FLUENT® finite volume CFD software.

In this, explored the concept of liquid cooling for enhanced heat dissipation and evaluates their performance with that obtained using conventional heat sink. For this study, an aluminium heat sink with appropriate number of fluid pockets in the heat sink base used for LED luminaries was selected in order to understand the effect of liquid cooling via natural convection.

The heat sink with fluid pockets for varying fin lengths with De-ionized water were analyzed for cooling high-power LED. The aluminium heat sinks of dimension 200 mm× 120 mm × 20 mm have aluminum rectangular fins for a length of 100 mm and 200 mm is considered for the current study. The analysis is carried out at constant heat supply of 80W for all the cases. For this, 80W cool weight Cree make LED was chosen to apply the heat to the heat sink and examined the performance of the heat sink when 80W heat is applied.

Discretising the transport equations, considering appropriate boundary conditions and providing grid-independent solutions are the major performance parameter considered in the present investigation.

The present study explores the solution in terms of fluid flow and heat transfer for natural convection for both steady and transient conditions for given fluid pockets in the heat sink. The law of conservation of mass, momentum and energy equations used in the domain is based on assuming a fluid with constant properties; the Boussinesq approximation was used for density.

3 Solution method and boundary conditions

Appropriate input data was provided to arrive at a proper and valid solution for a given problem. The simulation study is carried out for previously published experimentation, hence the test parameters were kept same to map with the experimental results. The variation in heat flux has not been considered for the simulation. The simulations were administered for both full length and half length fins with and without fluid pockets. The thickness of thermal interface material between the heat sink and LED was ignored in the simulations. The temperature locations were defined in the post processing of the simulations to maintain consistency with experimental results. The convergence criterion of the numerical simulations depends on the outright standardized residuals of the conditions. Convergence is considered as being accomplished at the point when these residuals turn out to be less.

The grid network in the regions of LED chips and little gaps between fins were refined. The no-slip condition was connected on the wall and the wall capacities were utilized at the close wall space. The thermal contact resistance along the chip, substrate and radiator were disregarded. Wall surface was coupled at the interface between fluid and solid regions to understand the heat transfer between the thermal radiator and the outside air space. The Neumann limit condition was applied on the surfaces of LED chips which were settled on MCPCB. Outside space was at open limit condition, which maintained the weight and temperature at 1.01×10^5 Pa and $27°$C respectively. The effect of different orientations (tilt angle) of the LED in line with the street light was also studied.

The following assumptions were made in the present analysis:

1　The variation in heat flux was not considered for the simulation.
2　The air flow field is incompressible, laminar and steady.
3　The thickness of thermal interface material between the heat sink and LED was ignored in the simulations.
4　The no-slip condition was connected on the wall and the wall capacities were utilized at the close wall space.
5　The thermal contact resistance along the chip, substrate and radiator were disregarded.
6　Wall surface was coupled at the interface between fluid and solid regions to understand the heat transfer between the thermal radiator.
7　The various fluid properties such as viscosity, thermal conductivity, etc. were assumed to be constant.
8　However to match with the experimental results, the temperature locations were defined in the post processing of the simulations to maintain consistency with experimental results.

Governing Equations for natural convection for a single-phase flow can be written as:

Continuity Equation:

$$\nabla.(\rho v) = 0 \qquad \qquad ...(1)$$

Momentum Equation:

$$\rho\frac{dv}{dt} = -\nabla p + \eta\nabla^2 v + F \qquad ...(2)$$

where, ρ denotes density, v is velocity, F is the net force and t is time in second

The various fluid properties such as viscosity, thermal conductivity, etc. were assumed to be constant. Daechon jeong *et al.*[1] utilized a polynomial to accurately determine the heat transfer coefficient of the air. Transient method was adopted and simple algorithm was utilized as the solution method with body force weighted for pressure, first order upwind for Momentum, Turbulent Kinetic Energy and turbulent dissipation rate. Energy equations were solved using second order upwind scheme. Second order implicit transient formulation was adopted. The average standard deviation was maintained in the range of 0.47487.

4 Mesh independency study

The Novel heat sink with fluid pockets was modeled and meshed using ANSYS workbench 16 as shown in Fig. 1. The complete geometric details of the heat sink test specimen along with fluid pockets were chosen for the mesh independency study to accomplish a numerical analysis to match with the experimental conditions. The initial mesh independence study was found to be satisfactory and it was decided to use
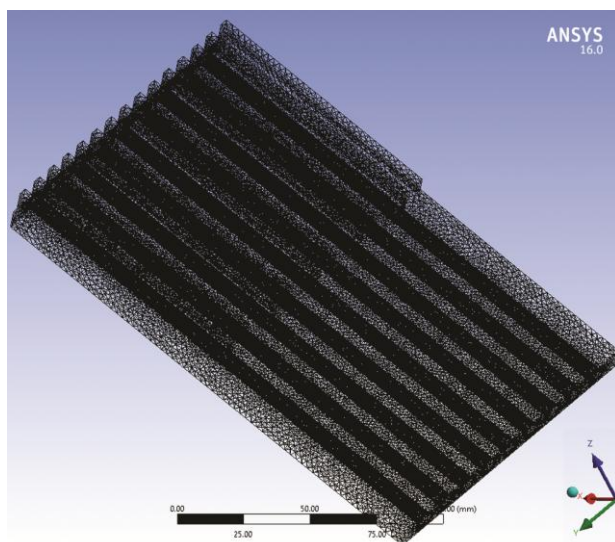

Fig. 1 — General view of the mesh on heat sink.

maximum mesh elements. Among various mesh types, grid with non-conformal structure comprising tetrahedral elements was adopted for discretisation of all portions of the model. The transition of the mesh was of extremely high density in the fluid pockets and also in pocket walls and moderate densities was at the outer surfaces as shown in Fig. 2. Hexahedral cells mesh structure did not suit the current test specimen because of the presence of circular structured fluid pockets. The relevance centre setting was fine. The maximum face and element size were limited to 2 mm and localised mesh refinements were performed with the help of sizing control.

Body sizing was applied on the faces of the holes to accurately capture the circular geometry. The mesh in the rectangular volume of heat sink wall and circular fluid pockets were all put together. A total of 471146 nodes and elements were found to be 1260946 in all domain of the mesh geometry. A total of 242383 elements were found particularly for fluid region in the fluid pockets. Various meshed geometrical views are shown in Fig. 1 to demonstrate the mesh deployment. The mesh, in all rectangular volumes of heat sink model, was maintained by using the "quad - map" meshing arrangement scheme.

The fluid flowing regions were employed with huge elements using the cooper scheme with quad–map face.

5 Results and Discussion

In this segment, the thermal performance and airflow for different heat sink configurations, especially for a novel cooling heat sink with multiple fluid pockets at the base, are analyzed and discussed.

5.1 Effect of fluid on junction temperature

Thermal performance of the heat sink with fluid pockets was examined numerically. The numerical result demonstrates temperature contour for full length fin heat sink with fluid pockets and conventional heat sink. It was found that the heat sink with fluid pockets offered least junction temperature among all the other types of heat sink. The fluid present in the pockets was able to minimize the junction temperature due to higher heat transfer coefficient and other thermal properties. The circulation of De-ionized water in the heat sink takes place due rise in temperature, capillary and gravity effect. The temperature difference between the heat sink with fluid pockets and conventional heat sink was found to be 13°C for full length and 40°C for half-
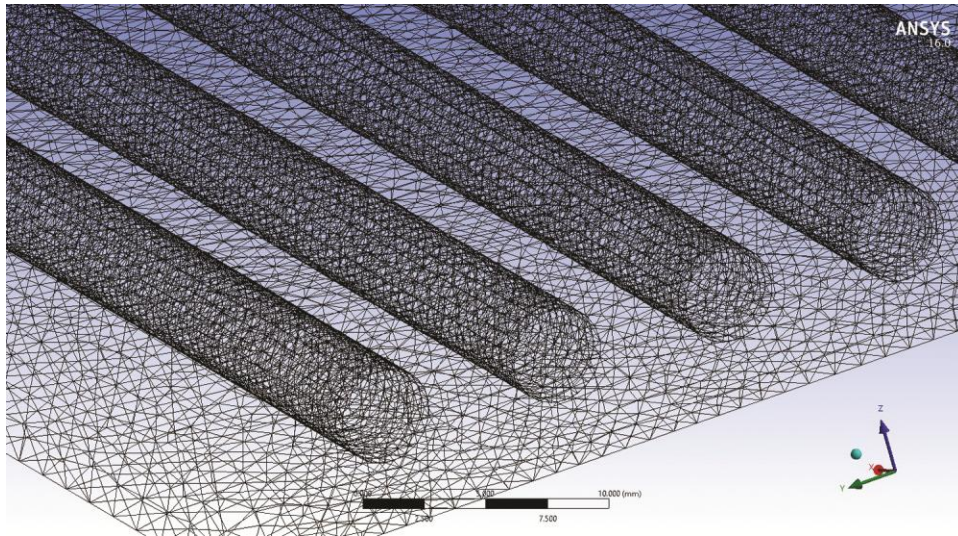
Fig. 2 — Close up view of the mesh zones shown over the heat sink along with fluid pockets.
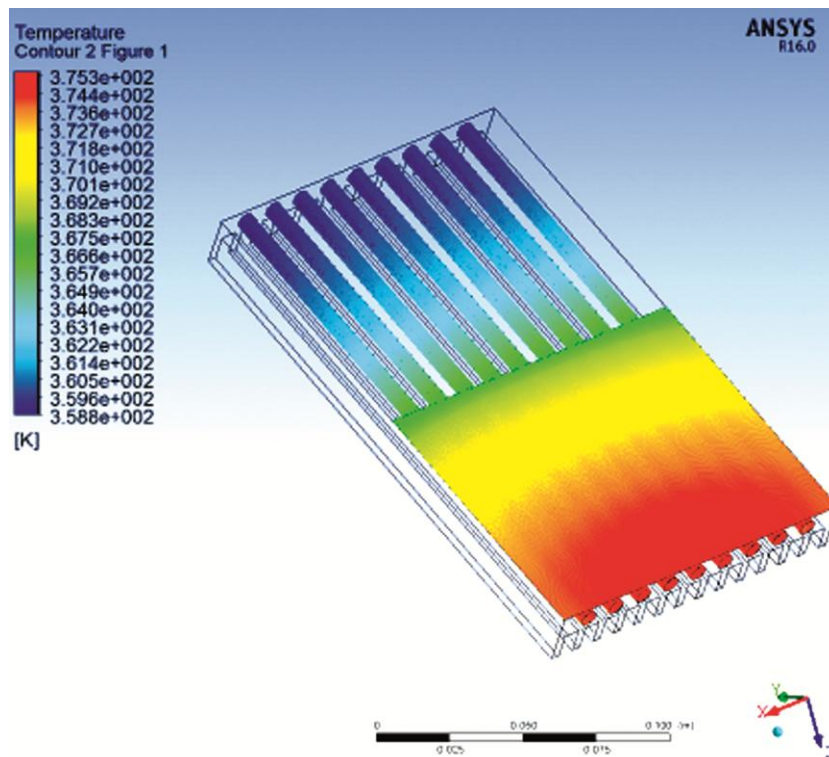
Fig. 3 — Temperature contours along with fluid pockets for full length fin heat sink with fluid pockets (HSHF01).

length fin heat sink respectively. It is noticeable from the fluid properties that water has most astounding boiling temperature, high density, latent heat, surface tension, thermal conductivity, viscosity and specific heat. This has created a viable heat exchange, prompting least junction temperature. Higher boiling temperature expands the sensible heat because of which the heat transfers rate increases. Higher thermal conductivity, surface tension and specific heat add to enhanced heat transfer.

The cooling fluid in the fluid pocket increases heat dissipation in the heat sink, accordingly enhancing cooling as shown in Fig. 3 and Fig. 4. The heat transfer enhancement because of fluid pockets in the heat sink was observed to be at the same temperature for both full length and half length fin heat sink with
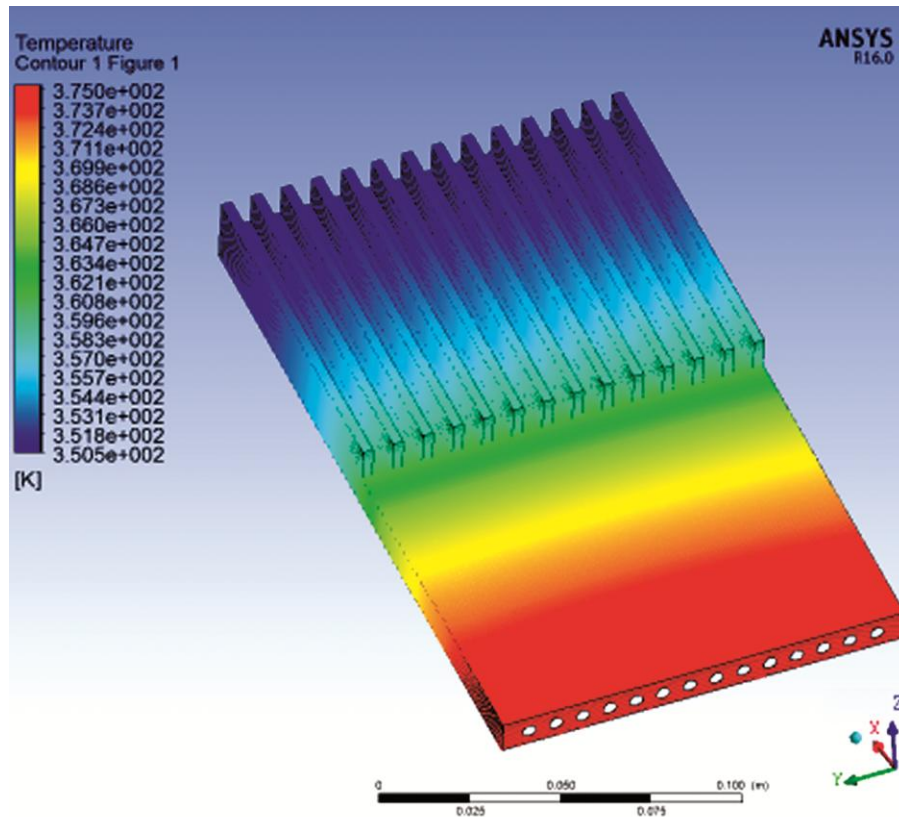
Fig. 4 —Temperature contours along with fluid pockets for half length fin heat sink with maximum fluid pockets (HSHH03).

fluid pockets. It was also demonstrated that the junction temperature was found to be lower when liquid cooling was used in the heat sink. The conventional heat sink with parallel fins proved to be the least effective.

5.2 Junction temperature in conventional heat sink

The flow pattern of atmospheric air has critical impact on the heat dissipation of LED lights. Under free convection condition, the flow pattern of atmospheric air is fundamentally dictated by the heat dissipation structure of LED illuminating presences. The heat dissipation of LEDs can be increased by enhancing the illuminators level structure to form a more sensible flow field. The heat dissipation in conventional heat sink was found to be lower than heat sink with fluid pockets due to the absence of heat transfer medium. This clearly depicts that the fluid in the heat sink rendered a positive result. In view of field synergy analysis, fluid pockets are utilized to enhance the LEDs' heat transfer structure. The homogeneous air stream leads the junction temperature of the LED is minimum and uniform over the surface of the fins. In this manner, the heat transfer execution

of each type of heat sink with liquid cooling is completely utilized, and the normal junction temperature of the LEDs is reduced by 14% for full length fin heat sink as shown in Fig. 5 and approximately 40% for half-length fin heat sink as shown in Fig. 6. In comparison with the conventional heat sink, the temperature of the heat sink with fluid pockets reduced by 14 °C for full length heat sink.

5.3 Effect of fluid flow on junction temperature

It is found that the fluid flow in the pockets moves from LED junction against gravity upwards, because of the increase in thermal energy, and this flows back to the bottom due to gravitational force. This creates a circulation of the fluid within the fluid pockets resulting in an improvement in the heat transfer. From the coordination of velocity and heat flow field, as appeared in Fig. 7, the velocity and heat flow vectors are quadrature just in a little region of balances and the normal crossing point edge between them.

As per the field synergy principle, convective heat transfer is credited not exclusively to temperature contrast, fluid motion and fluid properties, but to the match level of the velocity and heat flow fields. Smaller
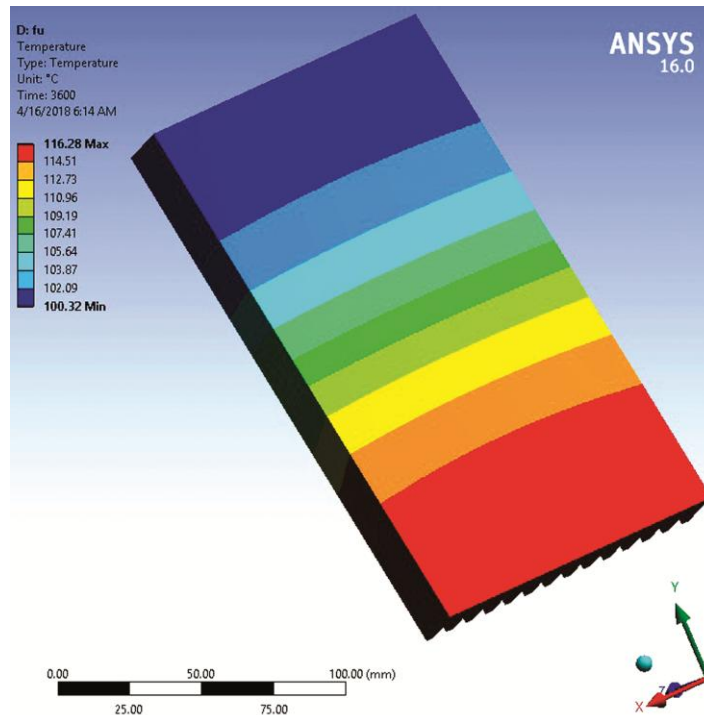
Fig. 5 — Temperature contours along the external surfaces and fins for conventional full-length fin heat sink (CHS01).
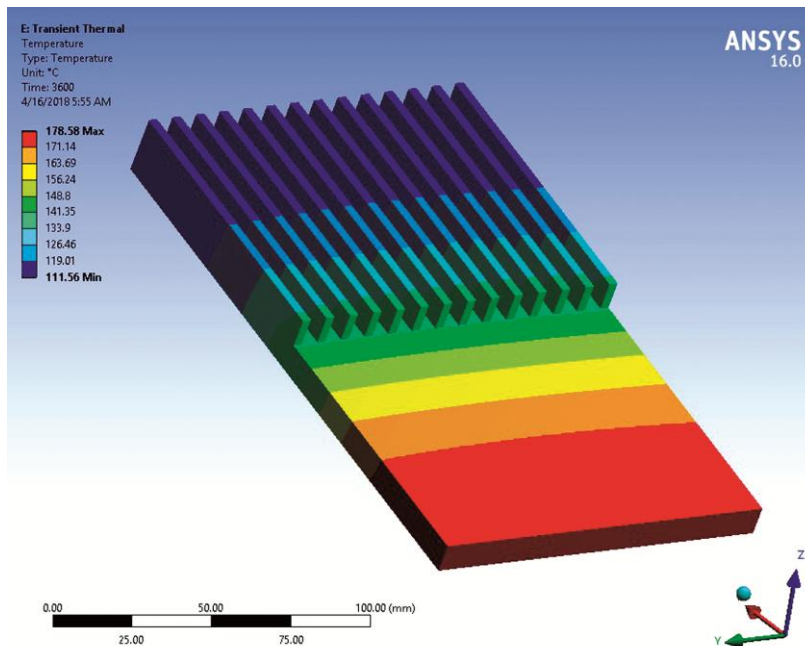
Fig. 6 — Temperature contours along the external surfaces and fins for conventional half-length fin heat sink (CHS02).

the crossing point edge amongst velocity and heat flow field, better is the heat transfer. At the point when the streamline and the isothermal line are quadrature, it implies the velocity and heat flow vector are parallel, the most satisfactory heat transfer rate is acquired. Fig. 8 and Fig. 9 show the flow appropriations of liquid

cooling in the heat sink. The measurement of the diameter of the hole was 4 mm opening and 12 mm spacing between two adjoining gaps.

By contrasting HSHF01, HSHH02 and HSHH03, it is demonstrated that the fluid flow is enhanced, in the range of 2 m/s. Fig. 8 demonstrates the heat transfer
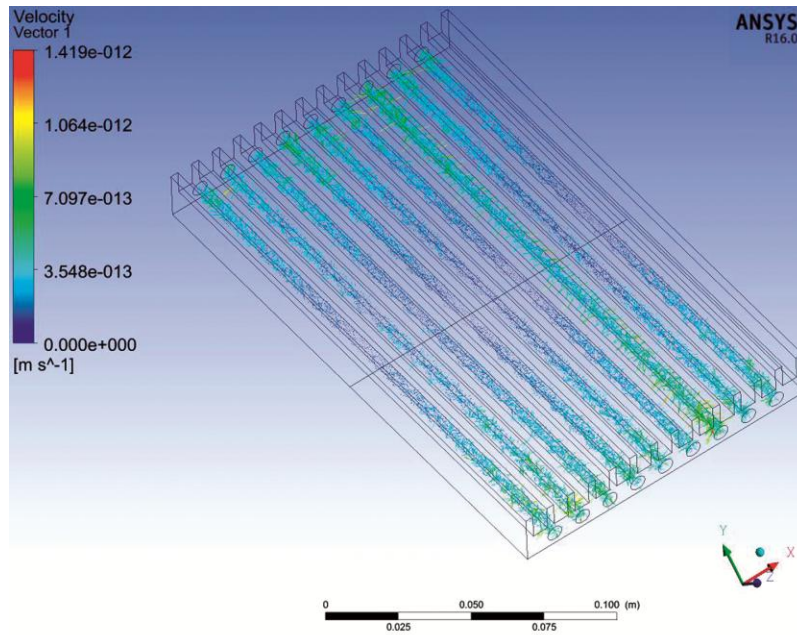
Fig. 7 — Velocity vectors along the fluid pockets for heat sink with fluid pockets for full-length fins (HSHF01).
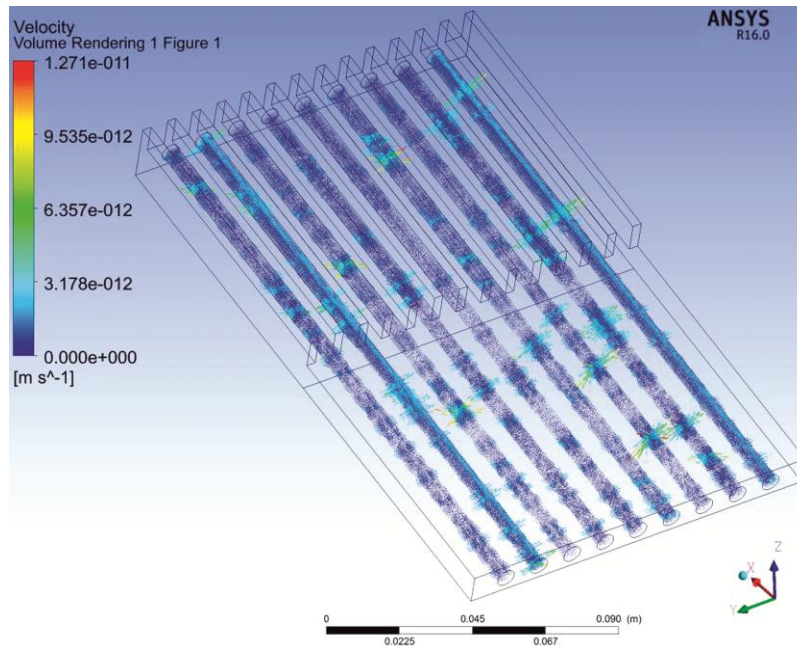
Fig. 8 — Velocity vectors along the fluid pockets for heat sink with fluid pockets for half-length fins (HSHH02).

coefficient improvement within the fluid pockets. The flow pattern surrounding the fluid pockets was seen to be improved for half-length fin heat sink in comparison to full length fin heat sink and was found to 2m/s higher than that of full-length fin heat sink.

Figure 9 demonstrates the heat transfer coefficient improvement within the fluid pockets. The flow pattern surrounding the fluid pockets was seen to be improved

for half-length fin heat sink in comparison to full length fin heat sink and was found to 2 m/s higher than that of full-length fin heat sink. As indicated in Fig. 9, nine fluid pockets are disseminated along the length of heat sink in which the fluid absorbs the heat and takes it away from the LED junction.

This demonstrates that drilling through-holes in the base of the heat sink can enhance heat transfer under

Fig. 9 — Velocity vectors along the fluid pockets for heat sink with fluid pockets for maximum number of fluid pockets (HSHH03).
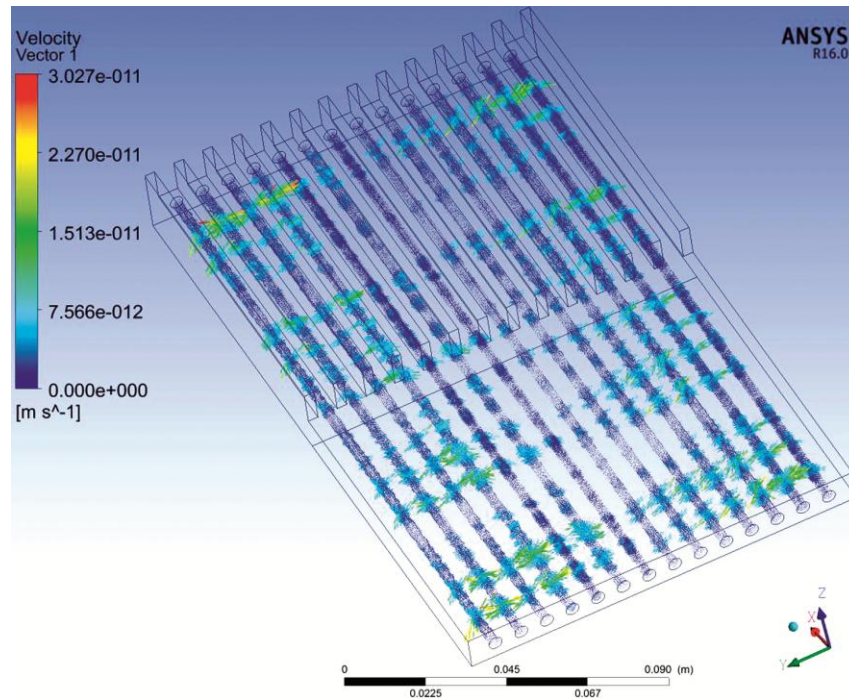
Table 1 — Comparison of results.

Heat Sink Type	Designation	Junction Temperature	
		Experiment (°C)	Numerical (°C)
Conventional Heat Sink without fluid and full length fins	CHS01	110.33	116.28
Heat Sink with fluid and full length fins	HSHF01	100.23	100.3
Conventional Heat Sink without fluid and half the length fins	CHS02	116.53	178.14
Heat Sink with fluid and half the length fins	HSHH02	97.33	103.7
Heat Sink with fluid and half the length fins(Diameter of hole 4mm)	HSHH03	94.37	100.7

natural convection conditions so that heat dispersal of the LEDs is upgraded drastically. To keep the coherence of air stream field, cool air flows upwards from the bottom. After the warm air ascends to a certain height, it is cooled off due to the presence of fins and the lightness of the buoyancy effect at which point it goes down into the free space amongst various fin geometry.

Based on field synergy analysis, incorporating fluid pockets in the heat sink improve the LEDs' heat dissipation structure. It shows that drilling through holes in the heat sink can optimize the flow pattern, and then reduce the intersection angle between velocity and heat flow field under natural convection so that the heat dissipation of the LEDs is enhanced dramatically.

5.4 Comparison study

The numerical results obtained by this study are compared with the results obtained in the previously published experimental work by Sangmesh *et al.*[11]. This study involves a representative study of numerical solutions to validate the experimental results obtained earlier to ascertain the concept of liquid cooling via natural convection in a heat sink. Hence, the simulations carried out for with De-ionized water for 100% filling rate. The numerical results are in good agreement with experimental results except in one case. A series of case studies were done for accurate and efficient heat transfer output; these results were then used as the benchmark to validate the experimental results.

The present study explores the solution in terms of fluid flow and heat transfer for natural convection for both steady and transient conditions for given fluid pockets in the heat sink. The laws of conservation of mass, momentum and energy equations used in the domain are based on assuming a fluid with constant

properties; the Boussinesq approximation was used for density.

The results were compared purely on output results (Junction Temperature of LED) obtained by the experiments and numerical study.

Simulation results are found to be same for HSHF01, HSHH02 and HSHH03. However, there is a negligible difference of 6°C attained for CHS01. There was a difference in case of CHS02 due to the half length fin arrangements in the heat sink. As many studies indicated that enhanced heat dissipation is observed with increase in surface area of heat sink fins but in case of CHS02 with limited in fin length would failed to extract heat where as the efficacy of the same improved with the use of fluid pockets. Hence, CHS02 obtained a maximum temperature compared to all other means of heat sinks considered in the study.

6 Conclusions

In this study, heat transfer performance of a novel heat sink with fluid pockets is presented numerically and the results were validated with experimental outcome obtained in the previous study as shown in Table 1. The thermal performance of the heat sink is evaluated in terms of reduced junction temperature of LED using De-ionized water as the heat transfer. The junction temperature reported by a heat sink with liquid is less than the conventional heat sink by at least 13%. The cooling mechanism of this device is an inspiration from conventional heat pipes where the fluid circulation is attained with condensation and evaporation of liquid. Whereas in this, the circulation of liquid may take place due to gravity force and thermal energy. The overall heat transfer of the heat sink with fluid pockets includes, both conduction and convection heat transfer. The cooling fluid inside the fluid pockets absorbs heat generated by LEDs resulting in exchange of heat from heat sink surface to the liquid medium in the fluid pockets. The heat gain causes the fluid to flow against gravity due to density variation, raises the mixture of liquid inside the fluid pockets and flow back by gravity effect when it is condensed by the extended fin surface.

References

1   Daechan J & Chan B, *Int J Heat and Mass Tra*, 113 (2017) 1086.
2   Royston M, Mendonca, Sai S Y & Chandrakant R K, *Int J Resin Eng Tech*, 41 (2015) 148.
3   Sung J K, Dong-Kwon Kim & Hwan H O, *J Heat Trans Eng,* 29 (2008) 169.
4   S C Wong & W Y Lee, *Int J The Sci*, 138 (2019) 116.
5   Hui Huang C & De Shau Haung M T L, *J Micro Ele Rel*, 52 (2012) 905.
6   Rasool K, Masoud A, Jalal A & Minh-Duc T, *J Energy,* 171 (2019) 1088.
7   Qie S, Daming S, Ya X, Tao J, Xu Z, Ning Z, Ke W & Zhiyi H, *Int J The Sci*, 28 (2015) 1.
8   Shangsheng F, Meng S, Hongbin Y, Shanyouming S, Feichen L & Tian J L, *J Appl Ther Eng*, 132 (2018) 30.
9   Chaudhary S, Kanika K M & Chaudhary S, *Ind J Eng Mater Sci*, 27 (2020) 33.
10   Sangmesh B , Gopalakrishna K, Manjunath S H, Narendra Kumar M &Vijay Kumar G, *J of Sci Ind Res*, 77 (2018) 600.
11   Sangmesh, Gopalakrishna K, Manjunath S H, Venkatesh K & Keertishekar M , *Int J Auto Mech Eng*, 14 (2017) 4846.

Fracture Toughness of CNT Filled Carbon Fabric Reinforced Epoxy Composites

M.D. Kiran[a], H.K. Govindaraju[a], Lokesh Yadhav B.R[b], B. Suresha[c] and T. Jayaraju[c]

[a]Department of Mechanical Engineering, BMS Institute of Technology and Management, Bangalore, India; [b]Department of Mechanical Engineering, R.L.Jalappa Institute of Technology, Doddaballapur, India; [c]Department of Mechanical Engineering, National Institute of Engineering, Mysore, India

ABSTRACT

In the present investigation, hand layup processed composites and hot-pressed Carbon matrix reinforced composites were manufactured with and without the addition of carbon nanotubes. The fabricated composites were tested for its mechanical and fracture properties using ASTM testing standards. The results showed that the carbon nanotubes reinforced composites have shown improved tensile and fracture properties when compared with carbon fabric reinforced epoxy composites. The main focus of the present investigation is to study the role and effect of CNT filler as a secondary reinforcement to carbon fibre reinforced epoxy composites. The results of these investigations provide insight into of fracture behaviour of CNT filled carbon fibre reinforced epoxy composites under autoclave chamber.

1 Introduction

In the area of automotive, aerospace and defence applications the scientists are extensively working for the development of strong, durable and light weight composite parts. The composite materials have advantages such as high strength, high stiffness, long fatigue life, low density, corrosion resistance, wear resistance, and environmental stability [1]. Although polymers have a higher strength-to-weight ratio than metals, their ability to replace them for such applications is hindered by their inherently low mechanical and fracture resistance properties.

The fibres significantly affect the mechanical properties of composites along the fibre direction; composites exhibit greater in-plane results. Woven fabrics type fibres are formed by the interweaving of warp fabrics in a regular weave pattern. Woven fabrics type fibres are attributed to the mechanical interlocking of the fibres which leads to effective load transfer between the matrix and fibre pays the main role [2]. In polymer composites, thermoset includes epoxy, polyurethane, polystyrene, polyamide, etc. and thermoplastics, such as polypropylene, polyethylene is used as matrix materials. Natural fibres and synthetic fibres includes Glass fibre, carbon fibre, etc. are used as reinforcements in the form of short/continuous/fabric [3]. Polymer composites reinforced with carbon fibre possess higher ductility than other fibres [4]. From the several investigation polymer matrix composites reinforced with plane woven fabric exhibits better mechanical properties [5].

The presence of nanoparticles in composites performs a vital role in the improvement of the mechanical properties. Stresses transfer and elastic deformation from the matrix to the fillers are governed by the interface quality [6]. The higher rigidity of fillers compared to epoxy; the deformation causes from the epoxy. Up to 1% of filler weight fraction, the nanoparticles are able to induce further mechanisms of failure without blocking matrix deformation. According to the crack pining theory, particles may act as obstacles to crack growth by pinning [7]. Mechanical properties of fibre reinforced polymer composites modify with the addition of different fillers in different ways. Particle size, quantity, and matrix particle interface have a major influence on the modification of mechanical properties of polymer matrix composites [8–12]. The addition of nanofillers with less than 100 nm dimensions leads to enhance the performance of polymer matrix composites [13]. Polymer composite with CNT shows high stiffness, high strength, better electrical and thermal properties due to their inimitable properties and high aspect ratio [14,15]. Tensile strength and young's modulus of epoxy composites were remarkably enhanced with the addition of CNT and it can provide better fracture toughness [16,17]. The addition of MWCNTs in epoxy composites shows enhancement of mechanical properties [18] and many researchers reported mechanical properties and fracture toughness of polymer composites are improved at a small percentage CNT addition.

Basic mechanical properties of the composites were studied and mode I fracture toughness of carbon fibre reinforced epoxy composites using Single Edge Notched Beam (SENB) specimens. The main objective of the present research is to study the mechanical and fracture properties of carbon fibre reinforced epoxy composite samples filled with multi-walled carbon nanotubes. Even though many researchers were worked on epoxy composites, very few researchers were reported mechanical properties of epoxy composites where the carbon nanotubes are used as reinforcements. Though there is similar material system, but in the present work carbon nanotubes are used as fillers (secondary reinforcements) for carbon fabric reinforced epoxy (CE) matrix composites. In the present work, the effect of the addition of carbon nanotubes on mechanical properties and fracture toughness is studied exclusively.

---

2 Experimental details

2.1 Materials and fabrication of composites

The composite materials considered in the present study consist of Araldite LY 1564 epoxy resin was used as a matrix with hardener (Aradur 22,962 grade) for room temperature curing. Both Epoxy resin and hardener are supplied by Huntsman Advanced Materials. Bi-directional carbon fabric of 200gsm 3k plain waving from pooja Fibres Ahmadabad, Gujarat was used as primary reinforcement. The mean diameter of the carbon yarns was 7 μm, whereas carbon nanotubes diameter ranges from 20 to 30 nm supplied by Sigma Aldrich, dispersed in epoxy as secondary reinforcement.

The composites were fabricated using hand lay-up method followed by curing in the autoclave [19]. Carbon nanotubes have been dispersed in epoxy through ultrasonic and high-speed shear mixer was used to achieve the uniform
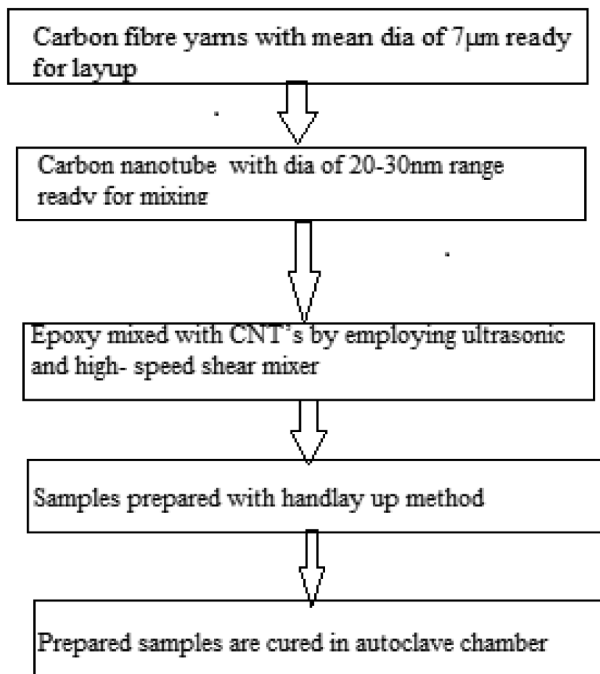

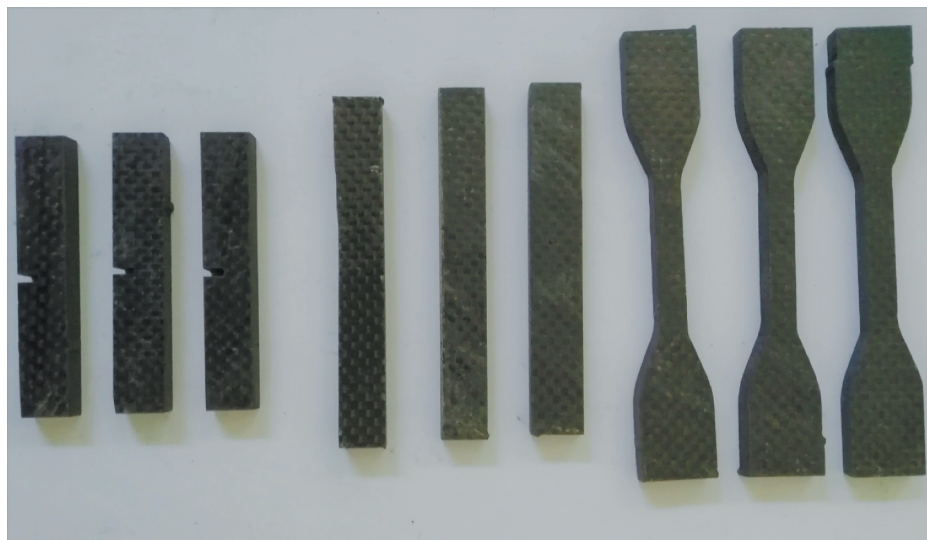Figure 1. Steps indicating the procedure for preparation of CFRP nano-composites.

distribution of Nanofillers in the epoxy matrix [20,21]. Figure 1 depicts the details of the production process of CFRP composites. Table 1 illustrates the designation and composition of CNT-epoxy with carbon fabric used in the present study.

2.3 Determination of voids

Void fraction is an amount of the voids present material and it is expressed as a fraction of the volume of voids over the total volume. There are various methods to determine the voids present in the composites. The theoretical density of the fabricated composite was calculated using the rule of mixture concept by considering the weight fraction of particulars. The actual density of the fabricated composites was measured as per the ASTM D792 standard employing a METTLER AE 200 densometer. In the present study for polymer composites, theoretical and actual densities were considered to calculate the volume fraction of voids using Equation 1.

$$V_v = \frac{\rho_t - \rho_m}{\rho_t} \times 100 \tag{1}$$

Where V_v is the void volume in percentage, ρ_t in g/cm^3 is the theoretical density of the composite specimen, and ρ_m g/cm^3 is the measured density of the composites, respectively.

2.4 Tensile test

To determine the ultimate tensile strength and Young's modulus of the composites tensile test has been conducted. The test specimens were prepared as per ASTM D638 standard of dimensions 165 mm × 19 mm × 4 mm. The tensile test was carried out on Kalpak-100 K computerised universal testing machine under displacement control with a crosshead speed of 2.5 mm/min.

2.5 Impact test

The impact strength of the composites was studied using the Izod impact test as per ASTM D256 standard with specimen dimensions of 63.5 mm × 12.7 mm × 3.2 mm. The impact test was carried out on a computerised impact testing
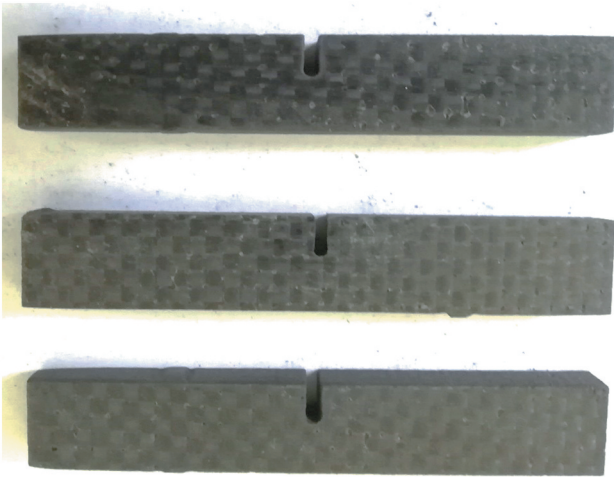

Figure 2. Image of prepared samples.

Figure 3. Image of fractured sample.

Figure 4. Image of SNEB samples.

Table 1. Composition of laminates.

Composites(Designation)	Carbon Fibre (wt%)	Epoxy (wt%)	CNT (wt%)
Carbon Epoxy (CE)	55	45	0
0.1% CNT+ CE (CE-C1)	55	44.9	0.1
0.2% CNT+ CE (CE-C2)	55	44.8	0.2
0.5% CNT+ CE (CE-C3)	55	44.5	0.5
0.75% CNT+ CE (CE-C4)	55	44.25	0.75

machine made International equipment, Mumbai, with the capacity of up to 25 J releasing angle of the pendulum 150°.

2.6 Mode I fracture test

Fracture toughness of the composite studied using a three-point bending test method in the form of critical-stress-intensity factor K_{IC} as per the ASTM D5045-99. The notched specimen comprises pre-crack or natural crack by using a sharp razor blade and tapping. The depth of the pre-crack developed by tapping must be two times larger than the width of the crack [22,23].

3 Results and discussion

3.1 Density and volume fraction

The density of composites is dependent on the ratio and density of the epoxy matrix, filler, and carbon fabric reinforcement. In the hand-layup technique, difficult to eliminate the presence of voids, and these voids were reduced by standard manufacturing technique. The existence of voids in composites habitually affects the mechanical properties of composites such as inter-laminar strength, tensile strength,

and fracture toughness [24]. The actual density is measured using densometer slighter than the theoretical density. The theoretical and experimental densities and volume fraction of voids of Carbon fibre reinforced epoxy composites with and without carbon nanotubes are shown in Table 2. The volume fractions of voids of composites are very less (<3%) which may due to the proper fabrication process involved in the manufacture of these composites. Images of prepared samples, fractured samples and SNEB samples are as shown in Figures 2–4, respectively.

3.2 Tensile properties

The stress–strain behaviour of epoxy composites reinforced carbon fibre with different percentage loading of carbon nanotubes as shown in Figure 5. The stress–strain graph composites plotted against the addition of CNT which leads to obtain the ultimate tensile strength, elongation and Young's modulus values and presented in Table 3.

As the table indicated, the tensile strength and young's modulus of CE composites improved as the addition of CNT increased up to a critical point shown in Figure 6. From the results, the addition of CNT is caused by increases in rigidity while enhancing tensile strength and ductility. The addition

Table 2. Densities and volume fraction of voids of CNT filled CE hybrid composites.

Composites	Theoretical density (g/cm³)	Measured density (g/cm³)	Volume fraction of voids (%)
CE	1.364	1.351	0.95
CE+C1	1.365	1.334	2.27
CE+C2	1.365	1.332	2.42
CE+C3	1.366	1.331	2.56
CE+C4	1.367	1.331	2.64

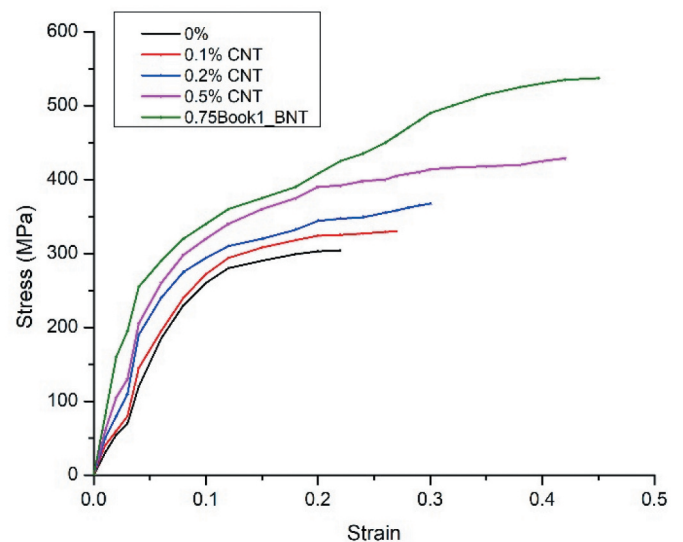Figure 5. A typical stress–strain curve of CNT filled CE Composites.

Table 3. Mechanical properties of unfilled and particulate filled CE composites.

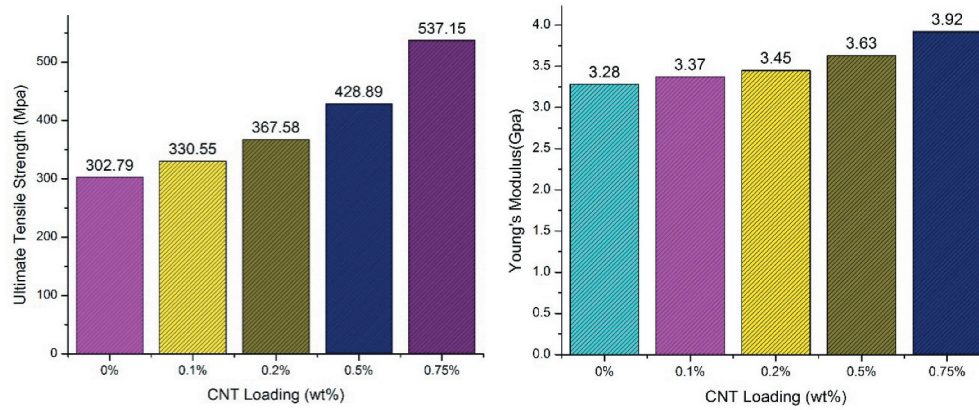| Composites	Tensile Strength (MPa)	Young's Modulus (GPa)	Fracture Strain
CE	302.79	3.28	0.226
CE+C1	330.55	3.37	0.262
CE+C2	367.58	3.45	0.291
CE+C3	428.89	3.63	0.375
CE+C4	537.15	3.92	0.462

Figure 6. Ultimate tensile strength and Young's modulus of CNT filled CE composites.

of 0.75% CNT filler to CE composites specimens shows 77 wt % enhancement of ultimate tensile strength. Similarly, the highest value of Young's modulus was reached up to 20% with the same 0.75 wt% addition to CE composites. This is because the higher aspect ratio of CNT used in the present investigation has a larger specific surface area and the alignment of CNT gives rise to germane toughening of the matrix against axial loading. Therefore, larger specific surface area leads to a stronger matrix–filler interface adhesion and are thought to better rigidity [25–28].

3.3 Impact strength

The Izod impact test was carried out to comprehend the effect of CNT on the impact strength of CE composites. Figure 7 shows the effect of the addition of CNT on the impact strength into the CE matrix composites. The results showed that the combination of carbon fabric and CNT achieved a significant improvement (approx. 40%) in impact Strength of epoxy resin. The 0.75% CNT filled composite has a substantial effect on the Impact strength of CE composites.

Carbon fibre plays a significant role in improving the impact resistance of the material, which leads to improving the overall toughness of the material. The interfacial bond between carbon fibre and epoxy resin increase with the increasing addition of CNT fillers, which leads to better load stress transfer between fibre and matrix [29]. Also, better interfacial adhesion between fibre and matrix increases the

Figure 8. Fracture toughness of CNT filled CE composites.

energy required to pull out the fibre from the matrix, and also reduces the friction and sliding of the fibre.

3.4 Fracture toughness

A fracture toughness test was carried using the SENB method to study the effect of CNT on the fracture toughness of CE composites. Fibre alignment with epoxy resembles the played improved toughness of the epoxy-based nanocomposites. The alignment of carbon fibre and better dispersion of CNT in the epoxy matrix leads to improving the fracture toughness of CE composites. This aids it with the improved load transfer and hence helps stress transfer between fibre to a matrix under the application of the load.

Figure 8 illustrates the effect of CNT on the fracture toughness of CE composites. The addition CNT filler to CE composites shows the improvement of fracture toughness of the composites. For the unfilled CE-composites, the value of K_{IC} is smaller than that of CNT filled CE composites. Fracture toughness of CNT filled the CE composites increased by 20% with the addition of 0.75%CNT due to the pinning effect of CNT and better interfacial bonding between filler and The addition of CNT filler to the epoxy matrix creates the pull-out mechanism and crack bridging perpendicular to the fracture surface [30]. Also, the addition of CNTs enhances the adhesive forces between the epoxy

Figure 7. Impact strength of CNT filled CE composites.

matrix and carbon fibres which leads to greater toughness and mechanical properties [31].

4. Conclusions

The effect of CNT filler loading on mechanical properties and fracture toughness of CE composites was studied. The enhancements in the mechanical properties and fracture toughness of the CNT filled CE composite were achieved. Some important conclusions of this research work are discussed as follows:

- The presence of voids at 0.75% volume fraction CNT filled composite is slightly higher than other volume fraction CNT loaded CE composites.
- Significant enhancements in mechanical properties and fracture toughness were obtained for the CNT filled CE composites in comparison with unfilled CE composites over the whole contents studied.
- The addition of 0.75% CNT filler to CE composites specimens shows 77 wt% enhancement of Ultimate Tensile Strength. Similarly, the highest value of young's modulus was reached up to 20% with the same 0.75 wt % addition to CE composites as CNT filler loading in the matrix improves the interface, which leads to better load transfer from fibre and nanofillers to the matrix.
- Combination of carbon fabric and CNT achieved a significant improvement of about 40% in impact Strength of epoxy resin which concludes 0.75% CNT filled composite have a substantial effect on the impact strength of CE composites. Due to better dispersion of particles have showed better matrix fibre interface which results in delayed crack propagation which leads to enhanced fracture toughness increased by 20% with the addition of 0.75%CNTs.

Disclosure statement

No potential conflict of interest was reported by the authors.

Notes on contributors

Mr. Kiran M D working as Assistant Professor in BMS Institute of Technology and Management, Bengaluru. Completed M.E in Machine Design in University Visvesvaraya College of Engineering, Bangalore. Research work focused on Material Science, Polymer Composite Materilas,Nanocomposites,Fracture Mechanics.

Dr H K Govindaraju working as Professor and Vice-Principal, BMS Institute of Technology and Management, Bengaluru. Obtained his Ph. D from NIE, Mysore from the Visvesvaraya Technological University. Research work focused on Material Science, Fatigue and Fracture Mechanics.

Lokesh Yadhav B R working as Assistant Professor in R.L Jalappa Institute of Technology, Doddaballapura, Bengaluru.Research work focused on Material Science, Polymer Composite Materilas, Tribology in Polymer Composites.

Dr. Suresha B working as Professor and Head of the department, NIE, Mysore. Completed his M.Tech from IITM, Chennai and Ph.D from Anna University, Chennai. Research work is focused on Material Science, Polymer Composite Materilas, Tribology in Polymer Composites, Nanocomposites.

Dr. T Jayaraju form Professor and Head of the department, NIE Institute of Technology, Mysore. Completed Ph.D from IIT Mumbai. Research work focused on Fracture Mechanics, Material Science.

References

[1] Tserpes KI, Labeas GN. Mesomechanical analysis of non-crimp fabric composite structural parts. Compos Struct. 2009;87:358–369.

[2] Fang Y, Zhao J, Zha JW, et al. Improved stability of volume resistivity in carbon black/ethylene-vinyl acetate copolymer composites by employing multi-walled carbon nanotubes as second filler. Polym. 2012;53:4871–4878.

[3] Yasmin A, Daniel IM. Mechanical and thermal properties of graphite platelet/epoxy composites. Polym. 2004;45:8211–8219.

[4] Jagannatha TD, Harish G. Mechanical properties of carbon / glass fiber reinforced epoxy hybrid polymer composites. Int J Mech Eng Rob Res. 2015;4(2).131-137.

[5] Vishwanath B, Verma AP, Rao CVSK. Effect of fabric geometry on friction and wear of glass-fiber-reinforced composites. Wear. 1991;145(2):315–327.

[6] Terrones M. Science and technology of the twenty first century: synthesis, properties, and applications of carbon nanotubes. Ann Rev Mater Res. 2003;33:419–501.

[7] Suresha B, Chandramohan G, Jawahar MA, et al. Mechanical and tribological properties of glass–epoxy composites with and without graphite particulate filler. J Reinf Plast Compos. 2009;28:225.

[8] Radford KC. The mechanical properties of an epoxy resin with a second phase dispersion. J Mater Sci. 1286;6:1291.

[9] Fu SY, Lauke B. Characterization of tensile behavior of hybrid short glass fiber calcite particle ABS composites. Compos Part A: Appl Sci. 1998;29:575–583.

[10] Cho J, Joshi MS, Sun CT. Effect of inclusion size on mechanical properties of polymer composites with micro and nano particles. Compos Sci Technol. 2006;66:1941–1952.

[11] Kiran MD, Govindaraju HK, Jayaraju T. Review-effect of fillers on mechanical properties of polymer matrix composites. Mater Today. 2018;5(10 Part 3):22355–22361.

[12] Lassila L, Garoushia S, Pekka KV, et al. Mechanical properties of fibre reinforced restorative composite with two distinguished fibre length distribution. J Mech Behav Biomed Mater. 2016;60:331–338.

[13] Tjong SC. Structural and mechanical properties of polymer nanocomposites. Mater Sci Eng R. 2006;53(3–4):73–197.

[14] Allaoui A, Bai S, Cheng HM, et al. Mechanical and electrical properties of a MWNT/epoxy composite. Compos Sci Technol. 2002;62(15):1993–1998.

[15] Cebeci H, Guzman de Villoria R, Hart J, et al. Multifunctional properties of high volumefraction aligned carbon nanotube polymer composites with controlled morphology. Compos Sci Technol. 2009;69:2649–2656.

[16] Yu M, Lourie O, Dyer M, et al. Strength and breaking mechanism of multiwalled carbon nanotubes under tensile load. Science. 2000;287(5453):637–640.

[17] Yakobson BI, Avouris P. Mechanical properties of carbon nanotubes, in carbon nanotubes. Berlin, Heidelberg, Houston, TX: Springer; 2001. p. 287–327.

[18] Hussain MT, Shivakumar Gouda PS, Siddhalingeshwar IG, et al. Effect of alcoholic treated MWCNT on tensile behavior of epoxy composite. Int J Eng Sci Technol. 2016;8(1):57–63.

[19] Suresha B, Saini MS. Fabrication and mechanical characterisation ofcarbon fabric reinforced epoxy with alumina andmolybdenum disulfide fillers. Int J Comput Aided Eng Technol. 2018;10:1/2.

[20] Withers GJ, Yu Y, Khabashesku VN, et al. Improved mechanical properties of an epoxy glass–fiber composite reinforced with surface organo-modified nanoclays. Compos Part B. 2015;72:175–182.

[21] Emrah B, Elcin K, Metin T. Mechanical and thermal behavior of non-crimp glass fiber reinforced layered clay/ epoxy nanocomposites. Compos Sci Technol. 2007;67:3394–3403.

[22] Kiran MD, Govindaraju HK, Jayaraju T. Evaluation of fracture toughness of epoxy-nickel coated carbon fiber composites with Al2O3 nano filler. Adv Polym Compos. 2018;2057:020002.1–020002.5.

[23] ASTM. D 5045-99 standard test methods for plane-strain fracture toughness and strain energy release rate of plastic materials. Philadelphia: American Society of Testing and Materials; 1999.

[24] Mehdikhani M, Gorbatikh L, Verpoest I, et al. Voids in fiber-reinforced polymer composites: A review on their formation, characteristics, and effects on mechanical performance. J Compos Mater. 2019;53(12):1579–1669.

[25] Gkikas G, Barkoula N-M, Paipetis A. Effect of dispersion conditions on the thermo-mechanical and toughness properties of multi walled carbon nanotubes–reinforced epoxy. Compos Part B Eng. 2012;43(6):2697–2705.

[26] Tajammul HM, Gouda PS, Siddhalingeshwar I, et al. Effect of alcoholic treated MWCNT on tensile behavior of epoxy composite. Int J Eng Sci Technol. 2016;8(1):57–63.

[27] Ervina J, Mariatti M, Hamdan S. Mechanical, electrical and thermal properties of multi-walled carbon nanotubes/epoxy composites: effect of post-processing techniques and filler loading. Polym Bull. 2016;1–21:2016.

[28] Zabet M, Moradian S, Ranjbar Z, et al. Effect of carbon nanotubes on electrical and mechanical properties of multiwalled carbon nanotubes/epoxy coatings. J Coat Technol Res. 2016;13(1):191–200.

[29] Tang L, Zhang H, Han J, et al. Fracture mechanisms of epoxy filled with ozone functionalized multi-wall carbon nano tubes. Compos Sci Technol. 2011;72(1):7–13.

[30] Yazman S, Samancı A. A comparative study on the effect of CNT or alumina nano particles on the tensile properties of epoxy nano composites. Arab J Sci Eng. 2018. DOI:10.1007/s13369-018-3516-4

[31] Chandra Shekar K, Anjaneya Prasad B, Eswara Prasad N. Strengthening in and fracture behaviour of CNT and carbon fibre reinforced, epoxy-matrix hybrid composite. Sadhana. 2016;41:1443–1461.

ELSEVIER

[ICAMBC 2020]

Three-point bending and impact behaviour of carbon/epoxy composites modified with titanium dioxide nanoparticles

Lokesh Yadhav B.R[1], H.K. Govindaraju[2*], M.D. Kiran[2]and B. Suresha[3*]

[1]Departmentof Mechanical Engineering R.L.Jalappa Institute of Technology, Doddaballapur 561203, India
[2] Departmentof Mechanical Engineering BMS Institute of Technology and Management, Bengaluru 560064, India
[3]Department of Mechanical Engineering, National Institute of Engineering, Mysore 570 008, India

Abstract

Nanofillers can be considered as viable strengthening agent in solid form which can advance the different properties of polymeric materials with minor lessening in the density of composites. Nanofillers are getting model changes the field of material science and polymer based composites. A study on the bending behaviour and impact energy of plain weave bidirectional carbon fabric reinforced epoxy (CE) filled by titanium dioxide (TiO_2) nanoparticles is presented in this paper. Test coupons as per ASTM standards are prepared by simple hand lay-up stacking followed by hot pressing. Mechanical properties for instance flexural strength, modulus and impact energy absorbed are obtained through three-point bend test and Izod impact test following ASTM D790-17 and ASTM D 256-10 (2018) standards. The results showed that the combination of carbon fabric and nano-TiO_2 achieved a significant improvement (around 35%) in impact energy of epoxy material. In terms of mechanical properties, flexural strength increased as the amount of nano-TiO_2 increased, up to a critical point. The outcomes showed that very low loading (up to 1 wt %) of TiO_2 enhances the CE composites resistance from bowing and impact loads. Overall, the nano-TiO_2 is a more cost-effective inorganic filler to effectively improve the flexural properties and impact energy of CE composites. Moreover, the failure mechanism and fractographic features of the three-point bend test failed specimens were examined utilizing the scanning electron microscope.

Keywords: Carbon fabric reinforced epoxy; Titanium dioxide; Hot pressing; Flexural strength; Flexural modulus; Failure mechanism; Impact energy

1. Introduction

In the past few years, conventional materials are supplanted by polymer based composites in light of high strength-to-weight ratio and stiffness to-weight proportions. These composites have interesting advantages, for example, high strength, high stiffness, long life, and low density, resistance to corrosion, superior wear resistance, and environmental friendly [1]. The abundant choice of materials and easy accessibility of thermoplastic and/ thermoset collections as well as their monetary practicality ensure these materials to be used in various sectors like vehicle, sport-goods, aviation, marine, chemical industries, and so forth [2]. Mechanical behaviour of fiber-reinforced polymeric composites specifically depends upon the type and fiber architecture, matrix type, surface treatment of fiber and matrix. Researchers concluded that tensile, flexural, impact, and inter laminar shear strengths were augmented in glass/phenolic modified poly vinyl butyral (PVB)/vinyl ester/epoxy composites [3-6]. It has been perceived that the plain weave fabric made of carbon fiber have preferable tribo-mechanical properties over the long carbon fibers [4]. The diverse weave types of the fiber yarns effects the mechanical properties of the polymer based composites. The carbon fiber mat with three diverse weave viz plain, twill and satin types are independently strengthened with polyetherimide (PEI) matrix and discovered that twill- weave pattern was the paramount from the point of view of flexural strength and/modulus as well as tensile strength and /modulus [5]. Carbon fabric reinforced vinyl ester composite is better than glass fabric reinforced vinyl ester composite as for strength concerned. It draws

an affirmation that high strength carbon fiber fortification roots to enhance the strength of vinyl ester composite [6]. Uniform scattering of nanoparticles in the epoxy resin materials promoted the superior mechanical properties of the composites by interfacing the fiber and matrix productively [7]. The inherent characteristic properties of nanofillers improved the mechanical, electrical, thermal, and magnetic properties of the hybrid composite systems [8, 9]. few of the investigations reveal that the modification of the epoxy matrix material with different organic and inorganic nanoparticles, for example, metal oxide particles, ceramics, montmorillonite, nano-cellulose and so forth., out of which apparent improvement in the tensile and flexural properties can be seen in TiO_2 modified epoxy composite systems [10].

Suresha and Manpinder, meticulous reported that the flexural strength and modulus increments with increased o-MMT nano layers stacking in carbon/epoxy composite [11]. The experimental examination on plain weave woven glass fabric strengthened epoxy stacked with nano TiO_2 concluded that the 1 wt % nano-TiO_2 filled glass/epoxy hybrid composite gave a 37% higher flexural strength and 28% higher flexural modulus contrast with the glass/epoxy composites [12]. Weikang et al. in one of their experimental investigations accentuated the enhancement in mechanical accompanied by thermal properties of glass fiber reinforced epoxy composites with CNTs–Al_2O_3 nanoparticles. As exhibited by the experiments, 0.5 wt % of each CNTs/Al_2O_3 stacking upgrades the flexural modulus, storage modulus, inter laminar shear strength and furthermore the glass transition temperature (T_g) [13]. Yuanxin et al. explored the impact of organo-modified MMT on the mechanical as well as thermal properties of carbon fiber-strengthened composites and are utilized customarily and portrayed that 2 wt % of organo-modified MMT in carbon fiber reinforced epoxy composite depicted the finest improvement in the flexural modulus, storage modulus, and glass transition temperature [14]. From the discussion it is noted that the presence of SiC filler in thermoset composites improved the flexural strength [15]. The outcomes demonstrated that Al_2O_3 and MoS_2 fillers have considerable impact on bending strength and bending modulus of carbon/epoxy composites [16]. In light of the work done on the impacts of the nano-$CaCO_3$ filler on mechanical properties of glass/epoxy composites, it can be concluded that addition of nano-$CaCO_3$ has altogether enhanced the bending properties, fracture toughness, and impact energy of the glass/epoxy hybrid composites [17]. The outcomes depict that, the rate of increase in bending strength with the incorporation of 1.25 wt % lead oxide (PbO) in the luffa fiber-fortified composite was 39.4% when contrasted with the luffa fiber-strengthened composites without nano-PbO and 1.25 wt% PbO modified epoxy composite with luffa fiber as strengthening material yielded superior impact strength [18].

Gradual increment in mechanical strength, for example, compressive strength, modulus, bending strength, impact energy, and surface hardness was seen up to 2 wt % fly-debris loading in the polymer matrix composite [19]. Experimental research revealed that, small amount of nanoclay (2 phr) included into the epoxy of carbon/epoxy composites can improve the flexural strength by 38%. [20]. The low –velocity impact strength data of glass fiber strengthened epoxy with nano-TiO_2 filler indicated that there is a gradual increment in impact strength from 33.52 kJ/m^2 for pristine epoxy to 95.21 kJ/m^2 for 3 wt % of nano- TiO_2 imbued composites [21]. Experimental results investigated by Bulut found that fuse of modest quantity of graphene nanoplatelets in the epoxy resin drastically improved the bending strength and modulus as well as impact strength [22]. The primary goal of this exploration work is to contemplate the mechanical properties, for example, flexural strength, flexural modulus and energy absorbed by conducting three-point bend test and Izod test as per ASTM D790-17 and ASTM D 256-10 (2018) respectively.

2. Experimental

2.1. Materials

Epoxy (Araldite LY 1564) was considered as a matrix material to prepare nanofiller filled hybrid composites in this study. For polymerization, room temperature curing agent (Aradur 22962 grade) was selected. Primary and secondary reinforcements were plain weave carbon fabric (200 gsm, 3K) and nano titanium dioxide (nano-TiO_2) in the final composites. The mean diameter of the carbon yarns was 7 μm, whereas particle size of TiO_2 was about 20-30 nm. The source and selected properties of the constituents of the composites are summarized in Table 1.

Table 1. Characteristics of constituents utilized for preparation of composites in this study

Constituent	designation	Density (g cm^{-3})	Source and Supplier
Epoxy (Araldite 1564)	E	1.1-1.2	HUNTSMAN, M/s CF Composites, New Delhi
Hardener (Aradur 22962)	H	0.89-0.90	HUNTSMAN, M/s CF Composites, New Delhi
Carbon fabric	C	1.8	Japan Toray 3K, Poojan Fibers, Ahmedabad, India
Titanium dioxide	TiO$_2$	3.9	Merck, Quesst International, Bangalore, India

2.2. Fabrication of composites

Epoxy resin (E) was preheated to 60 ^{o}C before anticipated amount of nano-titanium dioxide (TiO$_2$) were introduced and assorted utilizing mechanical stirrer for 25 min. In order to reduce the viscosity of E/TiO$_2$ blend and to enable uniform mixing, the temperature was maintained at 60 ^{o}C for the complete stirring time using a hot plate. Additionally, to remove trapped bubbles from the blend, degassing was performed for 45 min. Subsequently this blend was sonicated for 40 min utilizing ultrasonic processor. Curing agent (H) was poured to the E/TiO$_2$ blend at 100:25 (v/v) and wisely hand mixed to avoid any air bubbles. The composite slabs were prepared by hand lay-up method with plain weave carbon mat stacked upon one other with each layer being prudently impregnated with homogeneous mixture of epoxy resin mix, to produce a slab having dimensions; 250 mm × 200 mm × 3 mm. Hand roller was utilized to smear the resin mix for better wetting of fabric layers and to eradicate bubble formation. The consolidate stack was subjected to a constant pressure of 1MPa to enable uniform spreading of the resin mix into the stacked layers and to facilitate to squeeze out of the excess resin. The composite slab was cured at room temperature for 24 h shadowed by post-curing at 85 ^{o}C for 5 h. The step by step fabrication procedure is illustrated in Fig. 1. The test specimens (Fig. 2) as per ASTM standards for conducting flexure and impact tests were machined utilizing water jet machining. Table 2 shows the final composites prepared with weight percentages of the constituents.
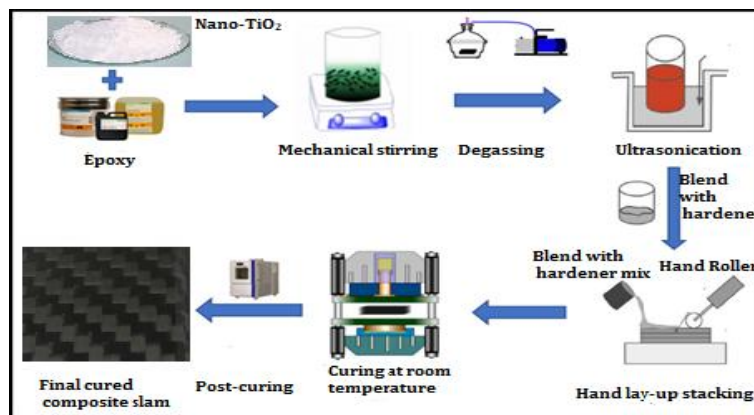

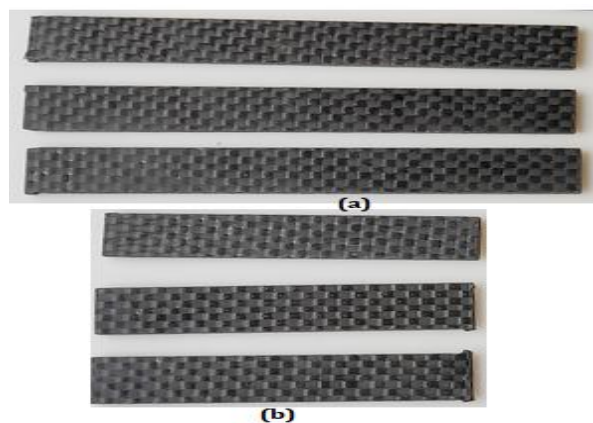Figure 1. Schematic representation of fabrication procedure of CE hybrid composites

Figure 2. Composite specimens for (a) flexural testing, (b) Impact testing

Table 2. Composition of nano-TiO$_2$ filled CE hybrid composites

Composites (Designation)	Carbon Fiber (wt %)	Epoxy (wt %)	TiO$_2$ (wt %)
Carbon Epoxy (CE)	55	45	0
0.25% TiO$_2$ + CE (CE-T1)	55	44.75	0.25
0.5% TiO$_2$ + CE (CE-T2)	55	44.5	0.5
1% TiO$_2$ + CE (CE-T3)	55	44	1
2% TiO$_2$ + CE (CE-T4)	55	43	2

2.3. Density and voids of the composites

The authentic densities of the prepared nanocomposites were calculated following the Archimedes principle. As per the Archimedes principle, when a body is inundated in a fluid, the actual loss in its weight is equivalent to the weight of the fluid it dislodges. To direct the test refined water was taken as the medium. This method is canvassed in ASTM D792 standard. The authentic density (ρ_a) of the composite was calculated by following the equation:

$$\rho_a = \frac{\rho_w \times W_a}{W_a - W_w} \tag{1}$$

where, ρ_w is the mass density of purified water, W_a is the mass of the specimen in air, and W_w is the mass of the sample in water.

The theoretical density (ρ_t) of the composite can be calculated by the following equation [23] :

$$\rho_t = \frac{1}{\left(^{w_f}/_{\rho_f}\right) + \left(^{w_m}/_{\rho_m}\right) + \left(^{w_p}/_{\rho_p}\right)} \tag{2}$$

where, w_f is the mass fraction of fiber, w_m is the mass fraction of matrix, w_p is the weight fraction of nanoparticles, ρ_f is the density of fiber, ρ_m is the mass density of matrix and ρ_p is the mass density of nanoparticles.

Volume fraction of voids (V_v) in % can be calculated from the following equation:

$$V_v(\%) = \frac{\rho_t - \rho_a}{\rho_t} \times 100 \tag{3}$$

where, ρ_t is the theoretical density of the composites, and ρ_a is the authentic density of the composite system.

2.4. Flexural testing

In order to evaluate the bending strength as well as bending modulus of the nanocomposites three-point bending test was accomplished. Specimens were prepared and test was carried out following ASTM D790-17 [24]. The bending test was conducted on a fully automated universal testing machine (100 kN load cell, Kalpak Instruments and Controls, Pune, India). The coupons were machined for dimensions having length of 90 mm, width of 12 mm and 2.5 mm thick. The span to depth ratio of the coupons was kept constant and the value was 16:1. For these samples testing, the load cell of 10 kN was used and the cross head speed of 2.5 mm/ min was kept constant. Five duplicate samples were prepared for each test. Photograph of the test conducted with specimen placed on the fixture is shown in Fig. 3. Scanning electron microscopy was utilized to identify the fracture mechanisms of failed specimens after flexural loading.
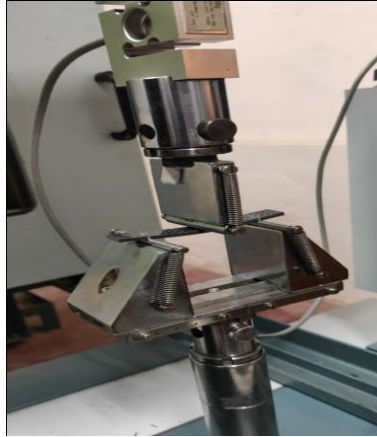
Figure 3. Composite coupon placed in UTM for the conduction of flexural test

2.5 Impact properties

Izod impact test was conducted on impact testing machine (From International Equipments, Fig. 4) with R2 hammer having the impact energy capacity of 0-5.24 J according to ASTM D256-10 [25]. A notch having an angle of 45º was made using a notch cutter restricting the width of the specimen to 10.16 mm. Four specimens of each series of composites of size 64 mm × 12.5 mm were tested, and the average values were reported.

Figure 4 Composite coupon placed in impact testing machine for the conduction of impact test

3. Results and Discussion

3.1. Effect of nanofiller on density and void fraction of CE composites

Density of composite material is very vital in accommodating for the various applications which are sensitive to weight. Composite's density majorly depends upon the relative portion of matrix to reinforcement. Theoretically, density can be found out following the rule of mixture and proportions of the integral materials used in the fabrication of composites. The density evaluated theoretically along with experimentally measured density and void fraction values are listed in Table 3. From the table, it can be observed that theoretical density is higher than that of the measured density and this could be due to the occurrence voids. The measured density of the unfilled CE composites is lowest (1.351 g cm^{-3}). However, among all TiO$_2$ filled CE nanocomposites (CE-T1 to CE-T4), CE filled with 2 wt % TiO$_2$ i.e., CE-T4 sample showed highest measured density of 1.372 g cm^{-3}. Also, the volume fraction of voids in 2 wt % TiO$_2$ filled CE (CE-T4, Table 3) composite is somewhat higher than the other composite

samples investigated. Furthermore, it can be observed that for unfilled CE and CE filled up to 1 wt % of TiO_2 (CE-T3) composites, the voids are < 0.65%. The differences among the measured and theoretical are due to fabrication procedure adopted. Many times, during stages of fabrication, the matrix squeeze out from the mould, and sometimes during fabric stacking have void space due to air tarp in the composite.

Table 3. Densities and voids of nano-TiO_2 filled CE hybrid composites

Composites	Theoretical density (g cm^{-3})	Measured density (g cm^{-3})	Volume fraction of voids (%)
CE	1.365	1.351	1.02
CE-T1	1.368	1.363	0.36
CE-T2	1.371	1.366	0.37
CE-T3	1.377	1.368	0.65
CE-T4	1.389	1.372	1.22

3.2. Flexural properties

In order to recognize how nano-TiO_2 filler would influence on the flexural strength and flexural modulus, the bending tests were conducted for unfilled CE composite and nano-TiO_2 filled CE hybrid composites. Experimental results of nano-TiO_2 filled CE hybrid composites based on different nano-TiO_2 loadings (CE-T1 to CE-T4) are illustrated in Fig. 5. Carbon fabric reinforced epoxy (CE) composite has a flexural strength of 578.03 MPa and when nano-TiO_2 is incorporated as secondary reinforcement in CE composite the values increased up to 1 wt of TiO_2 and it could be due to inform distribution of filler in the CE composites. Further, it can be seen that flexural strength drops with further increase in filler loading (>1 wt %). The hybrid composite with 1 wt % TiO_2 filler have significantly influenced the flexural strength and modulus of CE composite. The flexural strength and flexural modulus of 1 wt % TiO_2 filled CE increased by 13% and 18.5% respectively compared to unfilled CE composite strength (578.03MPa) and flexural modulus (32.67GPa) respectively.
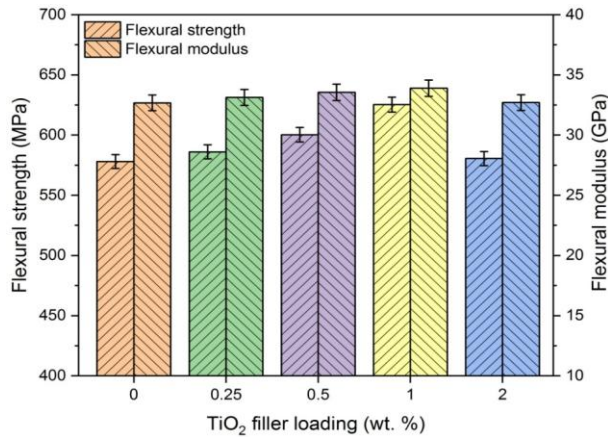

Figure 5. Flexural strength and modulus of nano-TiO_2 filled CE hybrid composites

The strength enhancement of any composite material is governed by the reinforcement and filler and matrix properties as well as on the fiber-filler weight fraction [27-31]. From figure 3, it is seen that for CE composite with 1 wt % TiO_2 (CE-T3) filler displayed best flexural strength (625.24 MPa) and flexural modulus (33.89 GPa) compared to unfilled CE composite. The presence of nano-TiO_2 in CE composite played a vital role in enhancing the mechanical properties. Load transfer and elastic deformation from the matrix to the nanofillers are directed by the fiber/matrix interface [32]. In the present work, the improvement in bending properties is owed to the improved dispersion and large interface areas of nanoparticles in contact with epoxy matrix, which considerably enhances the effective stress transfer from the matrix to the nanoparticles. The increased surface area of nano-TiO_2 particles led to enhanced interface for energy absorption. This produces a good interlocking mechanism with the surface of fiber, filler and the matrix. The rigid nature of TiO_2 in CE composite prevented the deformation of the epoxy material. Up to 1 wt % of nanofiller loading, the nanoparticles are able to resist transverse loads without matrix deformation. On the other hand, when fillers exceed more than 1 wt %, large number of nanoparticles participate leading to

agglomeration in the final composite. Finally, these results indicate that nano-TiO_2 loading of 1 wt % is optimum for improving the bending properties of CE hybrid composites. In this work, due to the improved rigidity, better interface area, and improved stiffness of the added nano-TiO_2 particles strongly contributed to the improvement of the bending properties of CE hybrid composites.

3.3. Impact strength

Izod impact test was carried out to apprehend the effect of nano-TiO_2 filler on the impact strength of CE hybrid composites. Fiber architecture played a major role in augmenting the impact strength offered by the epoxy based composite, and is always related to the toughness of the material. Alignment of fiber and better distribution of nano-TiO_2 in the epoxy matrix helped in improving the impact strength of CE hybrid nanocomposites. This aids it with better load transfer and hence promotes stress transfer that is being done via fiber to matrix with the application of the load. The impact strength of CE composites on the base of nano-TiO_2 appears as a function of filler loading (Fig. 6). Well dispersed TiO_2 nanoparticles notably increment the impact strength of CE hybrid nanocomposites. The increment of toughness might be expected to micro-plastic deformation around the TiO_2 nanoparticles. The filling of CE composite by nano-TiO_2 has got beneficial outcome to toughness too. Nevertheless in some cases, the energy absorbed by the CE composite declines with inculcation of fillers, and is attributed to the brittleness of the carbon fiber used [33]. Better bonding developed between fiber and matrix which can result in the increment of impact resistance.

Fig. 6 depicts the influence of nano-TiO_2 filler on the Izod impact strength of CE hybrid nanocomposites. With an increase in loading of nano-TiO_2 filler in CE composite, the impact strength upsurges up to a critical loading and declines subsequently. The impact strength of the nano-TiO_2 filler modified CE composite accomplishes its finest value at critical loading of 2 wt %. The enhancement in the impact strength was about 35% greater than that of unfilled CE composite and drops thereafter i.e., at 2 wt % of nano-TiO_2 loading. Furthermore, at 2 wt % loading of nano-TiO_2 filler, a significant drop in the impact strength was seen, but marginal improvement of 4.7% over the CE composite was noted.
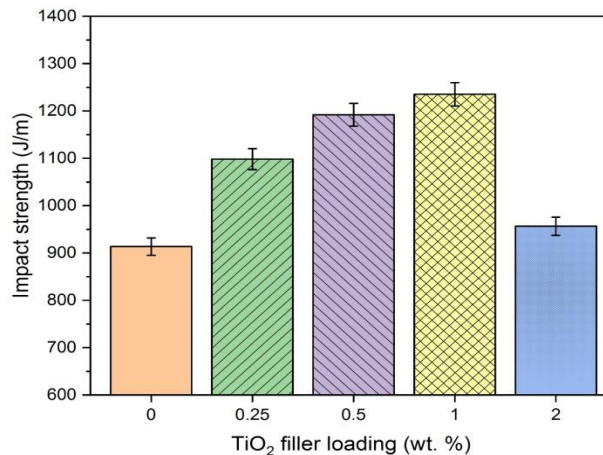

Figure 6. Impact strength of nano-TiO_2 filled CE hybrid composites

Runqin et al. [34] contemplated a progression of epoxy nanocomposites on impact behaviour and reported that up to certain critical loading of TiO_2 coated/CNT in poly(methyl methacrylate) (PMMA) matrix increased the impact strength of composites. At higher filler stacking, the impact strength drops unexpectedly. Moreover, the impact strength of 20 wt % TiO_2 changed PMMA is not as much as that of pristine PMMA. These outcomes can be interconnected with the stress concentration factors. Runqin et al. [34] had additionally conveyed that, the CNTs (>10%) into PMMA caused Izod impact strength to continuously diminish and associated to the decrease of interaction because of agglomeration of the CNTs. In this work, the upgrade in impact strength at lower stacking nano-TiO_2 filler is attributable to uniform distribution of TiO_2 that retains larger surface area at the filler/matrix interface. At higher stacking due to agglomeration diminished the impact strength of CE composite. Besides, as accumulated nano-TiO_2 particles tend to induct additional deformities viz., entrapment of minute air repositories in the epoxy. Huang et al. [35] expressed the comparative sort of impact for the clay/epoxy nanocomposites.

3.4. Fractography

In scanning electron microscope, micrographs have a huge profundity of field yielding a characteristic 3D appearance helpful for understanding the surface topography of multiphase composites. Carbon fabric strengthened epoxy (CE) composite in Fig. 7a has indicated the complete failure of specimen under bending load. The failure pattern along the width direction is nearly angular shape (Fig. 7a). Fig. 7a shows the crack in the matrix as well as the deboning between fiber and matrix. Moreover, fractographic features like pull-out, separation, debonding of a portion of the warp fibers and bowing of weft fibers can be seen which shows the poor interfacial adhesion of the carbon fibers with the epoxy matrix. Tearing of the weft fibers, and cut fiber tip is a plane round and perpendicular to the applied load and clean fiber surface can be found in Fig. 3b which could be because of the absence of epoxy in the fibers. Furthermore, figure 7b shows the huge degree of the fiber crack; void space and scarcely any fibers where the resin couldn't enter in the heap of fiber strands. This was principally a direct result of the weak bonding between the constituent carbon fiber and the epoxy matrix.
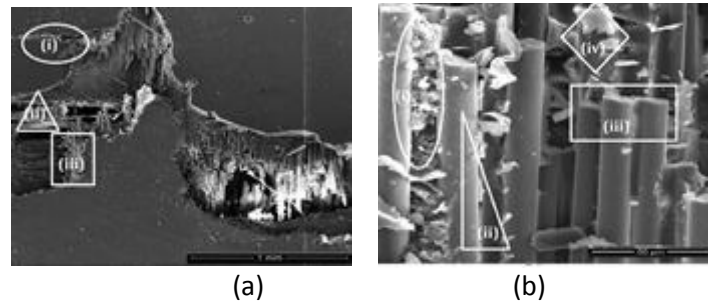

(a)   (b)

Figure 7. Micrographs of fractured CE specimen showing (a) lower maginfication, 100 X:(i) matrix crak opening path; (ii) pull-out of weft fibers; (iii) broken warp fibers, (b) higher maginfication, 500 X: (i) network of cracks in the matrix; (ii) debonding of warp fiber; (iii) broken fiber tip; (iv) voids
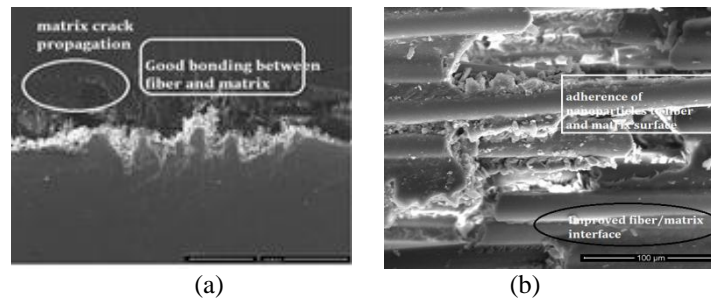

(a)   (b)

Figure 8. Micrographs of fractured 1 wt % TiO$_2$ filled CE specimen: (a) lower maginfication, 100X (b) higher maginfication, 500 X

Conversely, Fig. 8 shows good bonding between fibers, nanofillers and epoxy and practically no indications of fibers debonding, separation or pull-out mechanisms at the nano-TiO$_2$ filled CE composite fractured surface after flexural loading. This outcome proposes that interfacial adhesion between the carbon fibers, TiO$_2$ nanoparticles and epoxy matrix has acquired considerably more strong and solid upon consistently disseminated nanoparticles within the epoxy matrix. The modified epoxy with nanoparticles prompted increment in the interfacial adhesion among fiber and modified epoxy and further make a decent interlocking mechanism with the surface of the matrix. This phenomenon could be clarifying the explanation of bowing of weft fibers, as seen in Fig. 8b. Moreover, during the preparation of composites, the spaces between weft and twist fibers increment which empower modified epoxy to enter and occupy the spaces and consequently increment the area contact between the fiber and matrix and upgrade the interfacial adhesion, as depicted in Fig. 8b. These reasons could be credited to upgrade the interfacial adhesion and increment the integrity between the fibers and matrix as a bulk composite and lessen the defragment of fiber from the matrix material.

4. Conclusions

The influence of nano-TiO$_2$ filler loading on mechanical properties of carbon fabric reinforced epoxy (CE) hybrid composites was studied. The enhancements in the mechanical properties like bending properties and impact strength of the unfilled CE was achieved with lower nano-TiO$_2$ filler loadings. Some important conclusions of this research work are as follows:

- The presence of voids gives rise to the difference in theoretical and experimental density of the composites. The volume fraction of voids present in 2% TiO$_2$ filled composite is slightly higher than other filler loaded CE hybrid nanocomposites.
- Lower nanofiller loading (1 wt %) in the matrix develops a better interface, which aids in transferring the load from fiber and nanofillers to the matrix and thus improved the flexural properties and impact strength of CE composite. Furthermore, this improvement was attributed to the enhanced rigidity and stiffness of the composite by addition of nano TiO$_2$ particles.
- The higher loading of nano-TiO$_2$ filler in CE (> 1 wt %) results in an aggregation of nanoparticles in the epoxy matrix thereby decreased mechanical properties were observed in 2 wt % TiO$_2$ modified CE hybrid nanocomposites.
- On account of unfilled CE composite, the fractured features were debonding, tearing, and separations of warp fibers and also pull-out of weft fibers because of the poor interfacial adhesion between fiber and matrix. On the other hand, nano-TiO$_2$ modified epoxy with carbon fiber hybrid composite indicated improved adhesion between the fiber and nanoparticles modified epoxy. This modified epoxy with nanofillers and impregnated to the carbon mat had the option to carry the bowing load during the test. This was the primary explanation for the high flexural strength and modulus of TiO$_2$ filled CE hybrid nanocomposites.
- The combination of carbon fabric and titanium dioxide achieved a significant improvement (approx. 35%) in impact energy of the epoxy composite.

References
[1] Tserpes KI and Labeas GN, Compos Struct; 87(2009), pp. 358–369.
[2] Mallick, P.K. ed., 1997. Composites engineering handbook. CRC Press.
[3] Vishwanath, B., Verma, A.P. and Rao, C.V.S.K., Wear, 167 (1993), pp.93–99.
[4] D.C. Evans, J.K. Lancaster; RAE Technical Report (1978), 78147.
[5] Bijwe, J. and Rattan, R. Wear, 263 (2007), pp. 984–991.
[6] Suresha, B. and Kumar, K.N.S, Materials and Design, 30 (2009), pp. 2056– 2060.
[7] Wang H, Xian G, Li H., Compos Part A, 76 (2015), pp.172–80.
[8] Saba N, Paridah MT, Abdan K, Ibrahim NA, Construction and Building Materials, 123 (2016), pp.15–26,
[9] Kumar K, Ghosh PK, Kumar A, Compos Part B: Eng, 97 (2016), pp. 353–60
[10] Al-Turaif HA. Progress in Organic Coatings, 69 (2010), pp. 241–246.
[11] B Suresha and Manpinder S Saini, J Compos Mater, 50 (2015), pp. 3589-3601.
[12] S.Nallusamy, Journal of Nano Research, 40 92016), pp. 99-104.
[13] Li Weikang, Anthony D, Junwei Z, Composite Science Technology, 103 (2014), pp. 36–43.
[14] Yuanxin Z, Farhana P, Vijaya KR, Jounel of Material Processing Technology, 191(2007), pp. 347–351.

[15] Suresha B, Chandramohan G, Sadananda Rao PR, Sampathkumaran P, and Seetharamu S, Journal of Reinforced Plastics and Composites, 26 (2007), pp.565-578.

[16] Suresha B, and Manpinder Singh S, International Journal of Computer Aided Engineering and Technology, 10 (2018), pp. 89-101.

[17] Zulfli NM, Bakar AA. and Chow WS, Journal of Reinforced Plastics and Composites, 32 (2013), pp.1715-1721.

[18] Ashok KG, Kalaichelva, K, and Damodara, Journal of Natural Fibers, 1 (2020) pp.1-18.

[19] Sathishkumar GK, Rajkumar G, Srinivasan K, and Umapathy MJ, 37 (2018), pp.90-104.

[20] Xu Y and Hoa SV, Composites Science Technology, 68 (2008), pp. 854–861.

[21] Thiagarajan A, Madavan P, Parisithu B, Loganathan P, and Aravint, B, International Journal of Technical Research and Applications, 37 (2016), pp. 78-82.

[22] Bulut, M. Composites Part B Engineering, 122 (2017), pp. 71–78.

[23] Autar K Khaw, Mechanics of composite materials (second Ed.). 2006, CRC Press, Taylor & Francis Group.

[24] Standard, A.S.T.M., 2017. D790-17 standard test methods for flexural properties of unreinforced and reinforced plastics and electrical insulating materials. *West Conshohocken, PA: American Society of Testing* Materials.

[25] Standard, A.S.T.M., D256-10, 2010. Standard test methods for determining the izod pendulum impact resistance of plastics. ASTM International, West Conshohocken, PA.Withers GJ, Yu Y, Khabashesku VN, et al. Composites Part B, 72(2015): 175–182.

[26] Emrah B, Elcin K and Metin T. Composite Science Technology, 67(2007), pp. 3394–3403.

[27] Railsback LB, Geology, 31(2003), pp.737-740.

[28] Suresha, B, Varun CA, Indushekhara NM, and Vishwanath HR, IOP Conference Series: Materials Science and Engineering, 574 (2019), pp. 012010.

[29] Manjunath, M, Renukappa, NM, and Suresha B, Journal of Composite Materials, 50(2016), pp.1109-1121.

[30] Krishnan GS, Babu LG, Kumaran P, Yoganjaneyulu G, and Raj JS, Materials Research Express, 7(2019), pp.015310.

[31] Ganesh S, Gunda Y, Mohan SRJ, Raghunathan V, and Dhilip JDJ, Journal of Natural Fibers, (2020) pp.1-11.

[32] D.J. Green, P.S. Nicholson, J.D, Journal of Materials Science, 14 (1979), pp. 1657.

[33] Shafi UK, Kosar I, Arshad M, et al. Composites Part A, 42(2011), pp. 253–264.

[34] Runqin, H., Fenglian, N. and Qiuxiang, C., Journal of Experimental Nanoscience, 12 (2017), pp.308-318.

[35] Huang H, Talreja R., Composites Science and Technology. 65 (2005), pp. 1964-1981.

Fracture toughness study of epoxy composites reinforced with carbon fibers with various thickness

M.D. Kiran [a,*], H.K. Govindaraju [a], B.R. Lokesh Yadhav [b], B. Suresha [c], N. Keerthi Kumar [a]

[a] Department of Mechanical Engineering, BMS Institute of Technology and Management, Bengaluru 560064, India
[b] Department of Mechanical Engineering, R.L. Jalappa Institute of Technology, Doddaballapur 561203, India
[c] Department of Mechanical Engineering, National Institute of Engineering, Mysore 570 008, India

ARTICLE INFO

ABSTRACT

The objective of this paper is to evaluate the fracture toughness of carbon fibre/epoxy composite with different thickness of carbon fibers. The composites were fabricated using hand layup technique by resin infusion of 200gsm, 400gsm and hybrid carbon fabric lamina. The fracture toughness of composites with carbon hybrid carbon fibers were studied using single edge notched beam method at the room temperature (25 °C). From the experimental results it was found that epoxy composites reinforced with 200gsm carbon fiber better fracture toughness compare to composites reinforced with other fibers. And impact strength of epoxy composites with carbon fibers and hybrid carbon fibers also studied for comparison.
© 2021 Elsevier Ltd. All rights reserved.
Selection and peer-review under responsibility of the scientific committee of the International Conference on Smart and Sustainable Developments in Materials, Manufacturing and Energy Engineering.

1. Introduction

The thermoset polymer composites have extensive application in structural, automotive due to their better mechanical properties than thermoplastic polymer composites. Epoxy resin have numerous advantages as matrix of composites for structural applications largely due to their high stiffness, comparatively high temperature resistance and better chemical and corrosion resistance. The main disadvantage of epoxy as matrix is its inherent brittleness which leads to its notch sensitive and low toughness of composites. Polymer composites reinforced with carbon fiber possess better ductility than other fiber reinforced composites [1]. In recent years it has been developed that the carbon fiber reinforced polymer composites exhibit improved mechanical and thermal properties than the pure polymers [2]. Carbon fiber reinforced polymer composites are promising materials for light weight and low-cost components of aerospace and automotive application [3]. Also, these improvements are attained using conventional fabrication techniques without any defects in processing which leads to effect on density of polymer matrix composites [4]. The polymer composites reinforced with laminated fiber such as epoxy/carbon fiber composites are extensively used in automotive, structural and aerospace industries [5,6]. They exhibit high strength-to-weight and stiffness-to-weight ratios. These polymer composites have exclusive advantages over monolithic materials, such as high stiffness, high strength, long fatigue life, better resistance to wear and corrosion, and better environmental stability [7]. Better impact strength is one significant parameter for mechanical toughness or resistance to fracture of materials [8–10]. Carbon, glass and silk fibers reinforced epoxy composites can lead to better impact strengths more than 100 kJm^{-2}. Whereas carbon fiber and glass fiber reinforced composites exhibit clear dependence on volume fraction of reinforcement. The epoxy composite reinforced with T800-400gsm carbon fiber exhibits better mechanical properties under various load of carbon fiber and epoxy [11]. Carbon fiber of 400gsm have excellent strengthening effect of both tensile strength and flexural properties of carbon fiber epoxy composites [12].

From the literature survey it has been observed that very few research works was carried out on epoxy composites reinforced with different carbon fabric grades with the application of hand layup method. There is a lot of opportunity for improving the mechanical properties of epoxy composites using carbon fabric with different twill structures. Hence in this present research work epoxy composites reinforced with carbon fibers of different 200ghsm, 400gsm and combination of both were fabricated. The basic mechanical properties such as tensile and impact and fracture toughness of fabricated composites were studied and the effects of fiber upon the fracture properties were measured.

* Corresponding author.
  E-mail addresses: kiranmd@bmsit.in, kiranmdg@gmail.com (M.D. Kiran).

M.D. Kiran, H.K. Govindaraju, B.R. Lokesh Yadhav et al.

2. Materials

2.1. Materials used

Out of all fabrication process of polymer matrix composites, hand lay-up method is the one of the most widely used due to its low cost, simple and higher fibre contents and longer fibres as compared to other processes, hence it was suitable for present work and followed the same. The constituent materials for this research work were epoxy resin (Araldite 1564), Hardener (Aradur 22962) and carbon fabric (200 and 400gsm thick).

Initially preheated about 60 °C Epoxy resin was mixed with Hardener in the ratio of 100:25 (v/v) and carefully stirred with mechanical stirrer for uniform mixing and to avoid formation of air bubbles. Plain weave carbon fabrics were discretised to prepare composite plates with the dimension of 250 mm × 200 mm × 3 mm. To achieve 3 mm thickness 12 layers of 200gsm carbon fabrics were stacked one upon other, each layer was impregnated with epoxy resin. For complete wetting of carbon fabric with epoxy mixture and to avoid the formation of bubble, hand roller was passed over every layer. Constant pressure of 1 MPa was applied on consolidated stack to ensure evenly spreading of resin throughout the stacks. The same procedure was followed to prepare for 400gsm carbon fabric laminate composite, which consists of 12 layers of fabric. In hybrid composite preparation 3 layers of 200gsm were stacked at both ends and 4 layers of 400gsm carbon fabric were stacked at the centre and rest of the process remains unchanged. The composite plates were left for curing at room temperature around 24 h [13]. Water jet machining was adopted to prepare composites according to ASTM standards of experiments shown in Figs. 1 and 2. Before conducting testing, composites were subjected to post curing at 80 °C for 1 h to eradicate water content present in it if any. The Table 1 shows the details of composites with respect of designation and type carbon fabric reinforcement used in the present investigation.

3. Experiments

3.1. Tensile test

To determine the ultimate tensile strength and young's modulus of the composites tensile test has been conducted. The test specimens were prepared as per ASTM D638 standard of dimensions 165 mm × 19 mm × 4 mm [14]. The tensile test was carried
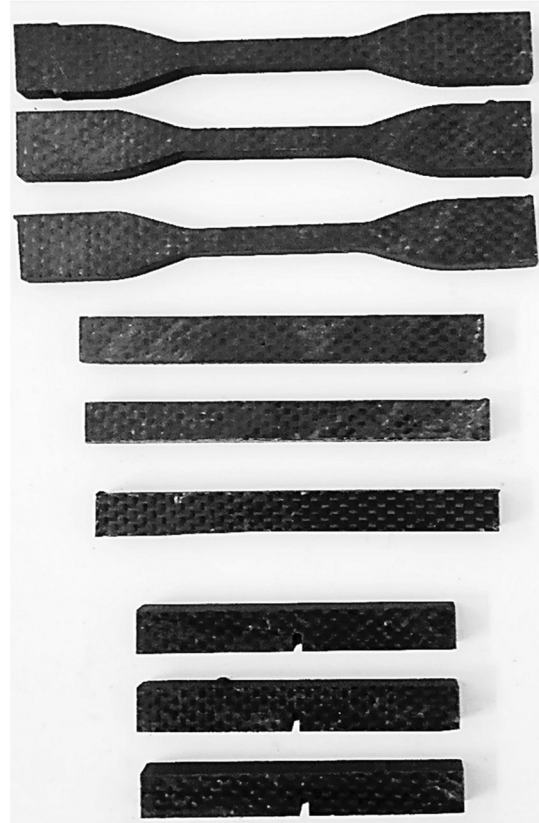
Fig. 2. Composite specimens for (a) Tensile testing, (b) Impact testing, (c) Fracture toughness testing.

Table 1
Composition of Laminates.

Carbon Fabric Used	Carbon Fiber (wt %)	Epoxy (wt %)
200GSM	55	45
400GSM	55	45
200 + 400 GSM	55	45

out on Kalpak-100K computerized universal testing machine under displacement control with a crosshead speed of 2.5 mm/min (Figs. 3–7).
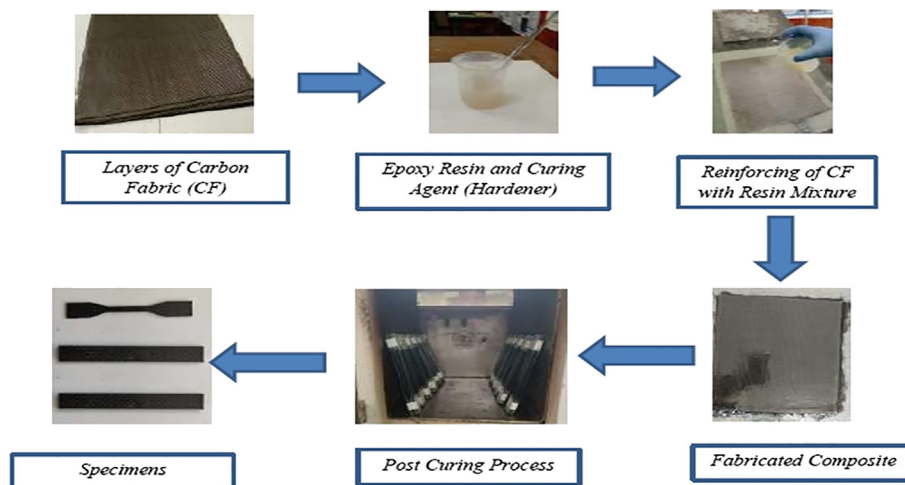
Fig. 1. Schematic representation of composite fabrication process.

M.D. Kiran, H.K. Govindaraju, B.R. Lokesh Yadhav et al.

3.2. Impact test

The impact strength of the composites was studied using the Izod impact test as per ASTM D256 standard with specimen dimensions of 63.5 mm × 12.7 mm × 3.2 mm [15]. The impact test was carried out on a computerized impact testing machine made International equipment, Mumbai, with the capacity of up to 25 J releasing angle of the pendulum 150°.

3.3. Mode I fracture test

Fracture toughness of the composite studied using a three-point bending test method in the form of critical-stress-intensity factor K_{IC} under plain strain condition. The single edge notched beam (SENB) specimen with pre-crack used to determine fracture toughness as per the ASTM D5045-99 [16]. The notched specimen comprises pre-crack as per standard was loaded using a three-point bending test [17]. The pre-crack introduced using sharp razor blade and the depth of the crack must be two times larger than width of the crack.

4. Results and discussion

The Table 2 indicated the Ultimate Tensile Strength, Young's modulus values, Impact strength and Fracture toughness of epoxy composites reinforced 200gsm, 400gsm and hybrid carbon fabric.

As the Table 2 indicated, the epoxy composites reinforced with 200gsm carbon fiber exhibits better tensile strength and young's modulus of shown in Fig. 8. From the results, the ultimate tensile strength of 200gsm carbon fabric reinforced composites shows 17% better than 400gsm and 13% better than hybrid carbon fabric reinforced composites. Also, hybrid carbon fabric reinforced composites exhibit 12% better than 400gsm carbon fabric reinforcement.

Impact strength of epoxy composite reinforced with 200gsm, 400gsm and hybrid carbon fiber shown in Fig. 9(a). Epoxy composite reinforced with 200gsm carbon fiber shows 15% better impact strength as compared 400gsm and 6% better than hybrid carbon fiber reinforced composites. Also, impact strength of hybrid carbon fabric reinforced composites 8% greater than 400gsm carbon fabric reinforcement.

Fracture toughness of epoxy composite reinforced with 200gsm, 400gsm and hybrid carbon fiber shown in Fig. 9(b). Epoxy

Fig. 4. Impact test experimental setup.
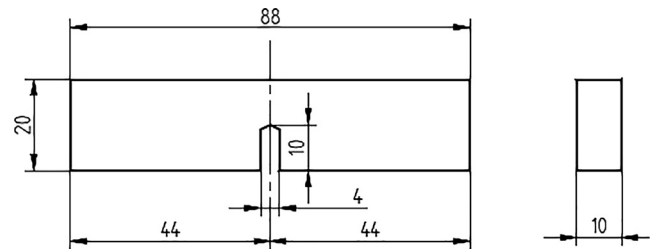
Fig. 5. SENB Specimens for fracture test (all dimensions are in mm).

Fig. 6. Three-point Bending setup for Fracture toughness test.

Fig. 3. Tensile test experimental setup.

composite reinforced with 200gsm carbon fiber exhibits better fracture toughness as compare to other fiber reinforced composites. The reinforcement of carbon fiber of thickness 200gsm with epoxy matrix shows 17% improved fracture toughness as

M.D. Kiran, H.K. Govindaraju, B.R. Lokesh Yadhav et al.

Fig. 7. Fractured specimens after testing.

compared to 400gsm carbon fiber reinforcement and 40% better fracture toughness than the hybrid carbon fiber reinforcement.

5. Conclusions

The mechanical properties and fracture toughness of carbon fabric reinforced epoxy (CE) composites with various thickness of carbon fiber fabric was studied. The epoxy composites reinforced with 200gsm carbon fiber fabric exhibits better mechanical properties as compared to 400gsm and hybrid carbon fiber reinforced epoxy composites due to 200gsm carbon fiber fabric have strong blending of filaments. The fiber architecture has a smaller amount effect on the density of the composites and effect seriously on the deformation and strength CE composites. Structure of weaves and integral properties of carbon fiber dominated the performance of composites. Therefore epoxy composites reinforced with lower thickness carbon fabric exhibits better mechanical properties and fracture toughness.
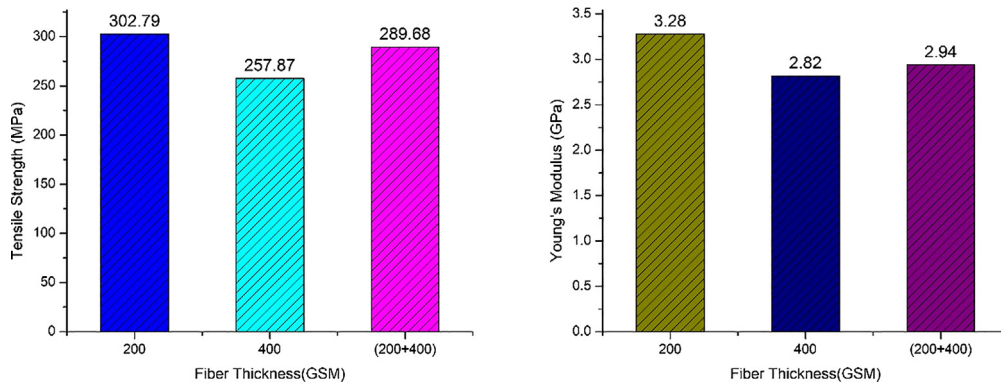
Fig. 8. Ultimate Tensile Strength and Young's modulus of composites.
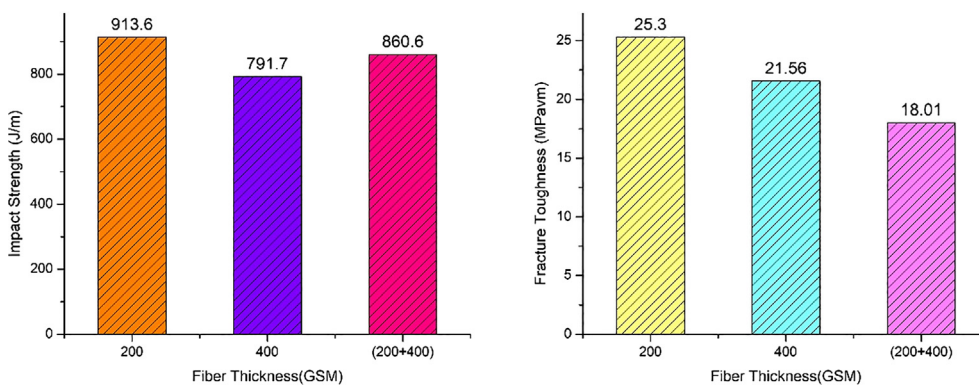
Fig. 9. (a) Impact Strength and (b) Fracture toughness of composites.

Table 2
Mechanical properties and Fracture toughness of composites.

Composites	Tensile Strength (MPa)	Young's Modulus (GPa)	Impact Strength (J/m)	Fracture Toughness (MPa$\sqrt{}$m)
200GSM	302.79	3.28	913.6	25.3
400GSM	257.87	2.82	791.7	21.56
200 + 400 GSM	289.68	2.94	860.6	18.01

CRediT authorship contribution statement

M.D. Kiran: Writing - original draft. **H.K. Govindaraju:** Supervision. **B.R. Lokesh Yadhav:** Data curation. **B. Suresha:** Conceptualization, Supervision. **N. Keerthi Kumar:** Writing - review & editing.

Declaration of Competing Interest

The authors declare that they have no known competing financial interests or personal relationships that could have appeared to influence the work reported in this paper.

References

[1] T.D. Jagannatha, G. Harish, Mechanical properties of carbon/glass fiber reinforced epoxy hybrid polymer composites, Int. J. Mech. Eng. Robotics Res. 4 (2) (2015).

[2] K. Zhang, Y. Gu, M. li, Z. Zhang, Effect of rapid curing process on the properties of carbon fiber/epoxy composite fabricated using vacuum assisted resin infusion molding, Mater Design 54 (2014) 624–631.

[3] A. Manalo, T. Aravinthan, A. Fam, B. Benmokrane, State-of-the-Art review on FRP sandwich systems for lightweight civil infrastructure, J. Compos. Construct. 21 (1) (2017) 04016068.

[4] I. Taraghi, A. Fereidoon, F. Taheri-Behrooz, Low velocity impact response of woven Kevlar/epoxy laminated composites reinforced with multi-walled carbon nanotubes at ambient and low temperatures, Mater Design 53 (2014) 152–158.

[5] M. Tehrani, A.Y. Boroujeni, T.B. Hartman, T.P. Haugh, S.W. Case, M.S. Al-Haik, Mechanical characterization and impact damage assessment of a woven carbon fiber reinforced carbon nano-tube-epoxy composite, Compos. Sci. Technol. 75 (2013) 42–48.

[6] S.S. Shams, R.F. El-Hajjar, Overlay patch repair of scratch damage in carbon fiber/epoxy laminated composites, Compos. Part A 49 (2013) 148–156.

[7] K.I. Tserpes, G.N. Labeas, Meso mechanical analysis of non-crimp fabric composite structural parts, Compos. Struc. 87 (4) (2009) 358–369.

[8] G. Wu, L. Ma, Y. Wang, L. Liu, Y. Huang, Interfacial properties and impact toughness of methylphenyl silicone resin composites by chemically grafting POSS and tetraethylenepentamine onto carbon fibers, Compos. Part. A-Appl. 84 (2016) 1–8.

[9] G. Davies, R. Olsson, Impact on composite structures, Aeronaut. J. (1968) 108 (1089) (2004) 541–563, https://doi.org/10.1017/S0001924000000385.

[10] M. Hagenbeek, Impact properties, Fiber Metal Laminates, Springer, Dordrecht, 2001.

[11] B. Muralidhara, S.P. Kumaresh Babu, B. Suresha, The effect of fiber architecture on the mechanical properties of carbon/epoxy composites, Mater. Today: Proceed. 22 (Part 4) (2020) 1755–1764.

[12] B. Muralidhara, S.P. Kumaresh Babu, B. Suresha, Utilizing vacuum bagging process to prepare carbon fiber/epoxy composites with improved mechanical properties, Mater. Today: Proceed. 27 (Part 27) (2020) 2022–2028.

[13] B. Suresha, M.S. Saini, Fabrication and mechanical characterisation of carbon fabric reinforced epoxy with alumina and molybdenum disulfide fillers, Int. J. Computer Aided Eng. Technol. 10 (1/2) (2018).

[14] ASTM D638-14, Standard Test Method for Tensile Properties of Plastics, ASTM International, West Conshohocken, PA, 2014.

[15] ASTM D256-10(2018), Standard Test Methods for Determining the Izod Pendulum Impact Resistance of Plastics, ASTM International, West Conshohocken, PA, 2018.

[16] ASTM D5045-99, Standard Test Methods for Plane-Strain Fracture Toughness and Strain Energy Release Rate of Plastic Materials, ASTM International, West Conshohocken, PA, 1999.

[17] M.D. Kiran, H.K. Govindaraju, T. Jayaraju, Evaluation of fracture toughness of epoxy-nickel coated carbon fiber composites with Al2O3 nano filler, Advances in Polymer Composites: Mechanics, Characterization and Application, AIP Conf. Proc. 2057:2018, 020002-1–020002-5; 10.1063/1.5085573.

Performance and Emission Characteristics of C.I Engine Fuelled with Hybrid Biodiesel

Veerbhadrappa Telgane[a,d], Sharanappa Godiganur[a], N. Keerthi Kumar[b] and T.K. Chandrashekar[c]

[a]*School of Mech. Engg., REVA University, Bengaluru, Karnataka, India*
[b]*Dept. of Mech. Engg., BMS Institute of Tech. and Management, Bangalore, Karnataka, India*
[c]*Dept. of Mech. Engg., MIT Mangaluru, Karnataka, India*
[d]*Corresponding Author, Email: Veerbhadrappa@reva.edu.in*

ABSTRACT:

In the present experimental investigation, the performance and emission characteristics of four stroke single cylinder water-cooled DI diesel engine using dual hybrid biodiesel is evaluated. Dual hybrid biodiesel produced from Simarouba Oil Methyl Ester (SuOME) and Jatropha Oil Methyl Ester (JOME) is used as a fuel to run the engine. Both the methyl esters are mixed in equal % and blended with diesel (B20 to B100). The fuel properties such as kinematic viscosity, calorific value, flash point, carbon residue and specific gravity were found for the prepared biodiesel. The results showed that B20 has almost closer brake thermal efficiency compared to that of the conventional diesel fuel. Except NO_x, B100 has recorded very less emission of CO, CO_2 and HC compared to that of diesel fuel.

KEYWORDS:

Hybrid biodiesel; Simarouba Oil Methyl Ester; Jatropha Oil Methyl Ester; Diesel engine; Performance; Emission

NOMENCLATURES:

B20   10% JOME, 10% SuOME and 80% diesel by volume
B40   20% JOME, 20% SuOME and 60% diesel by volume
B60   30% JOME, 30% SuOME and 40% diesel by volume
B80   40% JOME, 40% SuOME and 20% diesel by volume
B100   50% JOME and 50% SuOME

1. Introduction

Energy plays a substantial role in enhancing economic development of any country and the demand for conventional fuels remains to upsurge over the decades. The exhaustion of world oil reserves leads to search for better promising alternative substitute [1]. In this regard, it is anticipated that originated fuels will replace 20% of conventional diesel fuels by 2022. Biodiesels are produced from both edible and non-edible feedstock but the use of edible oil may cause scarcity of edible oil globally [2]. Hence, biodiesel produced from non-edible feedstock has been considered as a better substitute for diesel fuel. Though it is true, many factors like adequacy, type and harvesting capacity of plants has to be considered [3], biodiesels produced from various feedstocks may have different advantages. Hence, in the recent days it is necessary to obtain the benefits of biodiesels produced from one or more feedstock. Many researchers have adopted the concept of mixing of biodiesels with Jatropha and sesame oil methylesters at different ratios to run the diesel engines. It has been observed that due to mixing of two different feed stocks, there is an enhancement in physicochemical properties.

There is also an increase in heating value with reduced viscosity of blends relative to biodiesel produced from single feedstock. Results also revealed that, there is a reduction in CO and other emissions with slight increase in Brake Specific Fuel Consumption (BSFC). In general, it is observed that use of biodiesel up to 40% with diesel fuel in engine gives the results close to those of diesel fuels. Bora et al [4] made use of biodiesel produced from three different feedstock namely, polonga, koroch and Jatropha curcas, to study the performance of diesel engine. The results showed reduced performance compared to diesel fuel. However, mixed biodiesel showed that it had superior engine performance when compared to individual biodiesels. Further, reduction in BSFC of 3.65, 0.51 and 3.64% is observed when polonga, koroch and Jatropha curcas biodiesel is respectively used. Same trend is observed for CO, HC and smoke opacity with reverse trend for the brake thermal efficiency (BTE).

Padhee et al [5] reported that blending 20% Jatropha curcas biodiesel with diesel fuel results in higher BTE and exhaust gas temperature (EGT) but lower BSFC due to its higher viscosity and oxygen content. In addition, the CO emission is lower for all Jatropha curcas biodiesel-diesel blends. However, the nitrogen oxide (NO_x) emissions are higher for these blends. Vedharaj et al [6] analyzed the engine performance for 25% and 50% blends of ceiba pentandra. Higher BTE is observed with B50 due to higher combustion temperature and therefore NO_x emission increases. To reduce the NO_x emissions, urea-selective non-catalytic reduction system is adopted in the exhaust pipe. Simarouba biodiesel has been explored by many researchers as a potential substitute for diesel fuel. Ram et al [7] had studied the physical

properties of Simarouba fruit and concluded that Simarouba biodiesel can be a better substitute for diesel fuels. Keerthi et al [8] had used Simarouba oil methyl ester to study the effect of different combustion chamber. Due to higher viscosity of Simarouba oil compared to diesel fuel, it is observed that there is a reduction in performance of the engine. To increase the engine performance, various combustion chamber shapes have been adopted.

Even though many studies have been carried out concerning diesel engines and use of biodiesel, there is a lack of studies on the mixture of Jatropha and Simarouba biodiesel. In this paper, an in-depth investigation is carried out on the engine performance and emissions of biodiesel-diesel fuel blends at a ratio from 105 to 50% Jatropha curcas-Simarouba biodiesel. These test fuel samples are designated as B20, B40, B60, B80, and B100. The engine performance namely SFC, BTE and emission characteristics like CO, CO_2, HC, O_2 and NO_x are investigated for these biodiesel blends.

2. Materials and methodology

In the first phase of the work, esterification of selected oils and mixing of both the oil was done on volume basis and their properties have been evaluated. In the second phase, experiments were conducted using hybrid biodiesel blended with diesel for different blend ratio and also with neat diesel fuel. All the blend ratios were tested for different loading conditions and engine performance measurements such as brake specific fuel consumption, and emissions were measured to evaluate and compute the behaviour of diesel engine. Average reading of three runs was taken for tabulating the results. Initially, combustion and emission characteristics of test engine were investigated using conventional diesel fuel under standard operating conditions for different loads starting from no load to full load conditions. In the second phase of the work, hybrid fuel has been prepared by mixing Jatropha and Simarouba biodiesel in the ratio of 50% each, and blended with diesel in 20, 40, 60, 80 and 100%. Using the prepared fuel further tests was carried out to obtain the performance and emissions characteristics of engine when operated using test fuel. Average of three set of reading was considered to plot the graph. Finally, the results like BTE, BSFC, along with emissions like smoke capacity, HC, CO and NO_x were compared with baseline data and analyzed.

3. Experimental setup

The schematic of experimental engine test rig setup used for evaluation of performance, combustion and emission characteristics of hybrid fuel at standard operating conditions is shown in Fig. 1. Technical specifications of the engine setup used for present study are given in Table 1. The speed and torque of the engine is controlled automatically by an eddy current dynamometer. A hartridge smoke meter and delta 1600 S exhaust Gas analyzer was suitably employed to determine the regulated emission levels such as HC, CO and NO_x which uses non-dispersive infrared technology. Gas analyzers were initially calibrated before the start of trial tests. The in-cylinder pressure was obtained by using a

piezo-electric type pressure sensor mounted on the head of engine cylinder. Table 2 shows the physico-chemical properties of test fuels used.
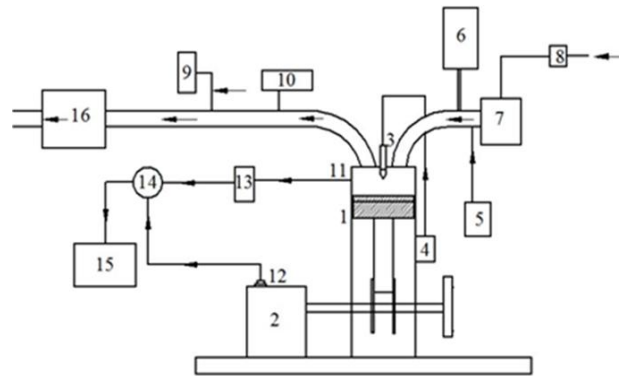
1. CI Engine, 2. Dynamometer, 3. Fuel Injector, 4. Fuel pump, 5. Fuel filter, 6. Fuel tank, 7. Air stabilizer tank, 8. Air filter, 9. Smoke meter, 10. Exhaust gas analyzer, 11. Pressure sensor, 12. TDC encoder, 13. Charge amplifier, 14. Indimeter, 15. Computer, 16. Exhaust pipe

Fig. 1: Line diagram of experimental setup

Table 1: Kirloskar TV 1 Engine and dynamometer specifications

Parameter	Specifications
Nozzle opening pressure	200 to 225 bar
Governer type	Mechanical centrifugal type
No. of cylinders	Single cylinder
Compression ratio	16.5:1
Bore diameter	80mm
Stroke length	110mm
Dynamometer	Electrical

Table 2: Physico-chemical properties of the crude Jatropha methyl ester (JOME) and Simarouba oil methyl ester (SuOME)

Property	Diesel	JOME	SuOME	B100
Density (kg/m^3)	840	876	865	875
Viscosity (mm^2/s)	2.98	4.8	4.68	4.72
Flash point (°C)	74	170	165	166
Calorific value (kJ/kg)	45,500	36,096	37,933	39,934
Acid value	0.35	4.9	5.34	5.02

4. Results and discussion

Studies were conducted on methyl esters of Jatropha and Simarouba dual biodiesel B100 and blends of B20, B40, B60 and B80. The fuel consumption test and rating test of a constant speed C.I engine was also conducted to evaluate the performance of the engine on diesel and different blends of biodiesel. Variations of BSFC in engine with various load for hybrid and diesel fuel is shown in Fig. 2. BSFC is inversely proportional to thermal efficiency of an engine. BSFC decreases sharply with the increase in load for all fuels. The main reason for this could be the increase in fuel which is required to operate the engine with increase in brake power because of its relatively less amount of heat lost at higher loads. The main reason for the variation of BSFC is the properties like density, viscosity and calorific value of the fuel used [9]. BSFC is lower for diesel fuel due to its lower viscosity than the hybrid fuel. However, B80 showed reduced BSFC than other blends and this may be attributed to higher combustion temperature of previous cycle leads to reduce the mixing time hence complete combustion happens.
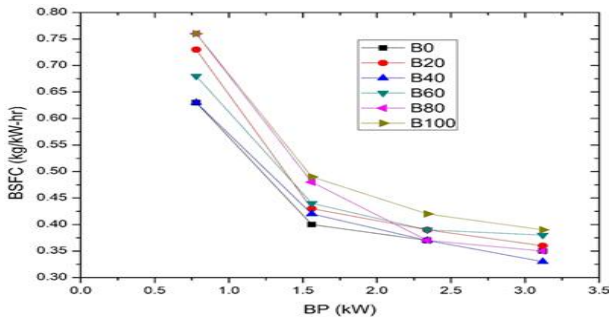
Fig. 2: Variation of BSFC with load

From Fig.3, the BTE of all the tested fuel increases with increase in brake power. This is due to the reduction in heat loss and increase in power and load. BTE for conventional diesel is found to be the highest because of its higher calorific value and proper air-fuel mixing. Hence, it results in complete combustion. It can be also observed that B20 and B100 exhibit highest and lowest BTE respectively when compared with all hybrid fuels. BTE of B20 and B100 is 26.5% and 24.2% respectively. This may be due to additional lubricity offered by B100 than B20, as a result of marginally higher viscosity of B100 test fuel.
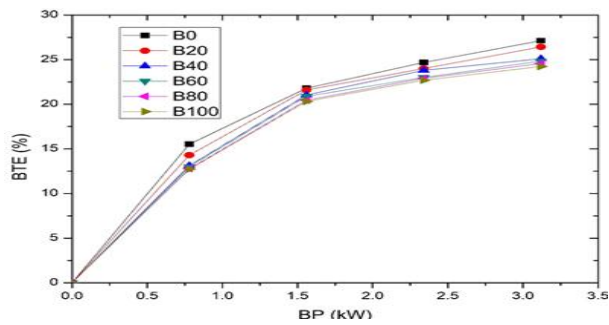

Fig. 3: Variation of BTE with load

Variation of CO emissions with engine loading for different test fuels is compared in Fig. 4. The major reason for CO emissions is lack of oxygen content in fuel air mixture [10]. It can be observed that, CO reduces drastically at a load of 10 and 15 N-m for all the test fuels. CO emissions for diesel fuel are 0.08% at a load of 15N-m whereas CO emissions for all other blends are lesser than that of diesel fuel. The lower CO emission of biodiesel blends maybe due to their more complete oxidation as compared to diesel. Some of CO produced during combustion of biodiesel may have converted into CO_2 by taking up extra oxygen molecules present in biodiesel chain and thus reduced CO formation. However CO emissions for B100 is 0.06% at 80% load whereas for B20 CO emission is same as diesel fuel and this may be attributed as % of biodiesel increases in diesel fuel, it leads to increase in oxygen content with in the combustion chamber due to rich oxygen content of hybrid fuel. The hydrocarbon emission trend for various blends of biodiesel is represented in Fig. 5. The reduction in HC was linear with the addition of biodiesel in the tested blends. These reductions indicate a more complete combustion of the fuel. The presence of oxygen in the fuel was thought to promote complete combustion.
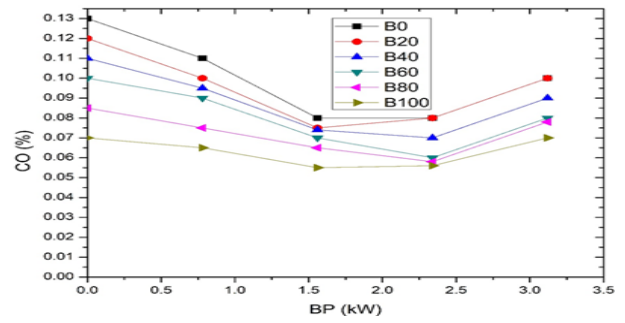
Fig. 4: Variation of CO with load

Fig. 6 shows the variation of CO_2 with respect to load. It is observed that as the load increases, CO_2 emission increases for all the test fuel. CO_2 emission from the engine using diesel fuel is 10% whereas for all other hybrid test fuels it is higher. This may be attributed to complete combustion due to the higher oxygen present in combustion chamber. CO_2 emission for B20 is 10.02% whereas for B100 is 11.25%. This may be attributed to lower calorific value of biodiesels as increase in percentage of blend leads to higher fuel consumption. The variation of NO_x with engine load for different fuels is represented in Fig. 7. NO_x formed in an engine is highly dependent on combustion temperature along with concentration of oxygen present in combustion products. In general, NO_x concentrations vary linearly with load of the engine. As the load increases, the overall air-fuel ratio increases resulting in increase in average gas temperature in the combustion chamber. Hence NO_x formation which is sensitive to temperature increases. The maximum NO_x emission for biodiesel is found to be 1312 ppm for B100 blend. It is 122 ppm higher than that of diesel fuel. The NO_x emissions may be eliminated by exhaust gas treatment.

Fig. 5: Variation of HC with load

Fig. 6: Variation of CO_2 with load

Fig. 7: Variation of NO$_x$ with load

5. Conclusion

Performance and emission results of single cylinder CI engine with hybrid mode of operation (SuOME and JOME) blended with diesel fuel were compared with baseline engine results. The production of dual (hybrid) biodiesel of non-edible oils involves a 2-stage transesterification process. Smooth engine operation has been observed for hyb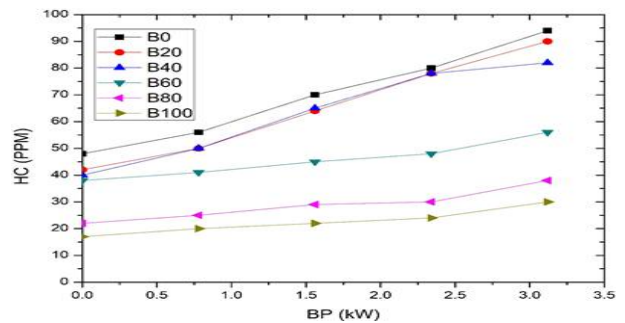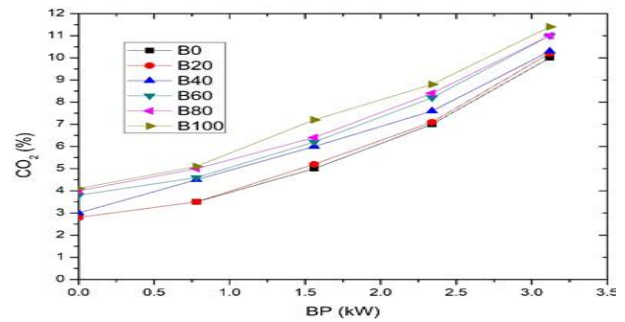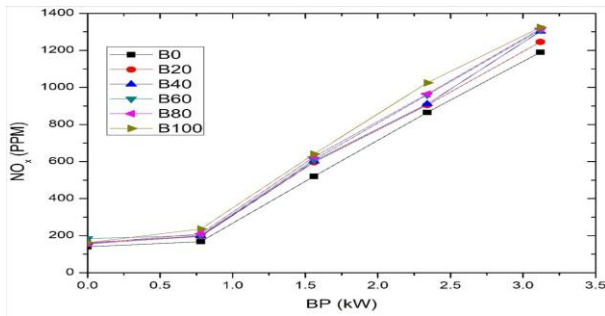rid fuel operation compared to diesel fuel operation. The maximum BTE is found to be 26.43% for B20 blend which is 0.69% lesser than that of diesel. The minimum BSFC of biodiesel is found to be 0.33 kg/kWh for B40 blend which is almost equal to that of diesel. The minimum CO emission for biodiesel is found to be 0.05 ppm for B100 blend which shows a 41.5% reduction as compared to diesel. The minimum HC emission for biodiesel is found to be 17 ppm for B100 blend which shows a 70.2% reduction as compared to diesel. CO$_2$ emission increases linearly as the load increases. The maximum CO$_2$ emission was found in B100 because of complete combustion of fuel. The maximum NO$_x$ emission for biodiesel is found to be 1312 ppm for B100 blend. Use of hybrid fuel may reduce hazardous emission and may become a substitute for conventional diesel.

REFERENCES:

[1] B. Nagaraj, T. Prakash and H. Rajashekhar. 2008. Performance and emission characteristics of a DI compression ignition engine operated on honge, Jatropha and sesame oil methyl esters, *Renewable Energy*, 33, 1982-1988. https://doi.org/10.1016/j.renene.2007.11.012.

[2] S. Dharma, M.H. Hassan, H.C. Ong, A.H. Sebayang, A.S. Silitonga, F. Kusumo and J. Milano. 2017. Experimental study and prediction of the performance and exhaust emissions of mixed Jatropha curcas-ceiba pentandra bio-diesel blends in diesel engine using artificial neural networks, *J. Cleaner Production*, 164, 618-633. https://doi.org/10.1016/j.jclepro.2017.06.065.

[3] N. Damanik, H.C. Ong, W.T. Chong and A.S. Silitonga. 2017. Biodiesel production from Calophyllum inophyllum-palm mixed oil, *Energy Sources, Part A: Recovery, Utilization, and Env. Effects*, 39(12), 1283-1289. https://doi.org/10.1080/15567036.2017.1324537.

[4] B.J. Bora, U.K. Saha, S. Chatterjee and V. Veer. 2014. Effect of compression ratio on performance, combustion and emission characteristics of a dual fuel diesel engine on raw bio-gas, *Energy Convers. and Mgmt.*, 87, 1000-1009. https://doi.org/10.1016/j.enconman.2014.07.080.

[5] P. Pradhan, H. Raheman and D. Padhee. 2014. Combustion and performance of a diesel engine with preheated Jatropha curcas oil using waste heat from exhaust gas, *Fuel*, 115, 527-533. https://doi.org/10.1016/j.fuel.2013.07.067.

[6] S. Vedharaj, R. Vallinayagam, W.M. Yang, S.K. Chou and P.S. Lee. 2014. Effect of adding 1, 4-dioxane with kapok bio-diesel on the characteristics of a diesel engine, *Appl. Energy*, 136, 1166-1173. https://doi.org/10.1016/j.apenergy.2014.04.012.

[7] S.K. Lohan, T. Ram, S. Mukesh, M. Ali and S. Arya. 2013. Sustainability of bio-diesel production as vehicular fuel in Indian perspective, *Renewable and Sustainable Energy Reviews*, 25, 251-259. https://doi.org/10.1016/j.rser.2013.04.024.

[8] N. Keerthikumar, T.K. Chandrashekar, N.R. Banapurmath and V.S. Yaliwal. 2018. Effect of combustion geometry, performance and emission characteristics of CI engine using Simarouba oil methyl ester, *IOP Conf. Series: Materials Sci. and Engg.*, 376, 1. https://doi.org/10.1088/1757-899X/376/1/012001.

[9] D.H. Qi, C.F. Lee, C.C. Jia, P.P. Wang and S.T. Wu. 2014. Experimental investigations of combustion and emission characteristics of rapeseed oil diesel blend in a two cylinder agricultural diesel engine, *Energy Convers. Mgmt.*, 77, 227-232. https://doi.org/10.1016/j.enconman.2013.09.023.

[10] S. Aydin and C. Sayin. 2014. Impact of thermal barrier coating application on the combustion, performance and emissions of a diesel engine fueled with waste cooking oil biodiesel-diesel blends, *Fuel*, 136, 334-340. https://doi.org/10.1016/j.fuel.2014.07.074.

Hybrid DC-AC homes with roof top solar power

Madhu M. C [1]*, K. Badari Narayana[2], J. Krishna Kishore[3]

[1] Department of Mechanical Engineering, BMS Institute of Technology and Management, Bengaluru, India
[2] Department of Mechanical Engineering, Ramaiah Institute of Technology, Bengaluru, India
[3] U R Rao Satellite Centre, Bengaluru, India

Abstract. The paper investigates the feasibility of a hybrid DC-AC home with roof top solar power. In recent times, roof top solar power has become popular for residential homes. Generally, the power obtained from roof-top solar panels is converted to AC with a power control unit and routed to the existing wiring network of the houses designed essentially to support the Electric Utilities which deliver AC power. Solar power with DC bus routing power to various sub-units and Brushless DC (BLDC) motor-based systems have been successfully flown in satellites for decades. The study presents the possibility of having a dedicated DC bus (24V / 48V) in the home connected directly to roof-top solar panels along with the traditional wiring network to support AC power (220-230V) from Electric Utilities. The recent success of the BLDC based home appliances further highlights the potential. This will also help to benefit from higher efficiency due to BLDC and avoid the conversion losses as home appliances that can run on DC power are presently available. It is now possible to have an independent local Roof Top solar power-based DC home-grid to support lighting circuit and home-appliances that operate on DC power. The existing wiring network for AC can continue to support high power equipment like motors, boilers, washing machines etc., It will also simplify the power control unit as the traditional inverter portion is avoided. Thus, the proposed hybrid DC-AC home needs be viewed in terms of an overall green approach which will be a paradigm shift for energy efficiency and lower carbon footprint. It has the potential to boost the sale of DC home appliances.

Key words: **DC power, electric utilities, green home, solar vehicle to home**

1. INTRODUCTION

In this article, the focus is to highlight the need to promote hybrid DC-AC homes with roof-top solar power. Residential homes across the nation have become significant consumers of electric power due to a modern lifestyle driven by urbanization. A typical urban home requires an average of 2 to 3 KW per family. The demand runs into Giga watts of power across the nation due to lakhs of All Electric Homes. India's solar potential of 6 Billion GWh as shown in Figure 1. can be used to generate roof-top solar power recognizing the crucial

role of solar power, the National Solar Mission (NSM) was launched in 2010, by the Gov. of India with the aim of installing 100 GWs solar power by 2022.
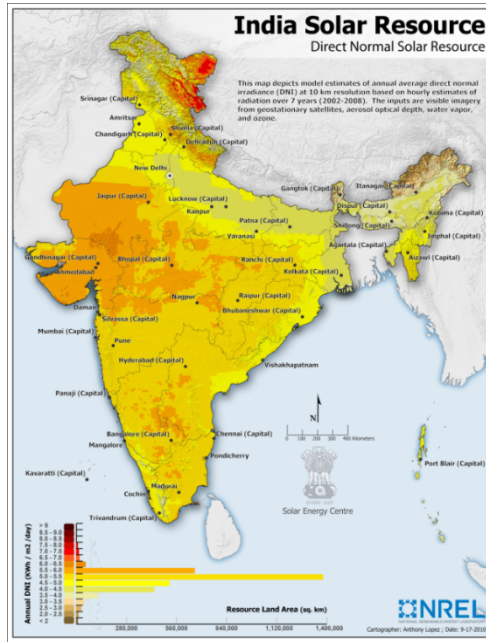
Figure 1: India's Solar Potential (National Resource Energy Laboratory)

Figure 2: Typical All Electric Home (AEH)

The power consumption in urban areas shows the socio-economic situation and the plight of rural areas. **Roof-Top** solar power supported **Hybrid DC-AC** homes has the potential to liberate Giga Watts of Power in Urban Areas from the grid which can be used for the development of rural areas and **Smart Villages** to improve their quality of life. This can possibly reduce the pressure on the already loaded urban infrastructure by reversing the migration from rural areas to urban areas. Figure 2. Represents a typical AEH home. Poor availability of electricity, education, employment, and health care due to lack of development in rural areas has led to migration from rural to urban areas. Hence, even small, and medium

enterprises are located in urban areas due to poor infrastructure and electricity access in rural areas. Mass migration to urban cities has invited younger people to find jobs and support themselves and support family and elders back home. Hence the labor cost and overall cost of living has increased even in urban areas. The recent pandemic COVID-19 has shown the need and urgency for distributed development across rural areas so that migration can be minimized. As the quality of life improves, the relentless migration to urban areas can be slowed down to improve social security and better health care.

Section 2 discusses the emerging trends, while in Section 3 discusses a typical hybrid DC-AC home and Section 4 gives the conclusion.

2. Emerging Trends

Roof top solar power has become popular for residential homes. The possibility of synergy exists between roof-top solar power and DC bus operated home appliances. Historically, these home appliances used single-phase AC induction motors. A new era has emerged, where DC power-based home appliances are available today in the consumer market due to BLDC. Most electrical devices even when supplied by AC operate on DC internally. The DC operated appliances avoid the rectifier electronics, thereby making devices simpler and more reliable with reduced power loss. For example, LED- lamps on DC supply can be realized with minimum components. Rooftop solar panels are a Photovoltaic source, and they generate DC power and can be used for DC based LED lamps, DC fans which will definitely reduce the electrical consumption from the grid, thereby saving electrical energy. This saved energy may be used for Industrial and agricultural sectors.

Figure 3 shows the typical home appliances which have traditionally operated on AC power. However, it is now possible to have DC power-based home appliances connected directly to DC bus derived from roof-top solar panels.

Figure 3:   Home Appliances

Figure 4 depicts a BLDC home appliance and Figure 5 shows how a DC grid works better than AC (and may reduce losses up to 5%). Figure 6 shows a DC fan which can replace AC

fans while Figure 7. gives a comparison between AC motor and BLDC based applications [11,12].
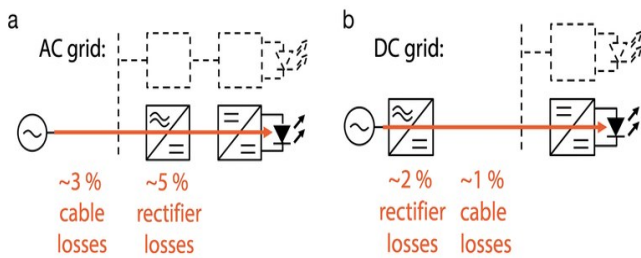

Figure 4: BLDC based home appliance – Mixie

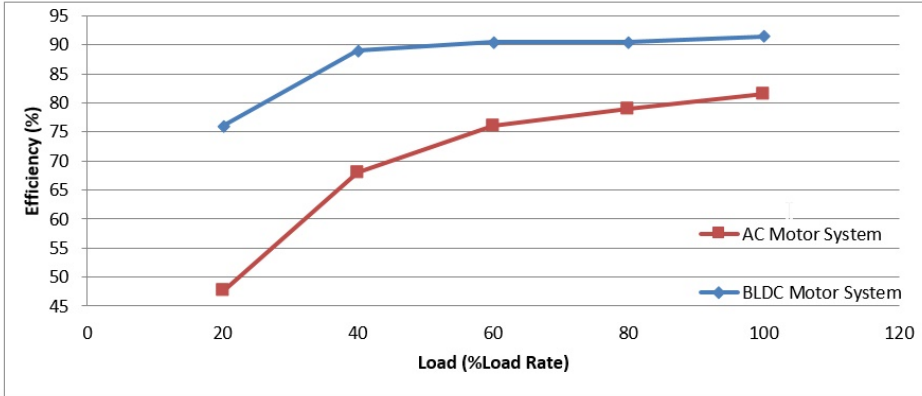**Figure 5**: AC and DC grid comparison   **Figure 6**: DC fan

Figure 7: Efficiency comparison

Since many appliances work on DC current, DC grids are becoming attractive in recent days. LED Lamps especially are the best example to be used in houses. These work on DC current and are examples to save power. During AC-DC conversion, the losses are around 5% for LED lamps, this loss of 5% does not occur if DC is used. DC fans consume less power than AC fans. BLDC motors have advantages such as reduced electricity consumption which gives advantage of longer backup on Inverters (even on Solar) and improved reliability. Noise reduction and longer lifetime. AC bus is also influenced by power factor aspects which is not present if DC bus rail is used to power home appliances. Many electrical appliances operate internally on DC power. Computers and electronic gadgets which are common in today's homes work on DC power.

LEDs are becoming popular in today's houses. They also contribute to the energy savings. An LED light has 40% of its components for AC-DC conversion. Which will make them simple to manufacture at lower cost and more reliable. DC bus at home is dependent on factors like conversion losses, electrical energy storage, length of the electric cables across the home and power consumption of the electrical appliances. The Figure 8 shows the components in an electronic circuit for AC supply.
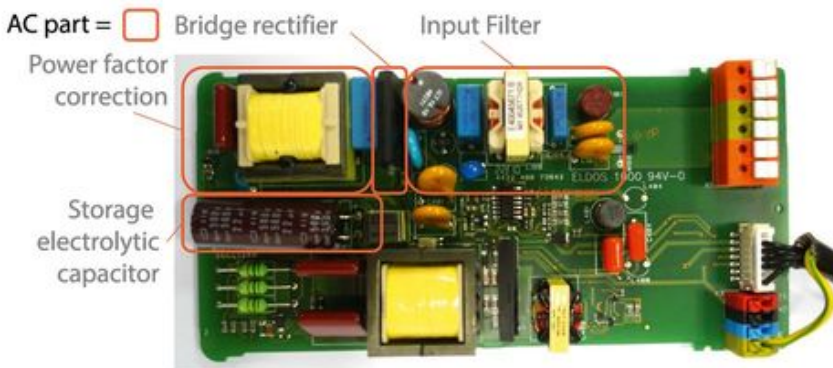

Figure 8: Components of an electronic circuit using AC power (11)

Drive motors of household appliances can be divided into AC and DC motors. Considerable progress in brushless DC motor (BLDC) has made household appliances possible like the

blender, juicer, coffee machine, tea machine, electric knife, eggbeater, rice cooker, food processor, grain grinder, straight mixer, and electric cutter. The same can be extended to floor cleaning devices also. The concept of low-carbon energy-saving products is vital to protect the environment. The brushless DC motor-based home appliances can help to meet the requirements of energy saving and low carbon footprint.

Rather than focusing on a dedicated DC home or AC home, a **hybrid AC-DC** home is proposed. A home DC grid can be set up for low power devices such as LED-lights, laptops, and TV, while a separate AC grid is used for high power devices. This approach can be adopted for homes and small offices.

3. Proposed Hybrid DC-AC home

Figure 9: Roof top Solar Power heater and plant

In a **hybrid DC-AC Bus** home, provision needs to be made for a DC bus from Roof Top Solar Power and AC bus from the Electric Utility. Thus, electricity used in residential homes can be divided into two categories: DC bus based circuitry (light, TVs, fans etc.,) and motor drive (refrigerator, washing machine, air conditioner, fan, vacuum cleaner, etc.), and give scope for future design of green buildings. Figure 9 shows roof top solar panels which can be used to generate 1 to 2 KW for the DC bus in a typical 2 Bedroom home as shown in Figure A1. The DC power generated from the solar panels can be supplied at 24V / 48V. The total load coming on the house can now be distributed between DC and AC buses. The DC power is distributed to all the power points in the house through cables. As many DC home appliances with same functionality are now available, it is possible to replace certain AC appliances like lamps, LED bulbs, fan etc., in the home. A DC bus rail can be used to avoid the traditional inverter/converter circuitry and losses. This can potentially help to reduce electrical energy drawn from the electrical grid which can be diverted to industry / agriculture usage etc.,

The future use of DC is also seen in the charging of Electric vehicles. All hybrid DC-AC homes can also have the advantage to receive energy from battery of Electric vehicles as shown in Figure 10 as Back-Up option in case of Emergency.

Figure 10: Charging an electric vehicle in a DC home

Socio-economic benefits of Hybrid DC-AC
- o   Generation of Gigawatts of roof top Solar Power
- o   Saves GWs of Power due to conversion losses due to DC home appliances and by avoiding Transmission & Delivery due to local generation and consumption.
- o   Increased strategic security due to local power generation unlike central power generation
- o   Enhanced tariffs in industry power will help to increase revenues of electricity boards.
- o   Saving of precious water used in thermal plants for power generation which can be used for agriculture to sustain food security and supplying drinking water to dry areas.
- o   Land acquisitions can be avoided as Roof-Top area is available...
- o   Human cost is avoided as there is no displacement and rehabilitation of people to alternate locations due to land acquisition as in case of Hydel / Thermal / Nuclear Projects etc.,
- o   Carbon footprint can be reduced per home
- o   High Job potential can be generated in Solar Sector / DC home appliance sector
- o   Boost to Manufacturing sector for DC Home appliances

4. Conclusion

The aim of the study is to present the feasibility of **hybrid DC-AC home** supported with **roof-top solar power** as BLDC based home appliances is possible. A typical room layout for a 2 or 3 BHK was taken to highlight how much load can be transferred to the DC bus. A home DC-grid at 24 V or 48 V can be considered. The conversion losses can be avoided. However, care needs to be taken w.r.t cabling network and associated losses. It has the potential to boost home DC appliances so that the power that is saved in residential homes can be diverted to industry and agriculture by Electric Utilities. A hybrid DC-AC home essentially further promotes the concept of a Green Building / home concept. The growth of **Electric Vehicles** also gives scope for a back-up supply to ensure lighting in case of emergency. Roof-top solar power adds to social security as massive power failures at Dams / Thermal Plants etc., will not lead to black-outs which existed in the past. It can be viewed as Personal Solar Power for a residential home.

5. REFERENCES:

1. W. J . Pellis, "The low voltage house", in *Electrtechniek:* Technische Uversiteit Endhoven, (1997), p.79
2. M. Friedman, "Concept for a DC low voltage house,' in *Sustainable building2002 Conference,* 2002, p.6
3. Giovanna Postiglione, "DC distribution system for home and office,' in Department of Electrical power engineering.vol.MSc Gartenberg, Sweden: Chalmers University of Technology, 2001, p.105
4 .Building Research Establishment, "The use of direct current output from PV systems in buildings', Department of Trade and Industry, London 2002.ETSU S/P2/00373/REP
5. Lasseter, R.and Paigi, P., "Micro grid: A conceptual solution", IEEE Power electronics specialist's conference, IEEE, 2004.
6. Ghareeb, A.T, Mohamed, A., &Mohammed, O.A,"DC micro grids and distribution systems: An overview", Power and Energy Society General meeting, .IEEE, 2013.
7. Electric Power Research Institute (EPRI), Duke Energy, "DC Powered data Centre demonstration": Executive summary, 2011.
8. Marnay C, "Building scales, building micro grids", 2012.
9. Nordman, B. & Christensen K, "DC local power distribution: technology, deployment and pathways to success", IEEE Electrification magazine, 2016.
10. Venkat Raja Raman, Ashok Jhunjhunwala, Prabjoth Kaur, Uma Rajesh, "Economic Analysis of deployment of DC power and appliances along with solar in urban multi-storied buildings." CEO, Cygni Energy Pvt Ltd, Hyderabad, India.
11.https://e2e.ti.com/blogs_/b/industrial_strength/archive/2018/02/06/cut-the-power-and-complexity-of-your-appliance-designs
12. https://www.bldcmotor.org/energy-saving-bldc-motor-for-household-application.html

APPENDIX A - Typical power requirements in a 2 BHK home (Hybrid DC-AC power)
In this appendix typical power requirements of hybrid AC-DC 2BHK home (Fig. A1) are given. A separate bus bar for AC and DC are assumed to be set up and with the AC appliances are cantered around the AC bus bar while the DC appliances are connected to the DC bus

bar. For the available rating of different AC and Dc appliances, the power required for a typical 2 BHK is shown in Table A1. The actual gain of the hybrid system depends on proper estimation of actual losses in each bus systems and cost of conversion equipment etc.,

Figure A1: Plan of a typical 2BHK home

Sl No	Description of Appliance	Qty	Average hours of each appliance/day	Power (W)	Energy consumed/day (kWh)	Energy consumed/month (kWh)
DC Power Units						
1	Lamp	6	3	10	0.18	5.4
2	Tube light	2	4	10	0.08	2.4
3	TV	1	8	36	0.288	8.64
4	Fan	4	4	18	0.288	8.64
5	Computer	1	2	24	0.048	1.44
Total DC power/month						26.52
AC Power Units						
6	Refrigerator	1	24	19	0.456	13.68
7	Water Geyser	1	1	2000	2	60.00
8	Washing machine	1	1	2000	2	60.00
9	Mixer Grinder	1	1	600	0.6	1.80
10	Pump Motor	1	1	740	0.74	22.00
Total AC power/month 157.48						

Table A1 : Typical power requirements for various AC and DC appliances

REVA UNIVERSITY

Bengaluru, India

Established as per the section 2(f) of the UGC Act, 1956
Approved by AICTE, COA and BCI, New Delhi

Certificate of Appreciation

School of Mechanical Engineering

Appreciates

KEERTHI KUMAR N

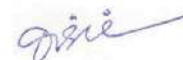of **BMS Institute of Technology and Management, Bengaluru**

presented on topic titled **Performance and Emission Characteristics of 4-Stroke Diesel Engine using Simarouba and Graphene Nanoparticles**

with Paper ID **TE024** in the 5th International Conference on Advanced Research in Mechanical, Materials and Manufacturing Engineering (ICAMMME - 2021), held on the 9th & 10th of July 2021.

Co-Authors : **Dr. Veerbhadrappa Telgane, Kiran M D, Pavan Kumar B K**

Director
School of Mechanical Engineering
REVA University

Vice-Chancellor
REVA University